rp 元素合成過程に関与する
陽子過剰な原子核の構造の研究

(研究課題番号：13640263)

平成 13 年～平成 16 年
科学研究費補助金（基盤研究 (C)(2)）研究成果報告書

平成 17 年 3 月

研究代表者 小 川 建 吾
（千葉大学理学部教授）

はしがき

本報告書は、平成13年度(2001年度)から平成16年度(2004年度)までの文部科学省科学研究費補助金(基盤研究(C)(2))「rp元素合成過程に関与する陽子過剰な原子核の構造の研究」(研究課題番号:13640263)による研究成果の報告書である。

宇宙の進化と元素合成の究明は自然科学における重要な課題である。これには宇宙物理学、原子核物理学など様々な分野が関係するが、原子核物理学が重要な鍵となっている。最近における原子核の微視的記述の進展により、宇宙の進化における核の役割が次第にあきらかになりつつある。質量数$A = 56$以上の重い元素の合成に関してs過程とr過程がよく知られているが,これらでは説明できない,陽子を過剰に含んだ核種が存在することが知られている。これらの核の生成は、陽子の捕獲反応なかでも新星や超新星において起こる水素の爆発的な元素合成過程(rapid-proton capture process,rp過程)の可能性が指摘され,陽子過剰核研究の重要さが増している。近年,短寿命核ビームの開発に伴って不安定核の研究が進んでおり,今後の陽子過剰核の構造の研究が急務とされている。

本報告書は、研究成果の概要、研究発表リスト、主要論文の収録から構成されている。関係する研究者各位のご参考になれば幸いである。

なお研究成果は松澤孝之氏をはじめ多くの研究者との共同研究や議論に負うところが多く、ここで改めて謝意を表する次第である。

2005年3月1日

研究代表者　　小川　建吾

研究組織

研究代表者　小川建吾　（千葉大学理学部・教授）

研究分担者　中田　仁　（千葉大学理学部・助教授）

研究経費

平成１３年　１，４００　千円

平成１４年　　８００　千円

平成１５年　　６００　千円

平成１６年　　７００　千円

合計　３，５００　千円

目　次

1. 研究成果の概要

1.1 はじめに

宇宙の進化と元素合成の究明は自然科学における重要な課題である。これには宇宙物理学、原子核物理学など様々な分野が関係するが、原子核物理学が重要な鍵となっている。最近における原子核の微視的記述の進展により、宇宙の進化における核の役割を正確に検討できる状況になりつつある。

質量数 $A = 56$ 以上の重い元素の合成に関して s 過程と r 過程がよく知られているが, これらでは説明できない, 陽子を過剰に含んだ核種が存在することも知られている。これらの核の生成は、陽子の捕獲反応なかでも新星や超新星において起こる水素の爆発的な元素合成過程 (rapid-proton capture process,rp 過程) の可能性が指摘され, 陽子過剰核研究の重要さが増している。近年, 短寿命核ビームの開発に伴って不安定核の研究が進んでおり, 今後の陽子過剰核の構造の研究が急務とされている。

1.2 本研究課題の目標

本研究では元素合成に関与する陽子過剰核の構造を微視的理論により調べ, 宇宙における rp 過程元素合成に関わる種々の原子核反応の可能性を研究することを目的とした。同時に安定核や中性子過剰核とは異なる陽子過剰核のさまざまな特徴を明らかにすることを目指した。当初においては特に,

(a) 軽い (p 殻及び sd 殻領域) 陽子過剰核における Thomas-Ehrman シフトの系統的研究,

(b) 陽子共鳴状態からの陽子放出確率の計算法の開発,

(c) 諸々の observable(β 崩壊確率や高スピン・アイソマーの性質など) から陽子過剰中重核の魔法数を調べること

に重点を置いて研究を開始した。

上記のうち (a),(b) については、軽い原子核合成における rp 過程の存在可能性が背景にある。陽子過剰核の構造は, クーロン障壁のため中性子過剰核とは様々な違いを持ち得る。陽子過剰核の特徴には, クーロン力の最低次の効果だけでなく高次の効果も重要な寄与を及ぼしている。従来 rp 過程に関与する未知の陽子過剰核の構造はその鏡映核のもので代用されてきたが, 例外的に不一致な状態が存在すること (Thomas-Ehrman シフト) も知られている。最近我々はこの Thomas-Ehrman シフトに関する新理論を提唱し, クーロン力の高次の効果が非常に大きな役割を果たすことを明らかにした。この効果は s 軌道陽子で特に大きいため,rp 過程元素合成のシナリオに大きな影響を与える可能性があり, 系統的な研究が望まれる。さらに, 共鳴状態からの陽子放出の研究も rp 過程との関連において重要であるが, その定量的評価が容易でない。近年の drip line 付近の核構造の理解や、共鳴状態に関する理論の進歩を生かして, 陽子放出確率の計算法を確立することを目指した。

１．３　本研究課題における主要な研究成果

(I) 軽い陽子過剰核の構造

陽子過剰核の構造は, クーロン障壁のため中性子過剰核とは様々な違いを持ち得る。陽子過剰核の特徴には, クーロン力の最低次の効果だけでなく高次の効果も重要な寄与を及ぼしている。従来rp過程に関与する未知の陽子過剰核の構造はその鏡映核のもので代用されてきたが, 例外的に不一致な状態が存在すること (Thomas-Ehrman シフト) も知られている。最近我々はこのThomas-Ehrmanシフトに関する新理論を提唱し, クーロン力の高次の効果が非常に大きな役割を果たすことを明らかにした。この効果はs軌道陽子で特に大きいため,rp過程元素合成のシナリオに大きな影響を与える可能性があり, 系統的な研究が望まれる。

1. 軽い核における Thomas-Ehrman Shift と有効相互作用

荷電対称性は核力に成立する重要な性質であり、実際に安定核領域の鏡映核のエネルギー準位はほぼ同じとみなせる。しかしながら安定領域から離れたれた原子核の構造が実験的に明らかになるにともない、鏡映核のレベルの中でいくつかのレベルに関して顕著なずれを示しているものが発見されている。なかには ^{16}N-^{16}F 対のように、基底状態のスピンが異なる鏡映核も存在している
このずれはThomas-Ehrman Shift とよばれている。本課題において我々はこのずれの原因が陽子過剰核における $s_{1/2}$ 陽子軌道の振る舞いにあるとして、理論的解析を行った。
まず陽子過剰核において、$1s_{1/2}$ 軌道上の陽子の動径方向波動関数に着目し、束縛エネルギーの減少に伴う、クーロン力に起因した動径成分の遠方へのしみだし効果の有効相互作用への影響を検討した。その効果は、弱束縛状態になると、$0d_{5/2}$ 陽子などにくらべ、$1s_{1/2}$ で大きく現われることが示された。我々はこの効果を $1s_{1/2}$ 陽子が関与する 2 体の有効相互作用行列要素に reduction factor を乗じ、より弱くすることで考慮できることを提案した。
具体的には p-sd 殻核を例とし、^{16}N-^{16}F の基底状態をはじめとした低い励起状態におけるエネルギー準位の大きな不一致を調べた。その結果、それぞれの核における陽子-中性子間有効相互作用の行列要素 $\langle 0d_{5/2}0p_{1/2}J|V_{\rm pn}|0d_{5/2}0p_{1/2}J\rangle$ と $\langle 0p_{1/2}0d_{5/2}J|V_{\rm pn}|0p_{1/2}0d_{5/2}J\rangle$ の差および $\langle 1s_{1/2}0p_{1/2}J|V_{\rm pn}|1s_{1/2}0p_{1/2}J\rangle$ と $\langle 0p_{1/2}1s_{1/2}J|V_{\rm pn}|0p_{1/2}1s_{1/2}J\rangle$ の差を比較すると、後者の差が著しく大きいことに依拠していることが、判明した。すなわち $\langle 1s_{1/2}0p_{1/2}J|V_{\rm pn}|1s_{1/2}0p_{1/2}J\rangle$ の値を対応する $\langle 0p_{1/2}1s_{1/2}J|V_{\rm pn}|0p_{1/2}1s_{1/2}J\rangle$ の約 0.8 倍した値とすることで、p 殻核の Thomas-Ehrman shift を統一的に理解できることを示した。さらに最近明らかにされた $sd-$ 殻核では ^{18}O-^{18}Ne に着目し、$J=0^+$ 状態の統一的理解に成功した。
従来 Thomas-Ehrman shift はエネルギー準位におけるずれを意味していたが、我々はこの考えをさらに発展させ、状態関数における鏡映核間のずれとして新たに軽い sd 殻核現象を見直すことの重要さを提案する。たとえば鏡映核のベー

タ崩壊における ft 値のずれなど、陽子過剰核の統一的理解のために検討すべき課題と位置づけている。これらに関しては今後の進展を目したい。

さらに, 共鳴状態からの陽子放出の研究も rp 過程との関連において重要であるが, 今回の研究課題においては Complex scaling 法による検討を開始はしたが、具体的な陽子放出確率の計算は継続課題となった。

2. ガモフ・テラー遷移におけるアイソスピン対称性の研究

多くの原子核のエネルギー準位から，アイソスピン対称性は非常によい近似的対称性と考えられている。他方，Thomas-Ehrman シフトのようなアイソスピン対称性の破れを表す現象を理解する上で，エネルギー準位だけでなく波動関数の性質を反映した他の物理量についても，アイソスピン対称性がどの程度成り立っているのか調べ，アイソスピン対称性をより精密に検証することが望まれる。その上で，ミラー核間のガモフ・テラー遷移強度は，明瞭でかつユニークな手段を与える。

最近の実験技術の進歩により，荷電交換反応によって β^+ 崩壊に相当する陽子過剰核側からのガモフ・テラー遷移強度が精密に測定できるようになり，sd 殻領域等でミラー核間のガモフ・テラー遷移強度の比較が可能となりつつある。本研究では，大阪大学理学部を中心とする実験グループに協力して，sd 殻領域のミラー核，^{26}Al(^{3}He, t) 荷電交換反応実験データと ^{26}Si のベータ崩壊強度の比較，またそれらと殻模型計算結果との比較によって，ガモフ・テラー遷移強度に関するアイソスピン対称性について調べ，^{26}Si と ^{26}Mg についてエネルギー準位だけでなくガモフ・テラー遷移強度についてもアイソスピン対称性がよく成り立っていると考えられること，また荷電交換反応の前方散乱強度とガモフ・テラー遷移強度がほぼ比例することを確認した。殻模型計算はガモフ・テラー遷移強度の実験データをよく再現しており，このミラー核に対するアイソスピン対称性を基礎とした従来の核構造の理解の正当性を示していると言えよう。これはまた，陽子過剰核に対して殻模型計算による研究を進める基盤の一つを与えたと見ることもできよう。但し，より一層陽子過剰になった場合にアイソスピン対称性の破れ がどう変化するかはまだ十分明らかでなく，今後の研究の発展が期待される。

また，アイソスピンの異なる状態間の磁気双極子遷移強度も，軌道角運動量の寄与，及び中間子交換流の寄与を補正することができれば，ガモフ・テラー遷移と類似の演算子によって起こる。逆に，上述のようにアイソスピン対称性がよく成り立っていることが確認できた場合，磁気双極子遷移強度をガモフ・テラー遷移強度と比較することにより，軌道角運動量の寄与に関する情報が得られる可能性がある。(^{3}He, t) のデータと既存の実験データを合わせ，また殻模型計算の結果とも比較しながら，核子の軌道運動の寄与についても調べた。

なお，この研究は上述のように大阪大学理学部の藤田佳孝氏らと協力して行ったもので，当該研究グループは特に殻模型に基づく理論計算及びそれに基づく議論を担当した。

(II) $N = 82$ 近傍の原子核の構造

1. $Z = 64$ 近傍の陽子過剰核の新たな描像の確立

Kleinheinz らによる陽子過剰な $Z = 64$ 核に関する実験的研究により、^{146}Gd は 2 重閉殻的様相を示していることが明らかにされ、さらに $Z \geq 64$ の $N = 82$ 核は $(0h_{11/2})^{Z-64}$ 配位で記述できるとする考えが、標準的とされていた。特に ^{152}Yb における $J = 10^+ \rightarrow J = 8^+$ の E2 遷移確率の現象は、$J = 10^+$ がセニオリティにもとずく選択則から説明できる典型例として、セニオリティアイソマーとして分類されていた。

我々はこの従来の見方に疑問を抱き、陽子過剰な $N = 82$ 核の再検討を行った。すなわち $Z = 64$ 領域に存在する $0h_{11/2}$ 軌道以外の $2s_{1/2}, 1d_{3/2}$ 軌道も取り入れたより現実的な模型で、統一的に理解されるべきであると考えた。

そこで第一段階として $(0h_{11/2}, 2s_{1/2}, 1d_{3/2})^{Z-64}$ 配位を仮定したより現実的な殻模型を採用し、これらの核のエネルギー準位ならびに E2 遷移確率をまず計算した。その結果、E2 遷移確率は $Z = 72$ 核で最低となり、実験と食い違うことを示した。この原因は陽子間の対相関により、$J = 10^+(^{152}\mathrm{Yb})$ において $0h_{11/2}$ 軌道の占有粒子数の期待値 $N(0h_{11/2})$ が減少し、$N(0h_{11/2}) < 6$ となることが明らかになった。

実験が示す ^{152}Yb において $N(0h_{11/2}) \sim 6$ を再現するため、従来 2 重閉殻核とみなし、芯として取り扱った ^{146}Gd の芯励起を考慮した殻模型計算に行い、$N = 82$ 核における一連の $J = 10^+$ 状態の分析を行った。その結果、芯励起を考慮することにより、$0h_{11/2}$ 軌道の占有粒子数が増加し、^{152}Yb において $N(0h_{11/2}) \sim 6$ を得るなど、エネルギー準位、$E2$ 遷移に関しての統一的かつ定量的な理解に成功した。

この結論は従来の陽子過剰な $N = 82$ 核についての認識を大きく変えるものである。特に従来のセニオリティアイソマーの概念をより普遍化した新しい概念「一般化されたセニオリティアイソマー」の重要性を示し、quasi spin との関連を明らかにした。

2. ^{136}Ba の新アイソマーの研究

^{132}Te,^{134}Xe, ^{138}Ce の $N = 80$ 核においてはいずれも $J = 10^+$ がアイソマーとして実験的に発見されていた。ところが同じ $N = 80$ 核である ^{136}Ba では、実験上の困難さから $J = 10^+$ のような高スピン状態の生成が難しく、未発見であった。最近日本原子力研究所の静間氏らの実験グループは、深部非弾性反応を用いた実験において、^{136}Ba の高スピン状態の生成に成功し、3.357MeV の励起エネルギー状態として $J = 10^+$ を発見した。

さらに $\gamma - \gamma$ 同時測定により、この $J = 10^+$ の寿命が $T_{1/2} = 94 \pm 10$ns であることが判明した。この E2 遷移強度は、近傍の ^{132}Te や ^{134}Xe の $J = 10^+$ の E2 遷移とくらべ、著しく小さく、きわめて特徴的な状態であることが判明した。

我々は理論的観点からこの $J = 10^+$ の理解を試みた。^{136}Ba を含む $N = 80$ 核に対して ^{132}Sn を芯とした殻模型を採用し、陽子に対して $(0g_{7/2}, 1d_{5/2})^{Z-50-r}$.

$(2s_{1/2}, 0h_{11/2}, 1d_{3/2})^r$ 配位（ここで $r = 0, 1, 2, 3, 4$）を、一方中性子には $(1d_{3/2}, 0h_{11/2}, 2s_{1/2}, 1d_{5/2}, 0g_{7/2})^{-2}$ 配位を仮定した。有効相互作用としては陽子-陽子間、中性子-中性子間にはSDIを採用し、陽子-中性子間には、最も陽子系-中性子系の相関に重要な4重極力 $(Q \cdot Q$ 力）を用いた。ハミルトニアン行列の計算に際しては、低い励起状態に対する影響がほとんど無視できると考えられ、陽子系のセニオリティ $v \geq 5$ の状態は除外して行った。

その結果、^{136}Ba の低い励起状態が再現され、$J = 10^+$ は 3.32MeV に得られ、2.94MeV の $J = 8^+$ と合わせ実験との十分な一致をみた。得られた波動関数から、E2遷移に関しても、一連の $N = 80$ 核における Z 依存性をよく説明した。特に ^{136}Ba の $J = 10^+$ 状態は、主として $|J_p = 0^+ \times J_n = 10^+\rangle$ からなることが判明し、またE2遷移で結ばれる $J = 8^+$ は $|J_p = 2^+ \times J_n = 6^+\rangle$ であることから、E2遷移確率の小ささが証明できた。

(III) ドリップライン近傍の Cu アイソトープの構造

陽子放出線 (proton drip line) 近傍の原子核研究には、その対極である中性子放出線 (neutron drip line) 近傍の原子核研究と密接なかかわりがあり、多くの示唆を得る可能性がある。特に荷電対称性にもとづき、中性子過剰核の構造から陽子過剰核の構造に関する大まかな情報を得ることが可能である。このような観点から、我々は原子力研究所のタンデム加速器を用いて行われた中性子数 $N = 40$ 近傍の Ni 領域の核構造に注目した。

^{68}Cu の低い励起状態は、$J = 1^+$(0keV), $J = 2^+$(84.1keV),$J = 3^+$(610keV), $J = 6^-$(721keV) であることが実験的に明らかになり、$N = 40$ 付近における中性子軌道として $f_{5/2}, p_{1/2}, g_{9/2}$ が存在している状況が明らかになった。特に第1励起状態 $J = 2^+$ から基底状態 $J = 1^+$ への M1 遷移が測定され、遷移確率の実験値は $|\langle 2^+||M1||1^+\rangle| = 0.197\mu_n$ と、単純な配位仮定 $\pi p_{3/2}\nu p_{1/2}$ 間の遷移確率 $|\langle \pi p_{3/2}\nu p_{1/2} 2^+||M1||\pi p_{3/2}\nu p_{1/2} 1^+\rangle| = 0.46\mu_n$ からは大幅に小さくなっていることが示された。一方 $J = 1^+$ の磁気モーメントの実験値は $g(1^+) = 2.48\mu_n$ と、ほぼ $|\pi p_{3/2}\nu p_{1/2} J = 1^+\rangle$ 状態での期待値に近いことが判明した。これらの値に統一した理論的解釈を行うため、我々は現実的な殻模型にもとづき状態を予測した。計算は陽子、中性子に対して $(p_{3/2}f_{5/2}, p_{1/2})^n + f_{7/2}^{-1}(p_{3/2}f_{5/2}, p_{1/2})^{n+1}$ 配位を仮定した。その結果、遷移確率と磁気モーメントの統一的理解には、芯部である $f_{7/2}$ からの励起モードを考慮することの重要性が示された。

(IV) 平均場近似での核内有効相互作用と不安定核の殻構造

最近の中性子過剰核における新魔法数の発見により，不安定核における殻構造が我々の従来の理解と異なっていることが明らかになった。これは核構造理解の根本に関わる問題であると言えよう。その原因として，核子が緩く束縛されていることによる効果や有効相互作用の影響などが議論されているが，まだ明確な答えは得られていない。この研究では，中性子過剰核だけでなく陽子過剰核も含め，β 安定線から離れた場合の殻構造の変化を自己無撞着な平均場近似により研究することを目指し，有効相互作用の検討やそれに適した数値計算アルゴリズムの開発を行った。

従来，原子核の平均場計算はゼロ・レンジに単純化されたSkyrme型相互作用を用いて行われることが多かった。しかし，ドリップ・ライン近傍までを含めた多様な核に対して，単一のSkyrme型相互作用で十分かどうかは自明でない。この研究では，核反応実験との首尾一貫性や殻模型との対応等も意識して，有限レンジ相互作用を含めた様々な相互作用を扱うことを意図し，それに適したアルゴリズムとして少数系の研究に用いられているガウス関数展開法が平均場計算にも有効であることを指摘し，その方法を定式化した上でプログラムを開発した。これはまた，緩く束縛された核子を扱うのにも効率的な方法である。

さらに，微視的なG行列に中間子交換の描像を組み合わせて提案され，核反応の解析等に広く用いられているいわゆるM3Y相互作用を基にし，核物質の性質等からこれを補正した新しい有効相互作用を提案した。この有効相互作用は，二重閉殻の原子核については従来のSkyrme型あるいはGogny型相互作用とほぼ同様の結果を与える一方，中性子過剰領域で$N \approx 16$や$N \approx 32$の殻構造が従来の相互作用と異なっており，新魔法数と矛盾しない。不安定核の殻構造に対して一定の予言性を持つことが期待される。しかし，まだ応用された範囲が限定されており，今後パラメータの数値も含め様々な角度からより詳しく検討することが望まれる。

(V) 殻模型モンテカルロ法による陽子過剰核の準位密度の研究

中質量$Z \approx N$核は，β安定線に比べて有意に陽子過剰側にあって，rp過程元素合成の経路となる可能性があり，rp過程元素合成の際の反応率を知るためその核準位密度が非常に重要である。核準位密度を理論的に求める上で，微視的な立場から殻模型による計算を実行するのが望まれること，またそのために量子モンテカルロ法(殻模型モンテカルロ法，略してSMMC法)が有効であることは，本研究の研究協力者である中田等が示してきた通りである。しかし，SMMC法を応用する場合，符号問題を避けるため通常は有効ハミルトニアンの一部を無視しており，そのためアイソスピンによるエネルギー分裂を正しく再現できないという問題があった。これは特に$Z \approx N$核の準位密度を計算する際に深刻な問題となり得る。

この研究では，SMMC計算実行の際に各サンプルに対してアイソスピン射影を実行する方法を新たに開発し，$Z \approx N$核に対してアイソスピン毎の準位密度を精度よく求めることに成功した。さらに，アイソスピンによるエネルギー分裂を実験値等から評価した上で，アイソスピン毎の準位密度を加え合わせることにより，全準位密度についても信頼性の高い計算が実行できることを示した。同時に，Ormandにより提案された摂動的なエネルギー分裂の補正が良くないことを明らかにした。

１．４　関連する研究成果

(I) jj 結合方式にもとづく殻模型計算コードの開発

本研究課題遂行に不可欠な前提として、原子核の微視的記述を行う最適な方法である原子核殻模型計算用プログラムコードの開発がある。少数多体系である原子核は2種類のフェルミオン陽子と中性子からなる量子系で、その粒子像にもとづいた記述に際してはパウリの排他律、角運動量保存則、核子数保存則など基本的に満たさねばならない基本則が存在する。これらを忠実に満たし、未確定である有効相互作用に多様な仮定を可能とするのが殻模型である。本研究課題で開発した殻模型コードは jj-coupling にもとづく殻模型で、後述するセニオリティ概念が有効に活用できる特徴をもっている。

1. Hamiltonian
   基本的には陽子、中性子がそれぞれの軌道空間にあるとしている。それぞれのハミルトニアンを $\mathcal{H}_p$ 、 $\mathcal{H}_n$ および陽子-中性子相互作用を V_{pn} とすると、ハミルトニアン $\mathcal{H}$ は

   $$\mathcal{H} = \mathcal{H}_p + \mathcal{H}_n + V_{pn}$$

   ここで $\mathcal{H}_p$ は1粒子エネルギー $\epsilon_p(i)$ および2体の相互作用 $V_{pp}(ij)$ を用いて

   $$\mathcal{H}_p = \Sigma_i \epsilon_p(i) + \Sigma_{i \neq j} V_{pp}(ij)$$

   と書け、中性子系に対しても同様に以下のようになる。

   $$\mathcal{H}_n = \Sigma_i \epsilon_n(i) + \Sigma_{i \neq j} V_{nn}(ij)$$

2. Basic Vectors
   陽子、中性子に対してそれぞれ6軌道までの空間を採用することが出来る。それぞれ、$j_{p1}, j_{p2}, j_{p3}, j_{p4}, j_{p5}, j_{p6}$ および、$j_{n1}, j_{n2}, j_{n3}, j_{n4}, j_{n5}, j_{n6}$ とすると、陽子系の基礎ベクトル、中性子系の基礎ベクトルは以下のようになり、

   $$|\alpha_p J_p\rangle = |j_{p1}^{n_{p1}}(\alpha_{p1} J_{p1}) j_{p2}^{n_{p2}}(\alpha_{p2} J_{p2})[J_{p12}] j_{p3}^{n_{p3}}(\alpha_{p3} J_{p3})[J_{p123}]$$
   $$\times\ j_{p4}^{n_{p4}}(\alpha_{p4} J_{p4}) j_{p5}^{n_{p5}}(\alpha_{p5} J_{p5})[J_{p45}] j_{p6}^{n_{p6}}(\alpha_{p6} J_{p6})[J_{p456}]\ J_p\ \rangle$$

   $$|\alpha_n J_n\rangle = |j_{n1}^{n_{n1}}(\alpha_{n1} J_{n1}) j_{n2}^{n_{n2}}(\alpha_{n2} J_{n2})[J_{n12}] j_{n3}^{n_{n3}}(\alpha_{n3} J_{n3})[J_{n123}]$$
   $$\times\ j_{n4}^{n_{n4}}(\alpha_{n4} J_{n4}) j_{n5}^{n_{n5}}(\alpha_{n5} J_{n5})[J_{n45}] j_{n6}^{n_{n6}}(\alpha_{n6} J_{n6})[J_{n456}]\ J_n\ \rangle$$

   その結果、系全体を記述する基礎ベクトルは

   $$|\alpha J\rangle = |\alpha_p J_p \times \alpha_n J_n :\ J\ \rangle$$

   となる。なお各軌道上での量子数 $\alpha_{p1}, \cdots, \alpha_{n1} \cdots$ にはセニオリティを含んでいる。したがって後述するこのセニオリティにもとづく状態制限が可能となる。

3. Effective Interaction
   2体の有効相互作用 $V_{pp}, V_{nn} V_{pn}$ としては各行列要素を数値で入力するが、標準

的なポテンシャル、すなわち中心力、LS力、テンソル力を、動径依存性としてYukawa型、Gauss型などをポテンシャルパラメターを用いて計算することも可能である。

4. Calculation of Hamiltonian matrix
計算対象の原子核の、芯の外側にある陽子数、中性子数を指定すれば、プログラムは自動的に状態を生成し、ハミルトニアン行列の各行列要素を計算し、格納する。この状態生成に際しては、上記基礎ベクトルに含まれる量子数（各軌道の粒子数、セニオリティ）にもとづく状態制限の導入も可能である。

5. Diagonalization
格納された行列要素を読み取り、ランチョス法にもとづいて固有値を最低固有値から指定個数だけ求める。

6. Calculation of nuclear property
得られた波動関数を用いて、電磁遷移確率、ベータ崩壊行列要素、1核子移行反応におけるspectroscopic factor、などの物理量を計算する。

(II) 重要な原子核構造研究課題への応用

本研究課題遂行上開発した上記のプログラムを用いて、核物理上きわめて重要な課題にも応用でき、注目される結果を得ることができた。本研究課題の成果の一つと位置づけ、その概要を以下に記す。

1. ハイパー原子核への応用
従来ハイパー核の生成には(K^-,π^-)反応や(π^+,K^+)反応が用いられていた。これらは運動量の小さなΛの生成など、ハイパー核研究上の利点あるが、入射粒子の強度が得にくいという大きな欠点があった。そこでこれらに代わる新たなハイパー核生成可能性として、電子加速器を用いた$(e,e'\gamma)$による、(γ,K^+)による反応が考えられる。すなわち

$$(\gamma,K^+): \qquad p(uud) \ + \ \gamma \ \rightarrow \ \Lambda(uds) \ + \ K^+(u\bar{s})$$

反応である。
この反応では核に持ち込む運動量が大きく、しかもスピン反転依存性も大きく、従来の低スピン状態よりも、高スピン状態が強く励起されることが予測される。例えば陽子 $|(0d_{5/2})_p^6 J=0^+\rangle$ が $|(0d_{5/2})_p^5\cdot(0d_{5/2})_\Lambda J\rangle$ 状態が生成されるとき、$J=5^+$状態生成確率が大きくなることである。そこで我々は元場俊雄氏らの研究グループと共同で、いくつかの原子核を標的にした(γ,K^+)実験を行った場合のシミュレーション計算を行った。特に実験可能性が高い、$^{28}\mathrm{Si}(\gamma,K^+)^{28}_\Lambda\mathrm{Al}$過程の検討を行った。始状態の$^{28}\mathrm{Si}(J=0^+)$として$(0d_{5/2},1s_{1/2},0d_{3/2})^{12}$、生成されるハイパー核$^{28}\mathrm{Al}_\Lambda$として$(0d_{5/2},1s_{1/2},0d_{3/2})^{11}\times(0d_{5/2},1s_{1/2},0d_{3/2})_\Lambda$を仮定した殻模型計算を行った。その結果を用いて$E_\gamma=1.3\mathrm{GeV}$における励起関数を求め、実験可能性を示した。これによりハイパー核研究の新局面の展開が期待される。

2. 乱雑な相互作用問題への応用

偶-偶核の基底状態のスピンは例外なく $J = 0^+$ で、これは核子間に働く対相互作用の影響と理解されていた。すなわち同種粒子間に働く相互作用 $\langle j^2 : J|V_{T=1}|j^2 : J\rangle$ で $J = 0$ 要素が他の要素とくらべ大きな引力傾向にあるからである。

ところが C.W.Johnson らは 2 体相互作用として乱数を用いた場合でも、統計的な分析を行うと、$J = 0^+$ スピン状態が基底状態となる確率が、他のスピン状態がなる確率とくらべ、著しく大きいことを示した。これは $J = 0^+$ 基底状態の出現が、対相互作用のみに依拠せず、空間に秘められた幾何学的な要因にもよることを示唆しているとして、大いに議論を呼んでいた。

これに関して Zhao-Arima の研究グループは、j^n 配位などの簡単な核状態に関する考察を行い、同じような結論を得ていた。これに対して我々研究グループは、より現実的な配位、すなわち陽子-中性子系でそれぞれが複数軌道空間上にある場合での検証を提案し、開発された殻模型計算コードを用いて共同研究を行った。具体的には sd 殻の特定核について、乱数表にもとづいた乱雑な相互作用を用いて全スピン状態の固有値計算を 1000 回繰り返すなどの計算が行われた。その結果、確かに $J = 0^+$ 基底状態の確率的多さが確認できた。さらにこれらの $J = 0^+$ 状態の波動関数を分析したところ、本来対相関から予測されるセニオリティ $v = 0$ が主成分ではなく、混合した各状態のセニオリティの平均値は、おおよそ $v = 4$ で、対相関による $J = 0^+$ とは全く別状態が基底状態になっていることが明らかにされた。

また乱雑な 2 体相互作用を用いた殻模型計算において、ハミルトニアン行列の対角要素の平均値 $E(J)$ を調べたところ、$E(J) \propto J(J+1)$ が成り立っていることが導かれた。これは対角化以前の段階で、$J = 0^+$ 基底状態優位性が現われていることを意味し、今後の研究にきわめて大きな影響を及ぼすものと思われる。

2. 発表論文リスト

(I) 学術雑誌等発表論文

1. H. Nakada and M. Sato
   A method of implementing Hartree-Fock calculations with zero- and finite-range interactions
   Nuclear Physics A 699, No. 3–4, pp. 511–537 (2002年2月) ;
   Erratum, Nuclear Physics A 714, No. 3–4, pp. 696–698 (2003年2月)

2. Y. Fujita, Y. Shimbara, A. F. Lisetskiy, T. Adachi, G. P. A. Berg, P. von Brentano, H. Fujimura, H. Fujita, K. Hatanaka, J. Kamiya, T. Kawabata, H. Nakada, K. Nakanishi, Y. Shimizu, M. Uchida and M. Yosoi
   Analogous Gamow-Teller and $M1$ transitions in ^{26}Mg, ^{26}Al and ^{26}Si,
   Physical Review C 67, No. 6, 064312 (12 pages) (2003年6月)

3. H. Nakada
   Hartree-Fock approach to nuclear matter and finite nuclei with M3Y-type nucleon-nucleon interactions
   Physical Review C 68, No. 1, 014316 (14 pages) (2003年7月)

4. L. Hou, T. Ishii, M. Asai, J. Hori, K. Ogawa and H. Nakada
   Measurement of $B(M1)$ for the $\pi p_{3/2}\nu p_{1/2}^{-1}$ doublet in ^{68}Cu
   Physical Review C 68, No. 5, 054306 (6 pages) (2003年11月) ;
   Publisher's Note, Physical Review C 68, No. 6, 069901(E) (1 pages) (2003年12月)

5. T. Shizuma, Z. G. Gan, K. Ogawa, H. Nakada, M. Oshima, Y. Toh, T. Hayakawa, Y. Hatsukawa, M. Sugawara, Y. Utsuno and Z. Liu
   A new isomer in ^{136}Ba populated by deep-inelastic collisions
   The European Physical Journal A 20, No. 2, pp. 207–210 (2004年5月)

6. Y. M. Zhao, A. Arima, N. Shimizu, K. Ogawa, N. Yoshinaga and O. Scholten
   Patterns of the ground states in the presence of random interactions: Nucleon systems
   Physical Review C 70, No. 5, 054322 (8 pages) (2004年11月)

7. Y. M. Zhao, A. Arima and K. Ogawa
   Energy centroids of spin I states by random two-body interactions
   Physical Review C 71, No. 1, 017304 (4 pages) (2005年1月)

(II) 国際会議報告

1. H. Nakada, K. Ogawa and R. Motegi
   Properties of nuclei around proton drip line and many-body effects on mirror asymmetry
   RIKEN Review No. 39, "Physics at Drip Lines", edited by H. Sagawa, T. Suzuki and A. Ozawa, pp. 161–165 (理化学研究所, 2001年9月)

2. H. Nakada, T. Matsuzawa, K. Ogawa and G. Momoki
   Seniority isomerism in proton-rich $N = 82$ nuclei and its indication to stiffness of the $Z = 64$ subshell
   "Nuclear Structure", Proceedings of the Conference: Bologna 2000 "Structure of the Nucleus at the Dawn of the Century", edited by A. Zichichi, G. C. Bonsignori, M. Bruno, A. Ventura and D. Vretenar, pp. 326–329 (World Scientific, 2001年)

3. H. Nakada
   Microscopic calculation of nuclear level densities with auxiliary-fields Monte Carlo method
   Journal of Nuclear Science and Technology Supplement 2, August 2002, Proceedings of the International Conference on Nuclear Data for Science and Technology, vol. 1, pp. 730–733 (Atomic Energy Society of Japan, 2002年8月)

4. K. Ogawa and H. Nakada
   Role of residual interaction in Thomas-Ehrman shifts in $A \sim 20$ nuclei
   Proceedings of the International RIKEN Symposium "Shell Model 2000", edited by T. Otsuka, H. Sakurai and I. Tanihata, pp. P11–P14 (North-Holland, 2002年)

5. H. Nakada, Y. Alhassid and S. Liu
   Shell model Monte Carlo approach to nuclear level densities
   Proceedings of the International RIKEN Symposium "Shell Model 2000", edited by T. Otsuka, H. Sakurai and I. Tanihata, pp. P35–P38 (North-Holland, 2002年)

6. H. Nakada
   A Hartree-Fock calculation with Yukawa interaction
   Progress of Theoretical Physics Supplement No. 146, Proceedings of the 10th Yukawa International Seminar "Physics of Unstable Nuclei", edited by K. Hagino, H. Horiuchi, M. Matsuo and I. Tanihata, pp. 442–446 (2002年12月)

7. T. Matsuzawa, H. Nakada and K. Ogawa
   Role of the $Z = 64$ core excitation in high-spin isomers in proton-rich $N \sim 82$

nuclei
Progress of Theoretical Physics Supplement No. 146, Proceedings of the 10th Yukawa International Seminar "Physics of Unstable Nuclei", edited by K. Hagino, H. Horiuchi, M. Matsuo and I. Tanihata, pp. 595–596 (2002年12月)

8. H. Nakada
Hartree-Fock calculations on unstable nuclei with several types of effective interactions
Nuclear Physics A 722, No. 1–4, pp. 117c–122c (2003年7月)

9. T. Ishii, M. Asai, M. Matsuda, P. Kleinheinz, L. Hou, J. Hori, A. Makishima, T. Kohno, M. Ogawa, K. Ogawa and H. Nakada
Nano-second isomers in neutron-rich nuclei around ^{68}Ni
Proceedings of the 3rd International Conference "Fission and Properties of Neutron-Rich Nuclei", edited by J. H. Hamilton, A. V. Ramayya and H. K. Carter, pp. 125–134 (World Scientific, 2003年)

10. H. Nakada, T. Matsuzawa and K. Ogawa
Survival of quasi-spin structure in isomers of $N \sim 82$ nuclei
"Symmetries in Science XI", edited by B. J. Gruber, G. Marmo and N. Yoshinaga, pp. 459–470 (Kluwer Academic, 2004年)

11. T. Motoba, P. Bydzovsky, M. Sotona, K. Itonaga, K. Ogawa and O. Hashimoto
Prospect of photoproduction of medium-heavy hypernuclei
"Electrophotoproduction of strangeness on nucleons and Nuclei" edited by K. Maeda et al., pp 221–232 (World Scientific, 2004年)

(III) その他の出版物

1. M. Sato and H. Nakada
   A modification of Gogny D1S interaction
   Bulletin of the American Physical Society 46, No. 7, p. 19 (2001年10月)

2. H. Nakada and Y. Alhassid
   Exact Isospin Projection in the Shell Model Monte Carlo Method and its Application to Nuclear Level Densities
   Bulletin of the American Physical Society 46, No. 7, p. 37 (2001年10月)

3. T. Matsuzawa, H. Nakada and K. Ogawa
   Role of $Z = 64$ core excitation in high-spin isomers in proton-rich $N \sim 82$ nuclei
   Bulletin of the American Physical Society 46, No. 7, p. 88 (2001年10月)

4. 中田 仁,
   陽子放出・捕獲に対する complex-scaled Hartree-Fock 計算の plan
   素粒子論研究 第104巻第2号, pp. B46–B47 (2001年11月)

5. H. Nakada
   Shell model study on Thomas-Ehrman shifts in *sd*-shell nuclei and its relevance to *rp*-process nucleosynthesis
   CNS-REP-42: CNS/RIKEN Workshop on Physics with Low-Energy RI Beams, pp. 65–72 (東京大学原子核科学研究センター, 2001年12月)

6. 中田 仁,
   殻模型モンテカルロ法による核準位密度の微視的計算
   筑波大学・計算物理学研究センター研究報告 "CP-PACSによる計算物理学2001", pp. 25–42 (筑波大学計算物理学研究センター, 2002年3月)

7. 中田 仁
   Shell Model Monte Carlo法による原子核準位密度の微視的計算
   核データニュース No. 72, pp. 4–11 (日本原子力研究所 核データセンター, 2002年6月)

8. 佐藤 真樹, 中田 仁
   平均場計算における Gauss 型有効相互作用の再考
   日本物理学会講演概要集 第57巻第2号第1分冊, p. 35 (日本物理学会, 2002年)

9. Z. Gan, 藤　暢輔, 小川　建吾, 大島　真澄, 宇都野　穣, 長　明彦, 初川　雄一, 静間　俊行, 早川　岳人, 石井　哲朗, 関　暁之, 木村　敏, 中田　仁, Z. Liu, Y. H. Zhang, 草刈　英榮, 菅原　昌彦
DIC による ^{136}Ba のアイソマー
日本物理学会講演概要集 第57巻第2号第1分冊, p. 50（日本物理学会, 2002年）

10. T. Motoba, K. Itonaga, K. Ogawa, P. Bydzovsky and M. Sotona
Photoproduction of p−shell and sd−shell hypernuclei
日本物理学会講演概要集 第57巻第2号第1分冊, p. 62（日本物理学会, 2002年）

11. 中田　仁
原子核の平均場と殻模型 — 現状と展望 —
原子核研究 第47巻第5号, pp. 65–123（2003年2月）

12. 佐藤　真樹, 中田　仁
平均場理論における有限レンジ相互作用の再考
原子核研究 第47巻第5号, pp. 215–219（2003年2月）

13. 佐藤　真樹, 中田　仁
波動関数の漸近形を考慮した ^{23}O の構造の研究
日本物理学会講演概要集 第58巻第1号第1分冊, p. 45（日本物理学会, 2003年）

14. 石井　哲朗, 侯　龍, 浅井　雅人, 堀　順一, 小川　建吾, 中田　仁
高速中性子により生成した ^{68}Cu の 2^+ 準位の寿命測定
日本物理学会講演概要集 第58巻第1号第1分冊, p. 58（日本物理学会, 2003年）

15. 中田　仁
殻模型モンテカルロ法による核準位密度の微視的計算
筑波大学・計算物理学研究センター研究報告 “CP-PACS による計算物理学2002”, pp. 51–63（筑波大学計算物理学研究センター, 2003年6月）

16. 中田　仁
M3Y 型有効相互作用による核物質及び有限核の性質の研究
日本物理学会講演概要集 第58巻第2号第1分冊, p. 33（日本物理学会, 2003年）

17. 佐藤　真樹, 中田　仁
酸素周辺核における波動関数の漸近形の重要性
日本物理学会講演概要集 第58巻第2号第1分冊, p. 34（日本物理学会, 2003年）

PHYSICAL REVIEW C 68, 014316 (2003)

Hartree-Fock approach to nuclear matter and finite nuclei with M3Y-type nucleon-nucleon interactions

H. Nakada*
Department of Physics, Faculty of Science, Chiba University, Yayoi-cho 1-33, Inage, Chiba 263-8522, Japan
(Received 7 April 2003; published 30 July 2003)

By introducing a density-dependent contact term, M3Y-type interactions applicable to the Hartree-Fock calculations are developed. In order to view basic characters of the interactions, we carry out calculations on the uniform nuclear matter as well as on several doubly magic nuclei. It is shown that a parameter set called M3Y-P2 describes various properties similarly well to the Skyrme SLy5 and/or the Gogny D1S interactions. A remarkable difference from the SLy5 and D1S interactions is found in the spin-isospin properties in the nuclear matter, to which the one-pion-exchange potential gives a significant contribution. Affecting the single-particle energies, this difference may play a certain role in the new magic numbers in unstable nuclei.

DOI: 10.1103/PhysRevC.68.014316 PACS number(s): 21.30.Fe, 21.60.Jz, 21.65.+f, 21.10.Dr

I. INTRODUCTION

Various models for nuclear structure have been developed in order to study low energy phenomena of the atomic nuclei. Whereas straightforward application of the bare *NN* interaction is yet limited only to light nuclei [1], the nuclear structure seems to be well described by relatively simple effective interactions at low energies. Although the effective interactions may depend on the models, there should be basic characters in the effective interactions for the low energy phenomena, irrespective of the model. On the other hand, since the invention of the secondary beam technology, experimental data on the unstable nuclei have disclosed new aspects of the nuclear structure. A remarkable example is the dependence of magic numbers on the neutron excess [2]. In regard to the new magic numbers discovered near the neutron drip line, a question has been raised on a character of the effective interactions relating to the spin-isospin flip mode [3].

Mean-field theories have successfully been applied to the nuclear structure problems, in particular for stable nuclei. They are also useful to investigate basic characters of the effective interactions. However, not many effective interactions have been explored for the nuclear mean-field calculations so far. The Skyrme interaction [4] has been popular in the Hartree-Fock (HF) calculations, since the zero-range form is easy to handle. Among a limited number of finite-range interactions, the Gogny interaction [5] is widely applied to the mean-field calculations, in which the Gaussian form is assumed for the central force. The parameter sets, both of the Skyrme and Gogny interactions, have been adjusted mainly to the data on the nuclei around the β stability. It is not obvious whether the available parameter sets of these interactions account for the new magic numbers properly.

In order to exploit effective interactions applicable also to unstable nuclei, guide from microscopic theories will be important. Brueckner's G matrix has been a significant clue to studies in this course. Although microscopic approaches using the G matrix have not yet been successful in reproducing the saturation properties, notable progress has been made recently. In the shell model approaches, microscopic effective interactions have been shown to reproduce observed levels remarkably well [6]. It should be noted, however, that the shell model interactions are usually specific to mass regions, and their global characters have not been discussed in detail, despite several exceptions [7]. The so-called Michigan three-range Yukawa (M3Y) interaction [8] has been derived from the bare *NN* interaction, by fitting the Yukawa functions to the G-matrix. Represented by the sum of the Yukawa functions, the M3Y type interactions will be tractable in various models. It has been shown that the M3Y interaction gives matrix elements similar to reliable shell model interactions [9]. Moreover, with a certain modification, M3Y-type interactions have successfully been applied to nuclear reactions [10]. By using a recently developed algorithm [11], a class of the M3Y-type interactions can be applied also to the mean-field calculations. Under such circumstances, it will be of interest to explore M3Y-type interactions and to investigate their characters in the mean-field framework. In this paper, we shall develop M3Y-type interactions and investigate their characters via the HF calculations.

II. MODIFICATION OF M3Y INTERACTION

Nuclear effective Hamiltonian consists of the kinetic energy and the effective interaction,

$$H=K+V; \quad K=\sum_i \frac{\mathbf{p}_i^2}{2M}, \quad V=\sum_{i<j} v_{ij}. \tag{1}$$

Here i and j are the indices of individual nucleons. It will be natural to assume the effective interaction v_{ij} to be translationally invariant, except for the density dependence mentioned below. We consider the effective interaction having the following form:

$$v_{12}=v_{12}^{(C)}+v_{12}^{(LS)}+v_{12}^{(TN)}+v_{12}^{(DD)},$$

*Email address: nakada@faculty.chiba-u.jp

$$v_{12}^{(C)}=\sum_n (t_n^{(SE)}P_{SE}+t_n^{(TE)}P_{TE}+t_n^{(SO)}P_{SO} + t_n^{(TO)}P_{TO})f_n^{(C)}(r_{12}),$$

$$v_{12}^{(LS)}=\sum_n (t_n^{(LSE)}P_{TE}+t_n^{(LSO)}P_{TO})f_n^{(LS)}(r_{12})\mathbf{L}_{12}\cdot(\mathbf{s}_1+\mathbf{s}_2),$$

$$v_{12}^{(TN)}=\sum_n (t_n^{(TNE)}P_{TE}+t_n^{(TNO)}P_{TO})f_n^{(TN)}(r_{12})r_{12}^2S_{12},$$

$$v_{12}^{(DD)}=t^{(DD)}(1+x^{(DD)}P_\sigma)[\rho(\mathbf{r}_1)]^\alpha\delta(\mathbf{r}_{12}). \quad (2)$$

The relative coordinate is denoted by $\mathbf{r}_{12}=\mathbf{r}_1-\mathbf{r}_2$ and $r_{12}=|\mathbf{r}_{12}|$. Correspondingly, the relative momentum is defined by $\mathbf{p}_{12}=(\mathbf{p}_1-\mathbf{p}_2)/2$. $\mathbf{L}_{12}$ is the relative orbital angular momentum,

$$\mathbf{L}_{12}=\mathbf{r}_{12}\times\mathbf{p}_{12}, \quad (3)$$

$\mathbf{s}_1$, $\mathbf{s}_2$ are the nucleon spin operators, and S_{12} is the tensor operator,

$$S_{12}=4[3(\mathbf{s}_1\cdot\hat{\mathbf{r}}_{12})(\mathbf{s}_2\cdot\hat{\mathbf{r}}_{12})-\mathbf{s}_1\cdot\mathbf{s}_2]. \quad (4)$$

$f_n(r_{12})$ represents an appropriate function of r_{12}, the subscript n corresponds to the parameter attached to the function (e.g., the range of the interaction), and t_n is the coefficient. Examples of $f_n(r_{12})$ are the delta, the Gauss, and the Yukawa functions. P_σ (P_τ) denotes the spin (isospin) exchange operator, while P_{SE}, P_{TE}, P_{SO}, and P_{TO} are the projection operators on the singlet-even (SE), triplet-even (TE), singlet-odd (SO), and triplet-odd (TO) two-particle states, respectively, which are defined by

$$P_{SE}=\frac{1-P_\sigma}{2}\frac{1+P_\tau}{2},\quad P_{TE}=\frac{1+P_\sigma}{2}\frac{1-P_\tau}{2},$$

$$P_{SO}=\frac{1-P_\sigma}{2}\frac{1-P_\tau}{2},\quad P_{TO}=\frac{1+P_\sigma}{2}\frac{1+P_\tau}{2}. \quad (5)$$

The nucleon density is denoted by $\rho(\mathbf{r})$. The original M3Y interaction is represented in the form of Eq. (2), with $f_n(r_{12})=e^{-\mu_n r_{12}}/\mu_n r_{12}$ and $v_{12}^{(DD)}=0$. As discussed in Ref. [11], the Skyrme and the Gogny interactions are obtained by setting $f_n(r_{12})$ appropriately, except for some parameter sets of the Skyrme interaction in which certain terms are expressed only in the density-functional form.

The saturation of density and energy is a basic property of nuclei. In developing effective interactions adaptable for many nuclei, it is required to reproduce the saturation property. However, the nonrelativistic G matrix fails to reproduce the saturation at the right density and energy. Therefore, it will not be appropriate to use the G matrix for HF calculations without any modification, although several HF approaches using interactions derived from the G matrix were tried in earlier studies [12]. The M3Y interaction was obtained so that the G matrix at a certain density could be reproduced by a sum of the Yukawa functions. The M3Y interaction gives no saturation point within the HF theory, unless density dependence is taken into account explicitly. Khoa *et al.* applied the M3Y interaction to nuclear reactions in the folding model, by making the coupling constants dependent on densities [10]. The exchange terms are treated approximately. However the exchange terms may contribute significantly to the nuclear structure. We here keep the coupling constants in $v_{12}^{(C)}$ independent of density, while introducing a density-dependent contact interaction [$v_{12}^{(DD)}$ in Eq. (2)], as in the Skyrme and the Gogny interactions. We can then treat the exchange (i.e., the Fock) terms exactly with the currently available computers. It should be mentioned that there has been an interesting attempt to approximate the exchange terms of the interaction in the density-matrix expansion [13], although the accuracy of the density-matrix expansion should be checked carefully.

We start from the Paris-potential version of the M3Y interaction [14]. This original parameter set with no density dependence is hereafter called "M3Y-P0." We shall modify this interaction so as to reproduce the saturation properties. In the isotropic uniform nuclear matter, matrix elements of $v_{12}^{(LS)}$ and $v_{12}^{(TN)}$ between the HF states vanish. Therefore $v_{12}^{(C)}+v_{12}^{(DD)}$ determines the bulk properties such as the saturation. The range parameters for the Yukawa functions $f_n^{(C)}(r_{12})=e^{-\mu_n r_{12}}/\mu_n r_{12}$ in $v_{12}^{(C)}$ are $\mu_1^{-1}=0.25$, $\mu_2^{-1}=0.4$, and $\mu_3^{-1}=1.414$ fm in the M3Y interaction, which correspond to the Compton wavelengths of mesons with masses of about 790, 490, and 140 MeV, respectively. We do not change these parameters. For the longest-range part ($n=3$), the coupling constants $t_3^{(SE)}$, $t_3^{(TE)}$, $t_3^{(SO)}$, and $t_3^{(TO)}$ are fixed to be those of the one-pion-exchange potential (OPEP), as in M3Y-P0. The interaction $v_{12}^{(DD)}$ in Eq. (2) acts only on the SE and TE channels,

$$v_{12}^{(DD)}=t^{(DD)}(1-x^{(DD)})\delta(\mathbf{r}_{12})P_{SE} + t^{(DD)}(1+x^{(DD)})\delta(\mathbf{r}_{12})P_{TE}. \quad (6)$$

Microscopic investigations have shown that the density dependence of the TE part is primarily responsible for the saturation [15], as a higher-order effect of the tensor force. While the interaction in the SE channel is attractive at low densities, it also has certain density dependence originating in the strong short-range repulsion. Thus, a possible way of modifying the M3Y interaction may be to replace a fraction of the repulsion in the SE and TE channels by $v_{12}^{(DD)}$.

In addition to the saturation properties that are relevant to the central force, the spin-orbit (LS) splitting is significant in describing the shell structure of nuclei. While true origin of the LS splitting is not yet obvious [16], LS splittings obtained from HF calculations with the G matrix interaction are too small, in comparison with the observed ones. From the HF calculations for finite nuclei, we find that $v_{12}^{(LS)}$ should be about twice as strong as that of M3Y-P0 to reproduce the observed LS splittings. The tensor force influences the ordering of the single-particle (s.p.) orbits. To reproduce the observed ordering, $v_{12}^{(TN)}$ should be smaller than that of

M3Y-P0. We here introduce an overall enhancement factor to $v_{12}^{(\mathrm{LS})}$ and an overall reduction factor to $v_{12}^{(\mathrm{TN})}$, as will be shown in Sec. V.

In this paper we shall use two parameter sets for modified M3Y interaction, "M3Y-P1" and "M3Y-P2," in order to show sensitivity to the parameters for some results. In M3Y-P1, we replace the shortest-range ($n=1$) repulsive part of $v_{12}^{(\mathrm{C})}$ by $v_{12}^{(\mathrm{DD})}$ in a simple manner. We reduce both $t_1^{(\mathrm{SE})}$ and $t_1^{(\mathrm{TE})}$ by a single factor, keeping the SE/TE ratio in $v_{12}^{(\mathrm{DD})}$ equal to $t_1^{(\mathrm{SE})}/t_1^{(\mathrm{TE})}$ in M3Y-P0, by imposing

$$x^{(\mathrm{DD})}=\frac{t_1^{(\mathrm{TE})}-t_1^{(\mathrm{SE})}}{t_1^{(\mathrm{TE})}+t_1^{(\mathrm{SE})}}. \tag{7}$$

The reduction factor and $t^{(\mathrm{DD})}$ are determined so as for the saturation density and energy in the nuclear matter to be typical values, as presented in the following section. Characters of M3Y-P1 will be investigated in the nuclear matter. Although this modification is too simple to reproduce properties of finite nuclei, the M3Y-P1 set will be useful to clarify what characters arise from the original M3Y interaction, relatively insensitive to the phenomenological modification. In the M3Y-P2 set, all t_n parameters belonging to the $n=1$ and 2 channels in $v_{12}^{(\mathrm{C})}$ are shifted from those of M3Y-P0. Although we have three ranges in $v_{12}^{(\mathrm{C})}$, the number of adjustable parameters is no greater than in the Gogny interaction, since we fix the OPEP part. We fit those parameters, together with the enhancement factor for $v_{12}^{(\mathrm{LS})}$ and the reduction factor for $v_{12}^{(\mathrm{TN})}$, to the binding energies of several doubly magic nuclei. The resultant values of the parameters will be shown later.

III. PROPERTIES OF NUCLEAR MATTER AT AND AROUND SATURATION POINT

Basic characters of nuclear effective interactions can be discussed via properties of the infinite nuclear matter; in particular, properties at and around the saturation point. In this section we investigate characters of the M3Y-type interactions via the nuclear matter properties within the HF theory. In comparison, we also discuss those of the Skyrme and the Gogny interactions. We use the D1S parameter set [17] for the Gogny interaction. In most of the Skyrme HF approaches, the LS currents arising from the momentum dependence of the central force are ignored, and the parameters are adjusted without their contribution. Although this treatment occasionally improves some characters of the interactions, in this paper we would focus on characters of the two-body interactions, rather than those of density functionals. For this reason we adopt the SLy5 set [18], which is devised for calculations including the LS currents.

In the HF theory of the nuclear matter, the s.p. wave functions can be taken to be the plane wave,

$$\varphi_{\mathbf{k}\sigma\tau}(\mathbf{r})=\frac{1}{\sqrt{\Omega}}e^{i\mathbf{k}\cdot\mathbf{r}}\chi_\sigma\chi_\tau. \tag{8}$$

Here χ_σ (χ_τ) denotes the spin (isospin) wave function, and Ω indicates the volume of the system, for which we will take the $\Omega\to\infty$ limit afterward. The s.p. energy for this state is defined as

$$\epsilon(\mathbf{k}\sigma\tau)=\frac{\mathbf{k}^2}{2M}+\frac{\Omega}{(2\pi)^3}\sum_{\sigma_2\tau_2}\int_{k_2\le k_{\mathrm{F}\tau_2\sigma_2}}d^3k_2 \times\langle\mathbf{k}\sigma\tau,\mathbf{k}_2\sigma_2\tau_2|v_{12}|\mathbf{k}\sigma\tau,\mathbf{k}_2\sigma_2\tau_2\rangle. \tag{9}$$

Energy of the nuclear matter is expressed by a function of densities depending on the spin and the isospin, $\rho_{\tau\sigma}$ ($\tau=p,n$; $\sigma=\uparrow,\downarrow$). The density variables can be converted to the total density $\rho=\Sigma_{\sigma\tau}\rho_{\tau\sigma}$, and the spin- and isospin-asymmetry parameters

$$\eta_s=\frac{\sum_{\sigma\tau}\sigma\rho_{\tau\sigma}}{\rho}=\frac{\rho_{p\uparrow}-\rho_{p\downarrow}+\rho_{n\uparrow}-\rho_{n\downarrow}}{\rho},$$

$$\eta_t=\frac{\sum_{\sigma\tau}\tau\rho_{\tau\sigma}}{\rho}=\frac{\rho_{p\uparrow}+\rho_{p\downarrow}-\rho_{n\uparrow}-\rho_{n\downarrow}}{\rho},$$

$$\eta_{st}=\frac{\sum_{\sigma\tau}\sigma\tau\rho_{\tau\sigma}}{\rho}=\frac{\rho_{p\uparrow}-\rho_{p\downarrow}-\rho_{n\uparrow}+\rho_{n\downarrow}}{\rho}, \tag{10}$$

where σ (τ) in the summation takes ±1, corresponding to $\sigma=\uparrow,\downarrow$ ($\tau=p,n$). By assuming that the s.p. states are occupied up to the Fermi momentum, the density is related to the Fermi momentum for each spin and isospin,

$$\rho_{\tau\sigma}=\frac{1}{6\pi^2}k_{\mathrm{F}\tau\sigma}^3. \tag{11}$$

The total energy of nuclear matter is given by

$$E=\frac{\Omega}{(2\pi)^3}\sum_{\sigma_1\tau_1}\int_{k_1\le k_{\mathrm{F}\tau_1\sigma_1}}d^3k_1\frac{\mathbf{k}_1^2}{2M} +\frac{\Omega^2}{2(2\pi)^6}\sum_{\sigma_1\sigma_2\tau_1\tau_2}\int_{k_1\le k_{\mathrm{F}\tau_1\sigma_1}}d^3k_1\int_{k_2\le k_{\mathrm{F}\tau_2\sigma_2}}d^3k_2 \times\langle\mathbf{k}_1\sigma_1\tau_1,\mathbf{k}_2\sigma_2\tau_2|v_{12}|\mathbf{k}_1\sigma_1\tau_1,\mathbf{k}_2\sigma_2\tau_2\rangle. \tag{12}$$

As already pointed out, only $v_{12}^{(\mathrm{C})}+v_{12}^{(\mathrm{DD})}$ contributes to the energy of the isotropic nuclear matter. In Appendix A, several formulas on the HF energy of the nuclear matter are derived for interactions expressed in the form of Eq. (2), with general and typical $f_n^{(\mathrm{C})}(r_{12})$. The nuclear matter energies are calculated for the Skyrme and the Gogny interactions, as well as for the M3Y-type interactions, by using these formulas.

In the spin-saturated symmetric nuclear matter, we have $\eta_s=\eta_t=\eta_{st}=0$, which indicates $k_{\mathrm{F}p\uparrow}=k_{\mathrm{F}p\downarrow}=k_{\mathrm{F}n\uparrow}=k_{\mathrm{F}n\downarrow}$ and $\rho_{p\uparrow}=\rho_{p\downarrow}=\rho_{n\uparrow}=\rho_{n\downarrow}=\rho/4$. In this case we denote the

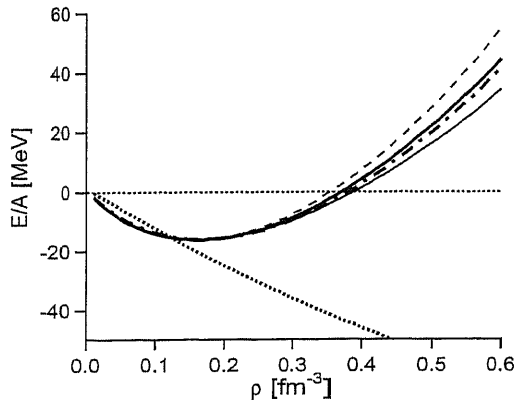

FIG. 1. Energies per nucleon $\mathcal{E}=E/A$ in the symmetric nuclear matter for several effective interactions. The thick dotted, dot-dashed, and solid lines represent the results with the M3Y-P0, M3Y-P1, and M3Y-P2 interactions, respectively, while the thin dashed and solid lines represent those with the SLy5 and D1S interactions.

Fermi momentum simply by k_F. The lowest energy for a given ρ normally occurs along this line. The saturation point is obtained by minimizing the energy per nucleon $\mathcal{E}=E/A$,

$$\left.\frac{\partial \mathcal{E}}{\partial \rho}\right|_{\text{sat.}}=0, \tag{13}$$

which yields the saturation density ρ_0 (equivalently, k_{F0}) and energy $\mathcal{E}_0$. Figure 1 illustrates $\mathcal{E}$ as a function of ρ for the symmetric nuclear matter with the M3Y type as well as with the SLy5 and D1S effective interactions. We set $M=(M_p+M_n)/2$, where M_p (M_n) is the measured mass of a proton (a neutron). The parameters for $v_{12}^{(C)}$ and $v_{12}^{(DD)}$ of the M3Y-type interactions are listed in Table I. As mentioned above, the M3Y-P0 interaction gives no saturation point. We do

TABLE I. Parameters of central forces (including $v_{12}^{(DD)}$) in the original and modified M3Y interactions. See text for the μ_n parameters.

Parameters		M3Y-P0	M3Y-P1	M3Y-P2
$t_1^{(SE)}$	(MeV)	11466	8599.5	8027
$t_1^{(TE)}$	(MeV)	13967	10475.25	6080
$t_1^{(SO)}$	(MeV)	−1418	−1418	−11900
$t_1^{(TO)}$	(MeV)	11345	11345	3800
$t_2^{(SE)}$	(MeV)	−3556	−3556	−2880
$t_2^{(TE)}$	(MeV)	−4594	−4594	−4266
$t_2^{(SO)}$	(MeV)	950	950	2730
$t_2^{(TO)}$	(MeV)	−1900	−1900	−780
$t_3^{(SE)}$	(MeV)	−10.463	−10.463	−10.463
$t_3^{(TE)}$	(MeV)	−10.463	−10.463	−10.463
$t_3^{(SO)}$	(MeV)	31.389	31.389	31.389
$t_3^{(TO)}$	(MeV)	3.488	3.488	3.488
α			1/3	1/3
$t^{(DD)}$	(MeV fm)	0	1212	1320
$x^{(DD)}$			0.09834	0.72576

TABLE II. Nuclear matter properties at the saturation point.

		M3Y-P1	M3Y-P2	SLy5	D1S
k_{F0}	(fm)	1.358	1.340	1.334	1.342
$\mathcal{E}_0$	(MeV)	−15.99	−16.14	−15.98	−16.01
$\mathcal{K}$	(MeV)	225.7	220.4	229.9	202.9
M_0^*/M		0.641	0.652	0.697	0.697
a_t	(MeV)	30.35	30.61	32.03	31.12
a_s	(MeV)	20.81	21.19	37.47	26.18
a_{st}	(MeV)	37.63	38.19	15.15	29.13

have saturation points in M3Y-P1 and M3Y-P2 owing to $v_{12}^{(DD)}$. Differences among the saturating forces, i.e., SLy5, D1S, M3Y-P1, and M3Y-P2, are small at $\rho\lesssim\rho_0$. At relatively high density ($\rho\gtrsim 0.3$ fm^{-3}), the M3Y-P1 and the M3Y-P2 interactions have lower $\mathcal{E}$ than SLy5 and higher than D1S. The values of k_{F0} and $\mathcal{E}_0$ are tabulated in Table II. The M3Y-P1 set has been determined so as to give $k_{F0}\simeq 1.36$ fm and $\mathcal{E}_0\simeq 16$ MeV.

In Figs. 2 and 3, contribution to $\mathcal{E}$ from each of the SE, TE, SO, and TO channels in $v_{12}^{(C)}+v_{12}^{(DD)}$ is shown as a function of k_F. Sum of all these channels and the kinetic energy $\langle K\rangle/A=(3/5)(k_F^2/2M)$ is equal to $\mathcal{E}$ in Fig. 1. As seen in Fig. 2, the TE channel takes a minimum at $k_F=1.3$–1.5 fm except for M3Y-P0 and M3Y-P1, primarily responsible for the

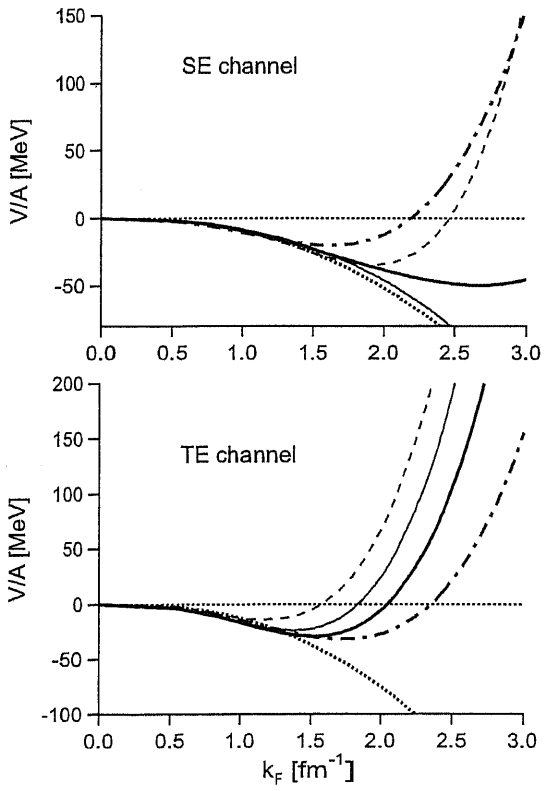

FIG. 2. Contribution of the SE and TE channels to $\mathcal{E}$. See Fig. 1 for conventions.

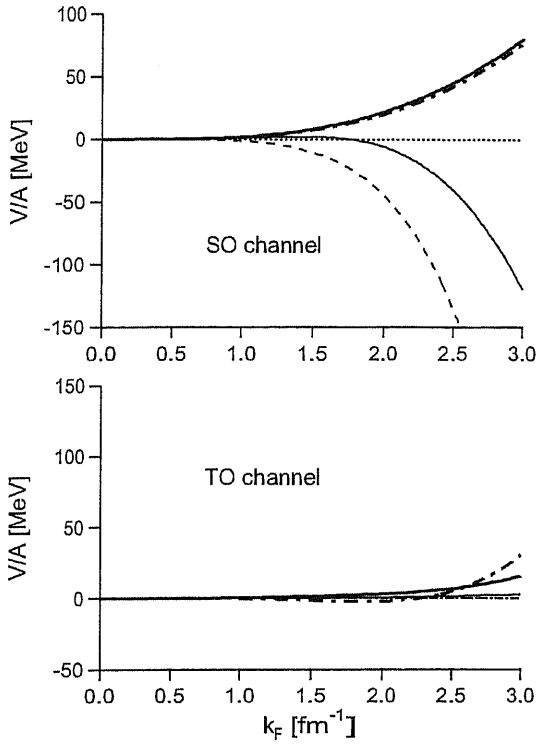

FIG. 3. Contribution of the SO and TO channels to $\mathcal{E}$. In both channels, the results of M3Y-P0 are equal to those of M3Y-P1, which are presented by the dot-dashed line. See Fig. 1 for the other conventions.

saturation at $k_{F0} \approx 1.3$ fm. In the D1S interaction, the energy out of the SE channel monotonically goes down. This is not compatible with the presence of the strong short-range repulsion in the NN force, and causes an unphysical property in the neutron matter, as will be shown in Sec. IV. Both the SO and TO channels do not contribute to $\mathcal{E}$ significantly for $\rho \lesssim \rho_0$ (i.e., $k_F \lesssim k_{F0}$). While the SO channel becomes attractive and the TO channel stays small in the SLy5 and the D1S interactions, both channels are repulsive in the M3Y-type interactions at $\rho > \rho_0$, including M3Y-P0. A certain part of this character of the M3Y-type interactions comes from the OPEP part.

The curvature at the saturation point with respect to ρ is proportional to the incompressibility,

$$\mathcal{K} = k_F^2 \frac{\partial^2 \mathcal{E}}{\partial k_F^2}\bigg|_{\text{sat.}} = 9\rho^2 \frac{\partial^2 \mathcal{E}}{\partial \rho^2}\bigg|_{\text{sat.}} . \tag{14}$$

The effective mass (k mass) at the saturation point M_0^* is defined by

$$\frac{\partial \epsilon(\mathbf{k}\sigma\tau)}{\partial k}\bigg|_{\text{sat.}} = \frac{k_{F0}}{M_0^*} . \tag{15}$$

The volume asymmetry energy corresponds to the curvature of $\mathcal{E}$ with respect to η_t:

$$a_t = \frac{1}{2} \frac{\partial^2 \mathcal{E}}{\partial \eta_t^2}\bigg|_{\text{sat.}} . \tag{16}$$

Analogously, the following coefficients are defined from the curvatures of $\mathcal{E}$ with respect to η_s and η_{st},

$$a_s = \frac{1}{2} \frac{\partial^2 \mathcal{E}}{\partial \eta_s^2}\bigg|_{\text{sat.}} , \quad a_{st} = \frac{1}{2} \frac{\partial^2 \mathcal{E}}{\partial \eta_{st}^2}\bigg|_{\text{sat.}} . \tag{17}$$

The coefficients a_s, a_t, and a_{st} are relevant to the spin and isospin responses in finite nuclei. In Table II we also compare $\mathcal{K}$, M_0^*, a_t, a_s, and a_{st} among the effective interactions.

The incompressibility $\mathcal{K}$ is sensitive to α in $v_{12}^{(\text{DD})}$. The experimental value of $\mathcal{K}$ has been extracted from the excitation energies of the giant monopole resonances. Despite a certain model dependence, most non-relativistic models are consistent with the experiments if $\mathcal{K} \approx 210$ MeV. For finite-range interactions, i.e., the Gogny and the M3Y-type interactions, $\alpha \approx 1/3$ seems to give reasonable values of $\mathcal{K}$, while in the Skyrme interactions $\alpha \approx 1/6$ looks favorable, because of the momentum-dependent terms in $v_{12}^{(\text{C})}$. The k mass is empirically known to be $M_0^* \approx (0.6\text{–}0.7)M$ [19]. The M3Y-type interactions tend to yield slightly smaller M_0^* than the SLy5 and the D1S interactions. The volume asymmetry energy a_t is important in reproducing global trend of the binding energies for the $Z \neq N$ nuclei. From empirical viewpoints $a_t \approx 30$ MeV seems appropriate, as is fulfilled in the M3Y-type interactions under consideration.

The a_s and a_{st} coefficients are relevant to the spin degrees of freedom. The kinetic energy has a certain contribution to a_s and a_{st}, as well as to a_t, which amounts to about 12 MeV at $\rho \approx \rho_0$ equally for a_t, a_s, and a_{st}. The interaction $v_{12}^{(\text{C})} + v_{12}^{(\text{DD})}$ gives rise to the rest of these coefficients. Both the M3Y-type interactions have similar tendency with respect to these coefficients. It is remarkable that a_{st} is substantially larger in the M3Y-type interactions than a_s. As is suggested by close a_s and a_{st} values between M3Y-P1 and M3Y-P2, the original M3Y interaction already carries this feature. In particular, the OPEP part included in the M3Y-type interactions plays a significant role, increasing a_{st} by about 11 MeV. On the other hand, a_s and a_{st} are comparable in the Gogny D1S interaction, and we have even $a_s > a_{st}$ in the Skyrme SLy5 interaction. In the SLy5 case, a_{st} is close to the value due only to the kinetic energy.

Global characters of the spin and isospin responses are customarily discussed in terms of the Landau parameters. Formulas on the Landau parameters at the zero temperature are given in Appendix B. We compute the parameters of Eq. (B22). The results are shown in Table III. It is remarked that the M3Y-P1 and M3Y-P2 interactions give similar results. The g_ℓ and the g'_ℓ parameters are closely related to the a_s and the a_{st} coefficients, respectively. It has been known that g_0 is small, while g'_0 should be relatively large [20]. Al-

TABLE III. Landau parameters at the saturation point.

	M3Y-P1	M3Y-P2	SLy5	D1S
f_0	−0.370	−0.357	−0.276	−0.369
f_1	−1.078	−1.044	−0.909	−0.909
f_2	−0.381	−0.436	0.0	−0.558
f_3	−0.191	−0.210	0.0	−0.157
f'_0	0.525	0.607	0.815	0.743
f'_1	0.537	0.635	−0.387	0.470
f'_2	0.250	0.245	0.0	0.342
f'_3	0.101	0.096	0.0	0.100
g_0	0.046	0.113	1.123	0.466
g_1	0.372	0.273	0.253	−0.184
g_2	0.199	0.162	0.0	0.245
g_3	0.088	0.078	0.0	0.091
g'_0	0.891	1.006	−0.141	0.631
g'_1	0.230	0.202	1.043	0.610
g'_2	0.073	0.040	0.0	−0.038
g'_3	0.008	−0.002	0.0	−0.036

though it is not easy to extract precise values of the Landau parameters from experimental data because they could depend on the interaction forms, qualitative trend will not depend on effective interactions. The M3Y-type interactions seem to have reasonable characters on the spin and isospin responses, while SLy5 and D1S do not, although the spin and isospin natures of the Skyrme interactions seem to be improved if the LS currents are ignored [21]. It is likely that the difference in these coefficients may significantly influence predictions of the spin and isospin responses of finite nuclei.

IV. PROPERTIES OF ASYMMETRIC NUCLEAR MATTER AND NEUTRON MATTER

We turn to the asymmetric nuclear matter. In Fig. 4, energies per nucleon $\mathcal{E}$ are depicted as a functions of ρ for the spin-saturated (i.e., $\eta_s=\eta_{st}=0$) nuclear matter with $\eta_t=-0.2$ and -0.5. The results from the M3Y-type interactions are compared with those of the Skyrme and the Gogny interactions. Energies of the spin-saturated neutron matter (i.e., $\eta_t=-1$) are presented in Fig. 5. Results from a microscopic calculation in Ref. [22] are also shown as a reference. Although the dependence on the interactions is not strong at low densities even for the neutron matter, it becomes stronger at $\rho>0.2$ fm as $|\eta_t|$ increases. In the D1S result for the neutron matter, $\mathcal{E}$ has a maximum at $\rho\approx 0.6$ fm and goes to $-\infty$ as $\rho\to\infty$. This unphysical behavior arises from $x^{(\mathrm{DD})}=1$ in the D1S set, which implies no density dependence in the SE channel [see Eq. (6)]. This could also give rise to a problem in practical calculations for finite nuclei. With the SLy5 interaction $\mathcal{E}$ goes up rapidly at any η_t, because of the momentum dependence of the interaction. In contrast to them, the M3Y-type interactions give moderate $\mathcal{E}$ for the neutron matter. The microscopic energy of Ref. [22] lies between those of M3Y-P1 and M3Y-P2. It will be possible, if necessary, to adjust the parameters of the M3Y-type interactions to the microscopic results.

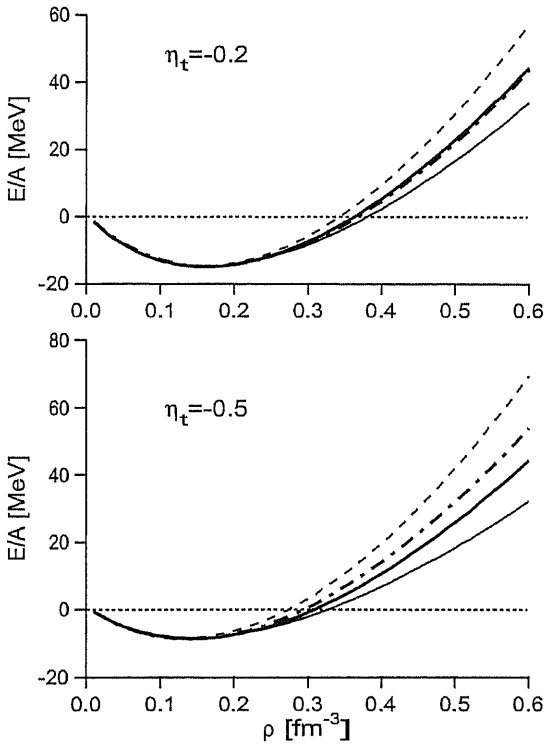

FIG. 4. Energies per nucleon $\mathcal{E}=E/A$ in the asymmetric nuclear matter with $\eta_t=-0.2$ and -0.5 for several effective interactions. See Fig. 1 for conventions.

V. PROPERTIES OF DOUBLY MAGIC NUCLEI

We next discuss properties of doubly magic nuclei in the HF approximation. In the calculations for finite nuclei, we use the algorithm presented in Ref. [11], where the following s.p. bases are employed:

$$\varphi_{\alpha\ell jm}(\mathbf{r})=R_{\alpha\ell j}(r)[Y^{(\ell)}(\hat{\mathbf{r}})\chi_\sigma]^{(j)}_m,$$

$$R_{\alpha\ell j}(r)=\mathcal{N}_{\alpha\ell j}r^{\ell+2p_\alpha}\exp[-(r/\nu_\alpha)^2]. \quad (18)$$

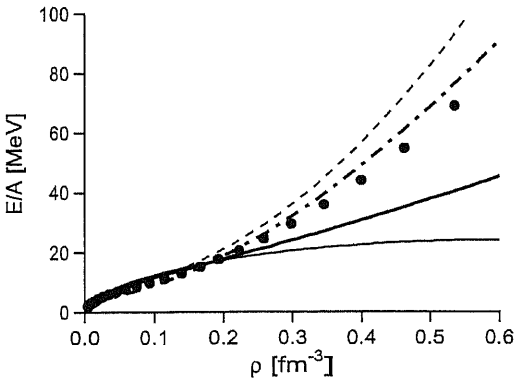

FIG. 5. Energies per nucleon $\mathcal{E}=E/A$ in the neutron matter for several effective interactions. The circles are the results of Ref. [22]. See Fig. 1 for the other conventions.

TABLE IV. Parameters of noncentral forces in the original and modified M3Y interactions. See text for the μ_n parameters.

Parameters		M3Y-P0	M3Y-P2
$t_1^{(\mathrm{LSE})}$	(MeV)	−5101	−9181.8
$t_1^{(\mathrm{LSO})}$	(MeV)	−1897	−3414.6
$t_2^{(\mathrm{LSE})}$	(MeV)	−337	−606.6
$t_2^{(\mathrm{LSO})}$	(MeV)	−632	−1137.6
$t_1^{(\mathrm{TNE})}$	(MeV fm^{-2})	−1096	−131.52
$t_1^{(\mathrm{TNO})}$	(MeV fm^{-2})	244	29.28
$t_2^{(\mathrm{TNE})}$	(MeV fm^{-2})	−30.9	−3.708
$t_2^{(\mathrm{TNO})}$	(MeV fm^{-2})	15.6	1.872

Here $Y^{(\ell)}(\hat{\mathbf{r}})$ expresses the spherical harmonics. We drop the isospin index without confusion. The index α indicates p_α (a non-negative integer) and ν_α, simultaneously. By choosing p_α and ν_α appropriately, these bases span the space equivalent to that of the harmonic-oscillator (HO) bases, and can also form the Kamimura-Gauss (KG) basis set [23]. Without parameters specific to mass number or nuclide such as $\hbar\omega$, a single set of the KG bases is applicable to a wide range of nuclides. In the following calculations we apply the hybrid basis set [11] for the nuclei with $A<50$, in which an HO basis is added to the KG basis-set, while the HO basis set with $N_{\mathrm{osc}}\leq 15$ and $\hbar\omega=41.2A^{-1/3}$ MeV for heavier nuclei.

In finite nuclei the noncentral forces are important as well. In the M3Y interaction, the LS force $v_{12}^{(\mathrm{LS})}$ and the tensor force $v_{12}^{(\mathrm{TN})}$ are taken by setting $f_n^{(\mathrm{LS})}(r_{12})=e^{-\mu_n r_{12}}/\mu_n r_{12}$ and $f_n^{(\mathrm{TN})}(r_{12})=e^{-\mu_n r_{12}}/\mu_n r_{12}$ in Eq. (2). We here fix the range parameters as in $v_{12}^{(\mathrm{C})}$; $\mu_1^{-1}=0.25$ fm, $\mu_2^{-1}=0.4$ fm for $v_{12}^{(\mathrm{LS})}$, and $\mu_1^{-1}=0.4$ fm, $\mu_2^{-1}=0.7$ fm for $v_{12}^{(\mathrm{TN})}$. The coupling constants in the M3Y-P2 set are tabulated in Table IV, together with those in the original M3Y-P0 set. In M3Y-P2, the enhancement factor for $v_{12}^{(\mathrm{LS})}$ is taken to be 1.8 and the reduction factor for $v_{12}^{(\mathrm{TN})}$ to be 0.12. The binding energies and the rms matter radii obtained from the HF calculations with M3Y-P2 are shown in Table V, in comparison with those of the SLy5 and the D1S interactions, as well as with the experimental data. The one-body terms of the center-of-mass (c.m.) energy are removed before iteration. The contribution of the two-body terms is subtracted from the convergent HF wave functions, in the D1S and the M3Y-P2 results. There are also spurious c.m. effects in the matter radii,

$$\begin{aligned}\langle r^2\rangle &= \frac{1}{A}\sum_i \langle(\mathbf{r}_i-\mathbf{R})^2\rangle \\ &= \frac{1}{A}\sum_i \langle r_i^2\rangle - \langle R^2\rangle \\ &= \frac{1}{A}\left[\left(1-\frac{1}{A}\right)\sum_i \langle r_i^2\rangle - \frac{1}{A}\sum_{i\neq j}\langle \mathbf{r}_i\cdot\mathbf{r}_j\rangle\right]. \end{aligned} \quad (19)$$

The first term in the right-hand side is expressed by one-body operators with a correction factor $(1-1/A)$. We need two-body operators for the second term. For the D1S and the M3Y-P2 interactions we fully remove the c.m. contribution according to Eq. (19). For the SLy5 interaction we use only the one-body terms with the correction factor, ignoring the two-body terms in Eq. (19), as in calculating the energies.

Wave functions of the doubly magic nuclei are considered to be well approximated in the spherical HF approaches. It should still be noted that correlations due to the residual interaction could influence their properties. Therefore we do not pursue fine tuning of the parameters. As shown in Table V, the M3Y-P2 set is fixed so as to reproduce the measured binding energies of the doubly magic nuclei, including ^{90}Zr, within about 5 MeV accuracy. The binding energies of these nuclei obtained from the SLy5 and the D1S interactions are in agreement with the experimental data within 3 MeV, slightly better than M3Y-P2. We do not have to take this difference seriously, before evaluating the influence of the residual interactions. In addition to the binding energies, the rms matter radii of these nuclei are reproduced by the M3Y-P2 set similarly well to the other available interactions. In Table VI we present the neutron s.p. energies $\epsilon_n(0p_{3/2})$ and $\epsilon_n(0p_{1/2})$ around ^{16}O. The enhancement factor for $v_{12}^{(\mathrm{LS})}$ in the M3Y-P2 set has been adjusted approximately to the experimental value of this s.p. energy difference. The reduction factor for $v_{12}^{(\mathrm{TN})}$ has been determined so as to reproduce the s.p. energy ordering for ^{208}Pb. Without this reduction factor, the orbits with higher ℓ have too high energies. The resultant s.p. levels in ^{208}Pb with M3Y-P2 are depicted in Fig. 6. The levels obtained from D1S and the experimental s.p. levels are also shown. The overall level spacings are related to M_0^* shown in Table II. In the usual HF calculations the level spacings tend to be larger than the observed ones,

TABLE V. Binding energies and rms matter radii of several doubly magic nuclei. Experimental data are taken from Refs. [24–26].

			Expt.	M3Y-P2	SLy5	D1S
^{16}O	$-E$	(MeV)	127.6	127.1	128.6	129.5
	$\sqrt{\langle r^2\rangle}$	(fm)	2.61	2.60	2.59	2.59
^{40}Ca	$-E$	(MeV)	342.1	338.7	344.3	344.5
	$\sqrt{\langle r^2\rangle}$	(fm)	3.47	3.37	3.29	3.36
^{48}Ca	$-E$	(MeV)	416.0	411.8	416.0	416.8
	$\sqrt{\langle r^2\rangle}$	(fm)	3.57	3.52	3.44	3.50
^{90}Zr	$-E$	(MeV)	783.9	778.7	782.4	784.5
	$\sqrt{\langle r^2\rangle}$	(fm)	4.32	4.25	4.22	4.23
^{132}Sn	$-E$	(MeV)	1102.9	1098.1	1103.5	1102.9
	$\sqrt{\langle r^2\rangle}$	(fm)		4.79	4.77	4.76
^{208}Pb	$-E$	(MeV)	1636.4	1635.8	1635.2	1638.1
	$\sqrt{\langle r^2\rangle}$	(fm)	5.49	5.53	5.52	5.51

TABLE VI. LS splitting around ^{16}O. Experimental data are extracted from Refs. [24,27].

		Expt.	M3Y-P2	SLy5	D1S
$\epsilon_n(0p_{3/2})$	(MeV)	−21.8	−22.6	−20.6	−22.3
$\epsilon_n(0p_{1/2})$	(MeV)	−15.7	−16.2	−14.4	−15.9

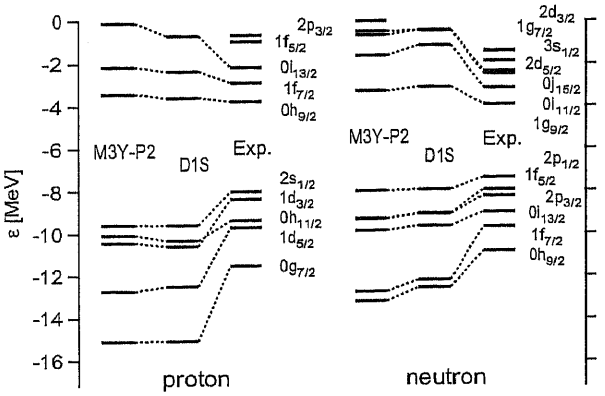

FIG. 6. Single-particle energies for ^{208}Pb. Experimental values are extracted from Refs. [24,27].

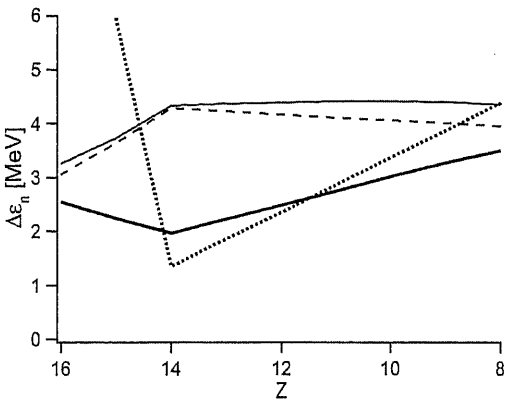

FIG. 7. $\Delta\epsilon_n$ for the $N=16$ isotones. The thick solid, dotted, thin solid, and dashed lines correspond to the results with the M3Y-P2, USD, D1S, and SLy5 interactions, respectively.

and it is not (and should not be) remedied until the correlations due to the residual interaction (or the ω mass) are taken into account [19]. This is also true in the present case. We find that M3Y-P2 yields as plausible s.p. levels as D1S does. We thus confirm that the M3Y-P2 interaction well describes the global nature of stable nuclei.

VI. SINGLE PARTICLE LEVELS IN $N=16$ ISOTONES

In the preceding section we have shown that the M3Y-P2 interaction reproduces the properties of the doubly magic nuclei to a similar accuracy to the SLy5 and the D1S interactions. At a glance, the spin-isospin characters in the nuclear matter, which have been discussed in Sec. III via a_{st} and g'_ℓ, do not seem to influence the nuclear properties around the ground states. However, the spin and isospin characters influence s.p. energies of finite nuclei. Thereby they may affect even the ground state properties. In this section we illustrate this point by the neutron orbits in the $N=16$ isotones, following the arguments in Ref. [3], although precise studies in this line are beyond the scope of this paper.

As was suggested in Ref. [3], the proton-number (Z) dependence of the neutron s.p. energy $\epsilon_n(0d_{3/2})$ relative to $\epsilon_n(1s_{1/2})$ can sizably be affected by effective interactions. Figure 7 depicts $\Delta\epsilon_n=\epsilon_n(0d_{3/2})-\epsilon_n(1s_{1/2})$ obtained from the spherical HF calculations in the $N=16$ isotones. Though it is not obvious whether the ground states of all of these isotones are well approximated by the spherical HF wave functions, it is meaningful to see the s.p. energies, which often give an indication to magic or submagic numbers. For D1S we reduce the number of bases in Eq. (18) to avoid instability occurring for some $N=16$ nuclei, which probably relates to the unphysical behavior in the neutron matter. It is found that, if viewed as a function of Z, $\Delta\epsilon_n$ strikingly depends on the interactions. With the M3Y-P2 interaction, $\Delta\epsilon_n$ increases as Z goes from $Z=14$ to $Z=8$. We have confirmed [28] that even M3Y-P1 (with appropriate $v_{12}^{(\mathrm{LS})}$ and $v_{12}^{(\mathrm{TN})}$) shows similar behavior and that a significant part of this feature originates in the OPEP part in $v_{12}^{(\mathrm{C})}$. It is thus suggested that this behavior of $\Delta\epsilon_n$ is correlated to the spin-isospin property in the nuclear matter.

For comparison, we also show the s.p. energies obtained from the reliable shell model interaction for the sd-shell nuclei, the so-called universal sd (USD) interaction [9]. For this purpose we define the effective values of s.p. energies for each nucleus A from the shell model space and interaction, which correspond to those of the spherical HF calculations, as

$$\epsilon_n^{\mathrm{USD}}(j;A)=\epsilon_n^{\mathrm{USD}}(j;^{17}\mathrm{O})+\sum_{j'}\langle N_{j'}\rangle_A\frac{2J+1}{(2j+1)(2j'+1)}\times\langle jj';J|v^{\mathrm{USD}}|jj';J\rangle, \quad (20)$$

where the sum with respect to j' runs over the valence orbits. For $\langle N_j\rangle_A$, we assume that the nucleons occupy the s.p. orbits from the bottom, according to $\epsilon(j)$. From these s.p. energies we obtain $\Delta\epsilon_n^{\mathrm{USD}}=\epsilon_n^{\mathrm{USD}}(0d_{3/2};A)-\epsilon_n^{\mathrm{USD}}(1s_{1/2};A)$ for individual nucleus. This definition is equivalent to the effective s.p. energies in Ref. [3] for the $Z\leqslant N(=16)$ nuclei. The $\Delta\epsilon_n^{\mathrm{USD}}$ values are also shown in Fig. 7. It is noted that in the shell model approaches the nucleus dependence of the s.p. wave functions is not fully taken into account. Effects of rearrangement in the wave functions of the deeply bound orbits are renormalized into the interactions among the valence nucleons. In contrast, in the HF approaches the s.p. wave functions are determined self-consistently, from nucleus to nucleus. Therefore, the shell model s.p. energies do not agree with their HF counterparts. However, there should be qualitative correspondence, which arises from basic characters of the effective interactions. It is remarked that the M3Y-P2 interaction has the same trend of $\Delta\epsilon_n$, in terms of the Z dependence, as the USD interaction. It has been suggested [3] that the interaction in the $(\boldsymbol{\sigma}\cdot\boldsymbol{\sigma})(\boldsymbol{\tau}\cdot\boldsymbol{\tau})$ channel, which will be linked to a_{st} or to g'_ℓ, is significant to the magic numbers in highly neutron-rich nuclei, and that the Z dependence of the s.p. energies in this region could be relevant to the new magic number $N=16$ [29]. The present results are fully consistent with the arguments in Ref. [3], although we cannot draw conclusions on the magic number problem without assessing the influence of residual interactions.

VII. SUMMARY AND OUTLOOK

We have developed effective interactions to describe low energy phenomena of nuclei. Starting from the M3Y interaction, we introduce a density-dependent contact term and modify several parameters in a phenomenological manner, whereas maintaining the OPEP part in the central force. In order to view basic characters of the interactions, the Hartree-Fock calculations are implemented for the infinite nuclear matter (for which useful formulas are newly derived) and for several doubly magic nuclei. We have shown that a parameter set called M3Y-P2 describes their properties plausibly. The properties that are well treated by the Skyrme SLy5 and/or the Gogny D1S interactions are also reproduced by the M3Y-P2 interaction. However, a remarkable difference is found in the properties relevant to the spin degrees of freedom in the nuclear matter. The M3Y-type interactions seem to give reasonable spin and isospin properties, in which the OPEP part contained in $v_{12}^{(C)}$ plays a significant role. We have also shown that the difference in the spin-isospin property affects the s.p. energies in finite nuclei to a considerable extent. It will be interesting to apply extensively the M3Y-type interactions, particularly to the magic number problems far from the β stability.

Although the M3Y-P2 interaction seems to have various desired characters, there still remains a certain room for further tuning of the parameters. It should be noted that this parameter set will not be a unique choice to reproduce the properties of the nuclear matter and the doubly magic nuclei. Effective interaction might not be constrained sufficiently only from the HF calculations. The pairing effects in nuclei give valuable information on the effective interaction, primarily on the SE channel. Comparison of the matrix elements with reliable shell model interactions will also be helpful, if the core polarization effects are treated appropriately. These points will be discussed in future publications.

ACKNOWLEDGMENTS

I am grateful to Dr. D. T. Khoa for discussions. This work was financially supported as Grant-in-Aid for Scientific Research (C), No. 13640263, by the Ministry of Education, Culture, Sports, Science and Technology, Japan. Numerical calculations were performed on HITAC SR8000 at Institute of Media and Information Technology, Chiba University, at Information Technology Center, University of Tokyo, and at Computing Center, Hokkaido University.

APPENDIX A: ANALYTIC FORMULAS FOR NUCLEAR MATTER ENERGY

In this appendix we derive formulas concerning the interaction part of Eq. (12). The form of Eq. (2) is assumed for v_{12}.

Each term of $v_{12}^{(C)}$ is expressed as $f_n^{(C)}(r_{12})\mathcal{O}_\sigma\mathcal{O}_\tau$. Its nonantisymmetrized matrix element in the plane wave states of Eq. (8) is evaluated as

$$\begin{aligned}
&\langle \mathbf{k}_1'\sigma_1'\tau_1', \mathbf{k}_2'\sigma_2'\tau_2'|f_n^{(C)}(r_{12})\mathcal{O}_\sigma\mathcal{O}_\tau|\mathbf{k}_1\sigma_1\tau_1, \mathbf{k}_2\sigma_2\tau_2\rangle_{\text{n.a.}} \\
&= \frac{1}{\Omega^2}\int d^3r_1 d^3r_2 e^{i(\mathbf{k}_1-\mathbf{k}_1')\cdot\mathbf{r}_1 + i(\mathbf{k}_2-\mathbf{k}_2')\cdot\mathbf{r}_2} f_n^{(C)}(r_{12}) \\
&\quad\times\langle\sigma_1'\sigma_2'|\mathcal{O}_\sigma|\sigma_1\sigma_2\rangle\langle\tau_1'\tau_2'|\mathcal{O}_\tau|\tau_1\tau_2\rangle \\
&= \frac{1}{\Omega^2}\int d^3R d^3r_{12} e^{i(\mathbf{K}-\mathbf{K}')\cdot\mathbf{R} + i(\mathbf{k}_{12}-\mathbf{k}_{12}')\cdot\mathbf{r}_{12}} f_n^{(C)}(r_{12}) \\
&\quad\times\langle\sigma_1'\sigma_2'|\mathcal{O}_\sigma|\sigma_1\sigma_2\rangle\langle\tau_1'\tau_2'|\mathcal{O}_\tau|\tau_1\tau_2\rangle \\
&= \frac{1}{\Omega}\delta_{\mathbf{K},\mathbf{K}'}\tilde{f}_n^{(C)}(|\mathbf{k}_{12}-\mathbf{k}_{12}'|) \\
&\quad\times\langle\sigma_1'\sigma_2'|\mathcal{O}_\sigma|\sigma_1\sigma_2\rangle\langle\tau_1'\tau_2'|\mathcal{O}_\tau|\tau_1\tau_2\rangle, \qquad \text{(A1)}
\end{aligned}$$

where $\mathbf{R}=(\mathbf{r}_1+\mathbf{r}_2)/2$, $\mathbf{r}_{12}=\mathbf{r}_1-\mathbf{r}_2$, $\mathbf{K}=\mathbf{k}_1+\mathbf{k}_2$, $\mathbf{K}'=\mathbf{k}_1'+\mathbf{k}_2'$, $\mathbf{k}_{12}=(\mathbf{k}_1-\mathbf{k}_2)/2$, $\mathbf{k}_{12}'=(\mathbf{k}_1'-\mathbf{k}_2')/2$, and $\tilde{f}(q)$ is the Fourier transform of $f(r)$,

$$\tilde{f}(q)=\int d^3r f(r) e^{-i\mathbf{q}\cdot\mathbf{r}}. \qquad \text{(A2)}$$

The density-dependent interaction $v_{12}^{(DD)}$ is also handled in a similar manner, since the density behaves like a constant in the nuclear matter. For the Hartree term we have $(\mathbf{k}_1\sigma_1\tau_1)=(\mathbf{k}_1'\sigma_1'\tau_1')$ and $(\mathbf{k}_2\sigma_2\tau_2)=(\mathbf{k}_2'\sigma_2'\tau_2')$, while $(\mathbf{k}_1\sigma_1\tau_1)=(\mathbf{k}_2'\sigma_2'\tau_2')$ and $(\mathbf{k}_2\sigma_2\tau_2)=(\mathbf{k}_1'\sigma_1'\tau_1')$ for the Fock term. Therefore both terms satisfy $\mathbf{K}=\mathbf{K}'$. For the relative momentum the Hartree term (the Fock term) yields $\mathbf{k}_{12}-\mathbf{k}_{12}'=0$ $(\mathbf{k}_{12}-\mathbf{k}_{12}'=2\mathbf{k}_{12})$. Contribution of the two-body interaction to the nuclear matter energy is obtained by integrating $\tilde{f}$ in Eq. (A1) up to the Fermi momenta.

We here consider general cases where the Fermi momentum may depend on spin and isospin. In order to take into account the spin-isospin dependence, we integrate $\tilde{f}$ in the range $k_1\leqslant k_{F1}$ and $k_2\leqslant k_{F2}$. The integration is immediately carried out for the Hartree term, as far as $f(r_{12})$ is momentum independent, since the integrand depends neither on $\mathbf{k}_1$ nor on $\mathbf{k}_2$,

$$\begin{aligned}
\mathcal{W}^{H}(k_{F1},k_{F2}) &= \int_{k_1\leqslant k_{F1}} d^3k_1 \int_{k_2\leqslant k_{F2}} d^3k_2 \tilde{f}(0) \\
&= \frac{16\pi^2}{9} k_{F1}^3 k_{F2}^3 \tilde{f}(0). \qquad \text{(A3)}
\end{aligned}$$

For the Fock term contribution, the integral with respect to $\mathbf{k}_1$ and $\mathbf{k}_2$ is converted to the one with respect to $\mathbf{K}$ and $\mathbf{k}_{12}$. We here assume $k_{F1}\leqslant k_{F2}$ without loss of generality, owing to the symmetry $\mathcal{W}(k_{F1},k_{F2})=\mathcal{W}(k_{F2},k_{F1})$. Handling the range of integral carefully, we obtain the following expression:

$$\mathcal{W}^{\mathrm{F}}(k_{\mathrm{F}1},k_{\mathrm{F}2})=\int_{k_1\leqslant k_{\mathrm{F}1}}d^3k_1\int_{k_2\leqslant k_{\mathrm{F}2}}d^3k_2\tilde{f}(2k_{12})$$
$$=8\pi^2\Bigg[\int_0^{(k_{\mathrm{F}2}-k_{\mathrm{F}1})/2}dk_{12}\frac{16}{3}k_{\mathrm{F}1}^3k_{12}^2\tilde{f}(2k_{12})$$
$$+\int_{(k_{\mathrm{F}2}-k_{\mathrm{F}1})/2}^{(k_{\mathrm{F}1}+k_{\mathrm{F}2})/2}dk_{12}\Bigg\{-\frac{1}{2}(k_{\mathrm{F}2}^2-k_{\mathrm{F}1}^2)^2k_{12}$$
$$+\frac{8}{3}(k_{\mathrm{F}1}^3+k_{\mathrm{F}2}^3)k_{12}^2-4(k_{\mathrm{F}1}^2+k_{\mathrm{F}2}^2)k_{12}^3$$
$$+\frac{8}{3}k_{12}^5\Bigg\}\tilde{f}(2k_{12})\Bigg]. \tag{A4}$$

These formulas are general to multicomponent uniform Fermi liquids with equal masses.

In handling the spin-isospin degrees of freedom, we rewrite the central force in Eq. (2) as

$$v_{12}^{(\mathrm{C})}=\sum_n\left(t_n^{(\mathrm{W})}+t_n^{(\mathrm{B})}P_\sigma-t_n^{(\mathrm{H})}P_\tau-t_n^{(\mathrm{M})}P_\sigma P_\tau\right)f_n^{(\mathrm{C})}(r_{12}). \tag{A5}$$

The relations between the coupling constants are

$$t_n^{(\mathrm{SE})}=t_n^{(\mathrm{W})}-t_n^{(\mathrm{B})}-t_n^{(\mathrm{H})}+t_n^{(\mathrm{M})},$$
$$t_n^{(\mathrm{TE})}=t_n^{(\mathrm{W})}+t_n^{(\mathrm{B})}+t_n^{(\mathrm{H})}+t_n^{(\mathrm{M})},$$
$$t_n^{(\mathrm{SO})}=t_n^{(\mathrm{W})}-t_n^{(\mathrm{B})}+t_n^{(\mathrm{H})}-t_n^{(\mathrm{M})},$$
$$t_n^{(\mathrm{TO})}=t_n^{(\mathrm{W})}+t_n^{(\mathrm{B})}-t_n^{(\mathrm{H})}-t_n^{(\mathrm{M})}. \tag{A6}$$

After summing over the spin-isospin degrees of freedom, the interaction energy is given by

$$\langle V\rangle=\frac{\Omega}{2(2\pi)^6}\sum_n\sum_{\sigma_1\sigma_2\tau_1\tau_2}[(t_n^{(\mathrm{W})}+t_n^{(\mathrm{B})}\delta_{\sigma_1\sigma_2}-t_n^{(\mathrm{H})}\delta_{\tau_1\tau_2}$$
$$-t_n^{(\mathrm{M})}\delta_{\sigma_1\sigma_2}\delta_{\tau_1\tau_2})\mathcal{W}_n^{\mathrm{H}}(k_{\mathrm{F}\tau_1\sigma_1},k_{\mathrm{F}\tau_2\sigma_2})$$
$$+(t_n^{(\mathrm{M})}+t_n^{(\mathrm{H})}\delta_{\sigma_1\sigma_2}-t_n^{(\mathrm{B})}\delta_{\tau_1\tau_2}$$
$$-t_n^{(\mathrm{W})}\delta_{\sigma_1\sigma_2}\delta_{\tau_1\tau_2})\mathcal{W}_n^{\mathrm{F}}(k_{\mathrm{F}\tau_1\sigma_1},k_{\mathrm{F}\tau_2\sigma_2})]. \tag{A7}$$

In Eq. (A7) we regard the sum over n to include $v_{12}^{(\mathrm{DD})}$. It is noted that $A=\Omega\rho$, which is used to obtain the energy per nucleon $\mathcal{E}$.

We next calculate the $\mathcal{W}$ functions for typical interaction forms.

(1) *δ interaction.* If $f(r_{12})=\delta(\mathbf{r}_{12})$, $\tilde{f}(q)=1$ and therefore we have

$$\mathcal{W}^{\mathrm{H}}(k_1,k_2)=\mathcal{W}^{\mathrm{F}}(k_1,k_2)=\frac{16\pi^2}{9}k_1^3k_2^3. \tag{A8}$$

(2) *ρ-dependent δ interaction.* Since the density is a constant in the uniform nuclear matter, the $\mathcal{W}$ functions for $f(r_{12})=\rho^\alpha\delta(\mathbf{r}_{12})$ are similar to the above case,

$$\mathcal{W}^{\mathrm{H}}(k_1,k_2)=\mathcal{W}^{\mathrm{F}}(k_1,k_2)=\frac{16\pi^2}{9}\rho^\alpha k_1^3k_2^3. \tag{A9}$$

Note that ρ is a function of the Fermi momenta, when we take derivatives of the $\mathcal{W}$ functions.

(3) *Gauss interaction.* For $f(r_{12})=e^{-(\mu r_{12})^2}$, we have $\tilde{f}(q)=(\sqrt{\pi}/\mu)^3e^{-(q/2\mu)^2}$, deriving

$$\mathcal{W}^{\mathrm{H}}(k_1,k_2)=\frac{16\pi^2}{9}\left(\frac{\sqrt{\pi}}{\mu}\right)^3k_1^3k_2^3, \tag{A10}$$

and

$$\mathcal{W}^{\mathrm{F}}(k_1,k_2)=\frac{32\sqrt{\pi}^7}{3}\Bigg[\mu\{(k_1^2-k_1k_2+k_2^2-2\mu^2)$$
$$\times e^{-[(k_1+k_2)/2\mu]^2}-(k_1^2+k_1k_2+k_2^2$$
$$-2\mu^2)e^{-[(k_2-k_1)/2\mu]^2}\}$$
$$-(k_1^3+k_2^3)\mathrm{erfc}\left(\frac{k_1+k_2}{2\mu}\right)+(k_2^3$$
$$-k_1^3)\mathrm{erfc}\left(\frac{k_2-k_1}{2\mu}\right)+\sqrt{\pi}k_1^3\Bigg], \tag{A11}$$

where

$$\mathrm{erfc}(x)=\int_x^\infty e^{-z^2}dz. \tag{A12}$$

In Eq. (A11) we have postulated $k_1\leqslant k_2$ again.

(4) *Yukawa interaction.* For the Yukawa interaction we set $f(r_{12})=e^{-\mu r_{12}}/\mu r_{12}$, leading to $\tilde{f}(q)=4\pi/\mu(\mu^2+q^2)$. This yields

$$\mathcal{W}^{\mathrm{H}}(k_1,k_2)=\frac{64\pi^3}{9\mu^3}k_1^3k_2^3, \tag{A13}$$

and

$$\mathcal{W}^{\mathrm{F}}(k_1,k_2)=\frac{2\pi^3}{3\mu}\Bigg[4k_1k_2\{3(k_1^2+k_2^2)-\mu^2\}$$
$$-16\mu\Bigg\{(k_1^3+k_2^3)\arctan\left(\frac{k_1+k_2}{\mu}\right)$$
$$-(k_2^3-k_1^3)\arctan\left(\frac{k_2-k_1}{\mu}\right)\Bigg\}-\{3(k_2^2-k_1^2)^2$$
$$-6\mu^2(k_1^2+k_2^2)-\mu^4\}\ln\frac{\mu^2+(k_1+k_2)^2}{\mu^2+(k_2-k_1)^2}\Bigg]. \tag{A14}$$

(5) *Momentum-dependent δ interaction.* In the Skyrme interaction we have momentum-dependent terms with the form $\frac{1}{2}\{\mathbf{p}_{12}^2\delta(\mathbf{r}_{12})+\delta(\mathbf{r}_{12})\mathbf{p}_{12}^2\}$ and $\mathbf{p}_{12}\cdot\delta(\mathbf{r}_{12})\mathbf{p}_{12}$. The former operates only on the even channels and yields

$$\mathcal{W}^{\mathrm{H}}(k_1,k_2)=\mathcal{W}^{\mathrm{F}}(k_1,k_2)=\frac{4\pi^2}{15}k_1^3k_2^3(k_1^2+k_2^2). \tag{A15}$$

The latter acts on the odd channels, giving

$$\mathcal{W}^{\mathrm{H}}(k_1,k_2)=-\mathcal{W}^{\mathrm{F}}(k_1,k_2)=\frac{4\pi^2}{15}k_1^3k_2^3(k_1^2+k_2^2). \tag{A16}$$

The incompressibility $\mathcal{K}$ and the spin-isospin curvatures a_t, a_s, a_{st} are expressed by the derivatives of the $\mathcal{W}$ functions.

The single-particle energy $\epsilon(\mathbf{k}\sigma\tau)$ defined in Eq. (9) is also expressed by the derivative of the $\mathcal{W}$ functions. We first rewrite the integral in Eq. (12) as

$$\int_{k_1'\le k_1}d^3k_1'\int_{k_2\le k_{\mathrm{F}\tau_2\sigma_2}}d^3k_2\langle\mathbf{k}_1'\sigma_1\tau_1,\mathbf{k}_2\sigma_2\tau_2|v_{12}|\mathbf{k}_1'\sigma_1\tau_1,\mathbf{k}_2\sigma_2\tau_2\rangle$$
$$=4\pi\int_0^{k_1}k_1'^2dk_1'\int_{k_2\le k_{\mathrm{F}\tau_2\sigma_2}}d^3k_2\langle\mathbf{k}_1'\sigma_1\tau_1,\mathbf{k}_2\sigma_2\tau_2|v_{12}|\mathbf{k}_1'\sigma_1\tau_1,\mathbf{k}_2\sigma_2\tau_2\rangle. \tag{A17}$$

This immediately gives

$$\frac{\partial}{\partial k_1}\int_{k_1'\le k_1}d^3k_1'\int_{k_2\le k_{\mathrm{F}\tau_2\sigma_2}}d^3k_2\langle\mathbf{k}_1'\sigma_1\tau_1,\mathbf{k}_2\sigma_2\tau_2|v_{12}|\mathbf{k}_1'\sigma_1\tau_1,\mathbf{k}_2\sigma_2\tau_2\rangle$$
$$=4\pi k_1^2\int_{k_2\le k_{\mathrm{F}\tau_2\sigma_2}}d^3k_2\langle\mathbf{k}_1'\sigma_1\tau_1,\mathbf{k}_2\sigma_2\tau_2|v_{12}|\mathbf{k}_1'\sigma_1\tau_1,\mathbf{k}_2\sigma_2\tau_2\rangle. \tag{A18}$$

Therefore,

$$\epsilon(\mathbf{k}_1\sigma_1\tau_1)=\frac{\mathbf{k}_1^2}{2M}+\frac{1}{(2\pi)^3}\frac{1}{4\pi k_1^2}\sum_n\sum_{\sigma_2\tau_2}[(t_n^{(\mathrm{W})}+t_n^{(\mathrm{B})}\delta_{\sigma_1\sigma_2}$$
$$-t_n^{(\mathrm{H})}\delta_{\tau_1\tau_2}-t_n^{(\mathrm{M})}\delta_{\sigma_1\sigma_2}\delta_{\tau_1\tau_2})\partial_1\mathcal{W}_n^{\mathrm{H}}(k_1,k_{\mathrm{F}\tau_2\sigma_2})$$
$$+(t_n^{(\mathrm{M})}+t_n^{(\mathrm{H})}\delta_{\sigma_1\sigma_2}-t_n^{(\mathrm{B})}\delta_{\tau_1\tau_2}$$
$$-t_n^{(\mathrm{W})}\delta_{\sigma_1\sigma_2}\delta_{\tau_1\tau_2})\partial_1\mathcal{W}_n^{\mathrm{F}}(k_1,k_{\mathrm{F}\tau_2\sigma_2})], \tag{A19}$$

where we use the shorthand notation

$$\partial_1\mathcal{W}_n^{\mathrm{H/F}}(k_1,k_2)=\frac{\partial}{\partial k_1}\mathcal{W}_n^{\mathrm{H/F}}(k_1,k_2). \tag{A20}$$

It is now obvious that the effective mass of Eq. (15) is expressed by using the second derivative of the $\mathcal{W}$ functions.

APPENDIX B: LANDAU PARAMETERS FOR SYMMETRIC NUCLEAR MATTER

Let us denote the occupation probability of the s.p. states of Eq. (8) by $n_{\tau\sigma}(\mathbf{k})$. The nuclear matter energy of Eq. (A7) can be rewritten as

$$\frac{\langle V\rangle}{\Omega}=\frac{\langle V\rangle_{\mathrm{H}}+\langle V\rangle_{\mathrm{F}}}{\Omega}, \tag{B1}$$

$$\frac{\langle V\rangle_{\mathrm{H}}}{\Omega}=\frac{1}{2(2\pi)^6}\sum_n\sum_{\sigma_1\sigma_2\tau_1\tau_2}\sum_{\mathbf{k}_1\mathbf{k}_2}n_{\tau_1\sigma_1}(\mathbf{k}_1)n_{\tau_2\sigma_2}(\mathbf{k}_2)\tilde{f}_n(0)$$
$$\times(t_n^{(\mathrm{W})}+t_n^{(\mathrm{B})}\delta_{\sigma_1\sigma_2}-t_n^{(\mathrm{H})}\delta_{\tau_1\tau_2}-t_n^{(\mathrm{M})}\delta_{\sigma_1\sigma_2}\delta_{\tau_1\tau_2}), \tag{B2}$$

$$\frac{\langle V\rangle_{\mathrm{F}}}{\Omega}=\frac{1}{2(2\pi)^6}\sum_n\sum_{\sigma_1\sigma_2\tau_1\tau_2}\sum_{\mathbf{k}_1\mathbf{k}_2}n_{\tau_1\sigma_1}(\mathbf{k}_1)n_{\tau_2\sigma_2}(\mathbf{k}_2)$$
$$\times\tilde{f}_n(2k_{12})(t_n^{(\mathrm{M})}+t_n^{(\mathrm{H})}\delta_{\sigma_1\sigma_2}-t_n^{(\mathrm{B})}\delta_{\tau_1\tau_2}$$
$$-t_n^{(\mathrm{W})}\delta_{\sigma_1\sigma_2}\delta_{\tau_1\tau_2}). \tag{B3}$$

The Landau coefficient is defined by

$$F^{(\ell)}_{\tau_1\sigma_1,\tau_2\sigma_2}(k_1,k_2)=\frac{2\ell+1}{2}\int_{-1}^{1}d(\hat{\mathbf{k}}_1\cdot\hat{\mathbf{k}}_2)P_\ell(\hat{\mathbf{k}}_1\cdot\hat{\mathbf{k}}_2)$$
$$\times\frac{\delta^2(\langle V\rangle/\Omega)}{\delta n_{\tau_1\sigma_1}(\mathbf{k}_1)\,\delta n_{\tau_2\sigma_2}(\mathbf{k}_2)}. \tag{B4}$$

For the interaction independent of momentum and of density, it is straightforward to write down the coefficients of Eq. (B4) in terms of $\tilde{f}$, within the HF theory at the zero temperature. Noticing that ρ also depends on $n_{\tau\sigma}(\mathbf{k})$, we evaluate the contribution of the density-dependent δ interaction $(1+x^{(\mathrm{DD})}P_\sigma)\rho^\alpha\delta(\mathbf{r}_{12})$ to $F^{(\ell)}_{\tau_1\sigma_1,\tau_2\sigma_2}(k_1,k_2)$ as

$$\frac{\delta_{\ell 0}}{(2\pi)^6}\left[\frac{\alpha(\alpha-1)}{2}\rho^{\alpha-2}\left\{\rho^2-\sum_{\sigma\tau}\rho_{\tau\sigma}^2+x^{(\mathrm{DD})}\left(\sum_{\sigma}\rho_{\sigma}^2-\sum_{\tau}\rho_{\tau}^2\right)\right\}+\alpha\rho^{\alpha-1}\{2\rho-\rho_{\tau_1\sigma_1}-\rho_{\tau_2\sigma_2}+x^{(\mathrm{DD})}(\rho_{\sigma_1}+\rho_{\sigma_2}-\rho_{\tau_1}-\rho_{\tau_2})\}+\rho^{\alpha}\{1-\delta_{\tau_1\tau_2}\delta_{\sigma_1\sigma_2}+x^{(\mathrm{DD})}(\delta_{\sigma_1\sigma_2}-\delta_{\tau_1\tau_2})\}\right], \tag{B5}$$

where $\rho_\sigma=\Sigma_\tau\rho_{\tau\sigma}$ and $\rho_\tau=\Sigma_\sigma\rho_{\tau\sigma}$. Apart from the spin and isospin degrees of freedom, the momentum-dependent δ interactions $\frac{1}{2}\{\mathbf{p}_{12}^2\delta(\mathbf{r}_{12})+\delta(\mathbf{r}_{12})\mathbf{p}_{12}^2\}$ and $\mathbf{p}_{12}\cdot\delta(\mathbf{r}_{12})\mathbf{p}_{12}$ contribute to $F^{(\ell)}_{\tau_1\sigma_1,\tau_2\sigma_2}(k_1,k_2)$ by

$$\frac{1}{(2\pi)^6}\left(\delta_{\ell 0}\frac{k_1^2+k_2^2}{4}-\delta_{\ell 1}\frac{k_1k_2}{2}\right). \tag{B6}$$

In characterizing effective interactions, we view the Landau coefficients for the symmetric nuclear matter, where $\rho_{\tau\sigma}=\rho/4$ for any τ and σ. While formulas for the Landau parameters were derived for the Skyrme interaction in Ref. [21] and for the Gogny interaction in Ref. [30], we here derive expressions for interactions with the form of Eq. (2) in a more general manner. It is customary to transform the (τ,σ) variables into the following ones:

$$\begin{aligned}
&1\cdots p\uparrow+p\downarrow+n\uparrow+n\downarrow,\\
&t\cdots p\uparrow+p\downarrow-n\uparrow-n\downarrow,\\
&s\cdots p\uparrow-p\downarrow+n\uparrow-n\downarrow,\\
&st\cdots p\uparrow-p\downarrow-n\uparrow+n\downarrow.
\end{aligned} \tag{B7}$$

Since $\Sigma_\sigma\sigma=\Sigma_\tau\tau=\Sigma_\sigma(\sigma\tau)=\Sigma_\tau(\sigma\tau)=0$, all the off-diagonal coefficients with respect to $(1,t,s,st)$ vanish. The diagonal coefficients are redefined as

$$\begin{aligned}
F_1^{(\ell)}(k_1,k_2)&=\frac{1}{16}\sum_{\sigma_1\sigma_2\tau_1\tau_2}F^{(\ell)}_{\tau_1\sigma_1,\tau_2\sigma_2}(k_1,k_2),\\
F_t^{(\ell)}(k_1,k_2)&=\frac{1}{16}\sum_{\sigma_1\sigma_2\tau_1\tau_2}\tau_1\tau_2F^{(\ell)}_{\tau_1\sigma_1,\tau_2\sigma_2}(k_1,k_2),\\
F_s^{(\ell)}(k_1,k_2)&=\frac{1}{16}\sum_{\sigma_1\sigma_2\tau_1\tau_2}\sigma_1\sigma_2F^{(\ell)}_{\tau_1\sigma_1,\tau_2\sigma_2}(k_1,k_2),\\
F_{st}^{(\ell)}(k_1,k_2)&=\frac{1}{16}\sum_{\sigma_1\sigma_2\tau_1\tau_2}\sigma_1\tau_1\sigma_2\tau_2F^{(\ell)}_{\tau_1\sigma_1,\tau_2\sigma_2}(k_1,k_2).
\end{aligned} \tag{B8}$$

The Hartree terms of the momentum- and density-independent interactions yield

$$\begin{aligned}
F^{(\ell)}_{1,\mathrm{H}}(k_1,k_2)&=\frac{\delta_{\ell 0}}{4(2\pi)^6}\sum_n(4t_n^{(\mathrm{W})}+2t_n^{(\mathrm{B})}-2t_n^{(\mathrm{H})}-t_n^{(\mathrm{M})})\tilde{f}_n(0),\\
F^{(\ell)}_{t,\mathrm{H}}(k_1,k_2)&=\frac{\delta_{\ell 0}}{4(2\pi)^6}\sum_n(-2t_n^{(\mathrm{H})}-t_n^{(\mathrm{M})})\tilde{f}_n(0),\\
F^{(\ell)}_{s,\mathrm{H}}(k_1,k_2)&=\frac{\delta_{\ell 0}}{4(2\pi)^6}\sum_n(2t_n^{(\mathrm{B})}-t_n^{(\mathrm{M})})\tilde{f}_n(0),\\
F^{(\ell)}_{st,\mathrm{H}}(k_1,k_2)&=\frac{\delta_{\ell 0}}{4(2\pi)^6}\sum_n(-t_n^{(\mathrm{M})})\tilde{f}_n(0),
\end{aligned} \tag{B9}$$

while the Fock terms

$$\begin{aligned}
F^{(\ell)}_{1,\mathrm{F}}(k_1,k_2)&=\frac{1}{4(2\pi)^6}\sum_n(4t_n^{(\mathrm{M})}+2t_n^{(\mathrm{H})}-2t_n^{(\mathrm{B})}-t_n^{(\mathrm{W})})G_n^{(\ell)}(k_1,k_2),\\
F^{(\ell)}_{t,\mathrm{F}}(k_1,k_2)&=\frac{1}{4(2\pi)^6}\sum_n(-2t_n^{(\mathrm{B})}-t_n^{(\mathrm{W})})G_n^{(\ell)}(k_1,k_2),\\
F^{(\ell)}_{s,\mathrm{F}}(k_1,k_2)&=\frac{1}{4(2\pi)^6}\sum_n(2t_n^{(\mathrm{H})}-t_n^{(\mathrm{W})})G_n^{(\ell)}(k_1,k_2),\\
F^{(\ell)}_{st,\mathrm{F}}(k_1,k_2)&=\frac{1}{4(2\pi)^6}\sum_n(-t_n^{(\mathrm{W})})G_n^{(\ell)}(k_1,k_2),
\end{aligned} \tag{B10}$$

where

$$G_n^{(\ell)}(k_1,k_2)=\frac{2\ell+1}{2}\int_{-1}^{1}d(\hat{\mathbf{k}}_1\cdot\hat{\mathbf{k}}_2)P_\ell(\hat{\mathbf{k}}_1\cdot\hat{\mathbf{k}}_2)\tilde{f}_n(2k_{12}). \tag{B11}$$

Contribution of the density-dependent interaction $t^{(\mathrm{DD})}(1+x^{(\mathrm{DD})}P_\sigma)\rho^\alpha\delta(\mathbf{r}_{12})$ is given by

$$\begin{aligned}
F^{(\ell)}_{1,\mathrm{DD}}(k_1,k_2)&=\frac{\delta_{\ell 0}}{4(2\pi)^6}t^{(\mathrm{DD})}\frac{3(\alpha+1)(\alpha+2)}{2}\rho^\alpha,\\
F^{(\ell)}_{t,\mathrm{DD}}(k_1,k_2)&=\frac{\delta_{\ell 0}}{4(2\pi)^6}t^{(\mathrm{DD})}(-2x^{(\mathrm{DD})}-1)\rho^\alpha,\\
F^{(\ell)}_{s,\mathrm{DD}}(k_1,k_2)&=\frac{\delta_{\ell 0}}{4(2\pi)^6}t^{(\mathrm{DD})}(2x^{(\mathrm{DD})}-1)\rho^\alpha,\\
F^{(\ell)}_{st,\mathrm{DD}}(k_1,k_2)&=-\frac{\delta_{\ell 0}}{4(2\pi)^6}t^{(\mathrm{DD})}\rho^\alpha.
\end{aligned} \tag{B12}$$

For momentum-independent interactions such as the Gogny interaction and the M3Y-type interactions, the Landau coefficients are obtained by $F_l^{(\ell)}(k_1,k_2)=F_{l,\mathrm{H}}^{(\ell)}(k_1,k_2)+F_{l,\mathrm{F}}^{(\ell)}(k_1,k_2)+F_{l,\mathrm{DD}}^{(\ell)}(k_1,k_2)$, and so forth. The momentum-dependent δ interactions yield

$$F_{l,\mathrm{MD}}^{(\ell)}(k_1,k_2)=\frac{1}{8(2\pi)^6}\left(\delta_{\ell 0}\frac{k_1^2+k_2^2}{2}-\delta_{\ell 1}k_1k_2\right)\times\begin{cases}3t_1^{(\mathrm{MD})}\\ 5t_2^{(\mathrm{MD})},\end{cases}$$

$$F_{t,\mathrm{MD}}^{(\ell)}(k_1,k_2)=\frac{1}{8(2\pi)^6}\left(\delta_{\ell 0}\frac{k_1^2+k_2^2}{2}-\delta_{\ell 1}k_1k_2\right)\times\begin{cases}t_1^{(\mathrm{MD})}(-2x_1^{(\mathrm{MD})}-1)\\ t_2^{(\mathrm{MD})}(2x_2^{(\mathrm{MD})}+1),\end{cases}$$

$$F_{s,\mathrm{MD}}^{(\ell)}(k_1,k_2)=\frac{1}{8(2\pi)^6}\left(\delta_{\ell 0}\frac{k_1^2+k_2^2}{2}-\delta_{\ell 1}k_1k_2\right)\times\begin{cases}t_1^{(\mathrm{MD})}(2x_1^{(\mathrm{MD})}-1)\\ t_2^{(\mathrm{MD})}(2x_2^{(\mathrm{MD})}+1),\end{cases}$$

$$F_{st,\mathrm{MD}}^{(\ell)}(k_1,k_2)=\frac{1}{8(2\pi)^6}\left(\delta_{\ell 0}\frac{k_1^2+k_2^2}{2}-\delta_{\ell 1}k_1k_2\right)\times\begin{cases}(-t_1^{(\mathrm{MD})})\\ t_2^{(\mathrm{MD})},\end{cases}\tag{B13}$$

where the upper row corresponds to the even channel interaction $\frac{1}{2}t_1^{(\mathrm{MD})}(1+x_1^{(\mathrm{MD})}P_\sigma)\{\mathbf{p}_{12}^2\delta(\mathbf{r}_{12})+\delta(\mathbf{r}_{12})\mathbf{p}_{12}^2\}$, while the lower to the odd channel interaction $t_2^{(\mathrm{MD})}(1+x_2^{(\mathrm{MD})}P_\sigma)\mathbf{p}_{12}\cdot\delta(\mathbf{r}_{12})\mathbf{p}_{12}$, respectively. Equation (B13) is available for the Skyrme interactions in which the LS currents are not ignored.

We next show explicit form of the $G^{(\ell)}$ factor in Eq. (B10) for typical interaction forms.

(1) *δ interaction.* Substituting $\tilde{f}(2k_{12})$ by 1, we obtain

$$G^{(\ell)}(k_1,k_2)=\delta_{\ell 0}.\tag{B14}$$

(2) *Gauss interaction.* Because $\tilde{f}(q)=(\sqrt{\pi}/\mu)^3 e^{-(q/2\mu)^2}$, Eq. (B11) leads to

$$G^{(\ell)}(k_1,k_2)=\frac{(2\ell+1)\sqrt{\pi}^3}{\mu k_1k_2}\sum_{m=0}^{\ell}\frac{(\ell+m)!}{m!(\ell-m)!}\left(\frac{\mu^2}{k_1k_2}\right)^m\times\{(-)^m e^{-[(k_1-k_2)/2\mu]^2}-(-)^\ell e^{-[(k_1+k_2)/2\mu]^2}\}.\tag{B15}$$

For $\ell=0$ and 1, we have

$$G^{(0)}(k_1,k_2)=\frac{\sqrt{\pi}^3}{\mu k_1k_2}\{e^{-[(k_1-k_2)/2\mu]^2}-e^{-[(k_1+k_2)/2\mu]^2}\},\tag{B16}$$

$$G^{(1)}(k_1,k_2)=\frac{3\sqrt{\pi}^3}{\mu k_1k_2}\left\{\left(1-\frac{2\mu^2}{k_1k_2}\right)e^{-[(k_1-k_2)/2\mu]^2}+\left(1+\frac{2\mu^2}{k_1k_2}\right)e^{-[(k_1+k_2)/2\mu]^2}\right\}.\tag{B17}$$

(3) *Yukawa interaction.* For the Yukawa interaction we use $\tilde{f}(q)=4\pi/\mu(\mu^2+q^2)$. Inserting it into Eq. (B11), we obtain for even ℓ,

$$\begin{aligned}G^{(\ell)}(k_1,k_2)&=\frac{2\pi(2\ell+1)}{\mu^3}\sum_{m=0}^{\ell/2}\left(\frac{\mu^2}{2k_1k_2}\right)^{2m+1}(-)^{\ell/2-m}\\&\times\frac{(\ell+2m-1)!!}{(2m)!(\ell-2m)!}\left[\left(1+\frac{k_1^2+k_2^2}{\mu^2}\right)^{2m}\ln\frac{\mu^2+(k_1+k_2)^2}{\mu^2+(k_2-k_1)^2}\right.\\&-\sum_{p=0}^{2m-1}\frac{(-)^p}{2m-p}\frac{(2m)!}{p!(2m-p)!}\\&\times\left(1+\frac{k_1^2+k_2^2}{\mu^2}\right)^p\left\{\left(1+\frac{(k_1-k_2)^2}{\mu^2}\right)^{2m-p}\right.\\&\left.\left.-\left(1+\frac{(k_1+k_2)^2}{\mu^2}\right)^{2m-p}\right\}\right]\end{aligned}\tag{B18}$$

and for odd ℓ

$$\begin{aligned}G^{(\ell)}(k_1,k_2)&=\frac{2\pi(2\ell+1)}{\mu^3}\sum_{m=0}^{(\ell-1)/2}\left(\frac{\mu^2}{2k_1k_2}\right)^{2m+2}(-)^{(\ell-1)/2-m}\\&\times\frac{(\ell+2m)!!}{(2m+1)!(\ell-2m-1)!}\\&\times\left[\left(1+\frac{k_1^2+k_2^2}{\mu^2}\right)^{2m+1}\ln\frac{\mu^2+(k_1+k_2)^2}{\mu^2+(k_2-k_1)^2}\right.\\&-\sum_{p=0}^{2m}\frac{(-)^{p+1}}{2m+1-p}\frac{(2m+1)!}{p!(2m+1-p)!}\\&\times\left(1+\frac{k_1^2+k_2^2}{\mu^2}\right)^p\left\{\left(1+\frac{(k_1-k_2)^2}{\mu^2}\right)^{2m+1-p}\right.\\&\left.\left.-\left(1+\frac{(k_1+k_2)^2}{\mu^2}\right)^{2m+1-p}\right\}\right].\end{aligned}\tag{B19}$$

For $\ell=0$ and 1, we have

$$G^{(0)}(k_1,k_2)=\frac{\pi}{\mu k_1 k_2}\ln\frac{\mu^2+(k_1+k_2)^2}{\mu^2+(k_2-k_1)^2}, \quad \text{(B20)}$$

$$G^{(1)}(k_1,k_2)=\frac{3\pi}{2\mu(k_1k_2)^2}\left[(\mu^2+k_1^2+k_2^2)\times\ln\frac{\mu^2+(k_1+k_2)^2}{\mu^2+(k_2-k_1)^2}-4k_1k_2\right]. \quad \text{(B21)}$$

Setting $k_1=k_2=k_{F0}$ and using the estimated level density at the Fermi momentum $N_0=(2\pi)^6 2k_{F0}M_0^*/\pi^2$, we define the usual Landau parameters,

$$f_\ell=N_0F_1^{(\ell)}(k_{F0},k_{F0}),\quad f'_\ell=N_0F_t^{(\ell)}(k_{F0},k_{F0}),$$
$$g_\ell=N_0F_s^{(\ell)}(k_{F0},k_{F0}),\quad g'_\ell=N_0F_{st}^{(\ell)}(k_{F0},k_{F0}). \quad \text{(B22)}$$

The second derivaties of $\mathcal{E}$ at the saturation point are connected to the Landau parameters. The following relations are verified:

$$\frac{M_0^*}{M}=1+\frac{1}{3}f_1,\quad \mathcal{K}=\frac{3k_{F0}^2}{M_0^*}(1+f_0),\quad a_t=\frac{k_{F0}^2}{6M_0^*}(1+f'_0),$$
$$a_s=\frac{k_{F0}^2}{6M_0^*}(1+g_0),\quad a_{st}=\frac{k_{F0}^2}{6M_0^*}(1+g'_0). \quad \text{(B23)}$$

[1] S.C. Pieper, K. Varga, and R.B. Wiringa, Phys. Rev. C **66**, 044310 (2002).
[2] I. Tanihata, Nucl. Phys. **A654**, 235c (1999).
[3] T. Otsuka *et al.*, Phys. Rev. Lett. **87**, 082502 (2001).
[4] D. Vautherin and D.M. Brink, Phys. Rev. C **5**, 626 (1972).
[5] J. Dechargé and D. Gogny, Phys. Rev. C **21**, 1568 (1980).
[6] L. Coraggio *et al.*, Phys. Rev. C **58**, 3346 (1998); **60**, 064306 (1999).
[7] J.P. Schiffer and W.W. True, Rev. Mod. Phys. **48**, 191 (1976).
[8] G. Bertsch, J. Borysowicz, H. McManus, and W.G. Love, Nucl. Phys. **A284**, 399 (1977).
[9] B.A. Brown, W.A. Richter, R.E. Julies, and B.H. Wildenthal, Ann. Phys. (N.Y.) **182**, 191 (1988).
[10] D.T. Khoa, W. von Oertzen, and A.A. Ogloblin, Nucl. Phys. **A602**, 98 (1996); D.T. Khoa, G.R. Satchler, and W. von Oertzen, Phys. Rev. C **56**, 954 (1997).
[11] H. Nakada and M. Sato, Nucl. Phys. **A699**, 511 (2002); **A714**, 696 (2003).
[12] J.W. Negele, Phys. Rev. C **1**, 1260 (1970); X. Campi and D.W. Sprung, Nucl. Phys. **A194**, 401 (1972).
[13] F. Hofmann and H. Lenske, Phys. Rev. C **57**, 2281 (1998).
[14] N. Anantaraman, H. Toki, and G.F. Bertsch, Nucl. Phys. **A398**, 269 (1983).
[15] H.A. Bethe, Annu. Rev. Nucl. Sci. **21**, 93 (1971).
[16] K. Andō and H. Bandō, Prog. Theor. Phys. **66**, 227 (1981); K. Suzuki, R. Okamoto, and H. Kumagai, Phys. Rev. C **36**, 804 (1987); S.C. Pieper and V.R. Pandharipande, Phys. Rev. Lett. **70**, 2541 (1993).
[17] J.F. Berger, M. Girod, and D. Gogny, Comput. Phys. Commun. **63**, 365 (1991).
[18] E. Chabanat, P. Bonche, P. Haensel, J. Meyer, and R. Schaeffer, Nucl. Phys. **A635**, 231 (1998).
[19] C. Mahaux, P.F. Bortignon, R.A. Broglia, and C.H. Dasso, Phys. Rep. **120**, 1 (1985).
[20] C. Gaarde *et al.*, Nucl. Phys. **A369**, 258 (1981); T. Suzuki, *ibid.* **A379**, 110 (1982); G. Bertsch, D. Cha, and H. Toki, Phys. Rev. C **24**, 533 (1981).
[21] M. Bender, J. Dobaczewski, J. Engel, and W. Nazarewicz, Phys. Rev. C **65**, 054322 (2002).
[22] B. Friedman and V.R. Pandharipande, Nucl. Phys. **A361**, 502 (1981).
[23] H. Kameyama, M. Kamimura, and Y. Fukushima, Phys. Rev. C **40**, 974 (1989).
[24] G. Audi and A.H. Wapstra, Nucl. Phys. **A595**, 409 (1995).
[25] D. T. Khoa, H. S. Than, and M. Grasso, Nucl. Phys. (to be published).
[26] G.D. Alkhazov, S.L. Belostotsky, and A.A. Vorobyov, Phys. Rep. **42**, 89 (1978).
[27] R. B. Firestone *et al.*, *Table of Isotopes*, 8th ed. (Wiley, New York, 1996).
[28] H. Nakada, Nucl. Phys. **A722**, 117c (2003).
[29] A. Ozawa, T. Kobayashi, T. Suzuki, K. Yoshida, and I. Tanihata, Phys. Rev. Lett. **84**, 5493 (2000).
[30] J. Ventura, A. Polls, X. Viñas, and E.S. Hernandez, Nucl. Phys. **A578**, 147 (1994).

Measurement of $B(M1)$ for the $\pi p_{3/2}\nu p_{1/2}^{-1}$ doublet in ^{68}Cu

L. Hou,* T. Ishii,† and M. Asai
Advanced Science Research Center, Japan Atomic Energy Research Institute, Tokai, Ibaraki 319-1195, Japan

J. Hori‡
Department of Fusion Engineering Research, Japan Atomic Energy Research Institute, Tokai, Ibaraki 319-1195, Japan

K. Ogawa and H. Nakada
Department of Physics, Faculty of Science, Chiba University, Inage, Chiba 263-8522, Japan
(Received 12 May 2003; published 18 November 2003; publisher error corrected 26 November 2003)

Lifetimes of excited states in ^{68}Cu were measured by the γ-γ-t coincidence using two BaF_2 detectors through the decay of ^{68}Cu^m produced by the (n,p) reaction. The half-life of the 2^+ state at 84 keV was obtained as 7.84(8) ns, corresponding to the $B(M1;2^+\rightarrow 1^+)$ value of $0.00777(8)\mu_N^2$. A shell model calculation with a minimum model space of $\pi p_{3/2}\nu p_{1/2}^{-1}$ gives a good prediction of this $B(M1)$ value by using experimental g factors of neighboring nuclei. This small $B(M1)$ value can also be explained by a shell model calculation in the $f_{7/2}^{-r}(p_{3/2}f_{5/2}p_{1/2})^{n+r}(r=0, 1)$ model space.

DOI: 10.1103/PhysRevC.68.054306 PACS number(s): 21.10.Tg, 23.20.−g, 21.60.Cs, 27.50.+e

I. INTRODUCTION

The nuclear structure around ^{68}Ni, with Z=28 and N=40, provides important knowledge of the shell structure in the neutron-rich Ni region and thus many studies have been made with the progress of experimental techniques [1–18]. Among these studies, the magic properties of ^{68}Ni have been discussed from different angles. One of the issues is whether one can treat the ^{68}Ni nucleus as a core in a shell model calculation. We previously demonstrated that the energy levels in ^{71}Cu can be predicted very accurately by a shell model calculation with the $\pi p_{3/2}\nu g_{9/2}^2$ model space, using experimental energy levels in neighboring nuclei as residual two-body interactions [7]. It is interesting to study to what extent such a calculation is valid to explain the properties of nuclei around ^{68}Ni.

In the $^{68}_{29}Cu_{39}$ nucleus, the proton (π) $p_{3/2}$ and the neutron (ν) $p_{1/2}$ orbitals lie near the Fermi surface. Therefore, the 1^+ ground state and the 2^+ first excited state in ^{68}Cu are expected to have a large component of the $\pi p_{3/2}\nu p_{1/2}^{-1}$ configuration. This simple configuration gives an insight into the nuclear structure around ^{68}Ni. In particular, the $B(M1;2^+\rightarrow 1^+)$ value provides a good test of a shell model calculation. Furthermore, this $B(M1)$ value gives information on the core excitation, in particular, for the Z, N=28 core.

Excited states in ^{68}Cu were first studied through the γ decay of the ^{68}Cu isomer ($T_{1/2}$=3.75 min) produced by the ^{68}Zn(n,p) reaction [19–22]. Sherman *et al.* [23] studied energy levels in ^{68}Cu by the $(t, ^3\mathrm{He})$ transfer reaction. Recently, the g factors of the ground and the isomeric states were measured in ^{68}Cu separated from fission products using a mass separator with a chemically selective laser-ion-source [24]. We found a nanosecond isomer in ^{68}Cu [25] produced in heavy-ion deep-inelastic collisions using an isomer-scope [26].

In the present study, we have carried out a decay experiment of ^{68}Cu^m produced by the ^{68}Zn(n,p) reaction using 14-MeV neutrons. This reaction provides an almost pure ^{68}Cu^m source without chemical or mass separation. We have measured the lifetime of the first excited state and obtained a small $B(M1;2^+\rightarrow 1^+)$ value. We show that a parameter-free shell model calculation within the $\pi p_{3/2}\nu p_{1/2}^{-1}$ model space correctly predicts this $B(M1)$ value by using experimental g factors of neighboring nuclei. Furthermore, we show that this small $B(M1)$ value can be explained by a shell model calculation in the $f_{7/2}^{-r}(p_{3/2}f_{5/2}p_{1/2})^{n+r}(r=0, 1)$ model space.

II. EXPERIMENTS

The ^{68}Cu^m source ($T_{1/2}$=3.75 min) was produced by the ^{68}Zn(n,p) reaction at FNS (fusion neutronics source) in JAERI. Three ^{68}Zn targets of 0.2 g and 10 mm in diameter were prepared from the 99.4% enriched ^{68}ZnO powder by the following procedure. The ^{68}ZnO powder was dissolved in a 0.1M H_2SO_4 solution. Then, the ^{68}Zn metal was deposited by electrolysis on a thin platinum wire. The ^{68}Zn metal removed from the Pt wire was shaped by pressing it in a mold 10 mm in diameter. Each target was sealed in thin paraffin paper and in a polyethylene film.

The ^{68}Zn target was irradiated by 14-MeV neutrons at a place of about 5×10^9 cm^{-2} s^{-1} neutron flux; FNS generates 4×10^{12} s^{-1} neutrons by the ^{3}H(d,n) reaction using a 37 TBq tritium rotating target. The ^{68}Zn target was irradiated for 10 min and then transferred through a pneumatic tube to the outside of the irradiation room. The irradiated target was cooled for about 2 min. Thus, the cycle of 10-min irradiation, 2-min cooling, and 8-min measurement was repeated

*On leave from China Institute of Atomic Energy, P.O. Box 275(67), Bejing 102413, China.
†Electronic address: ishii@popsvr.tokai.jaeri.go.jp
‡Present address: Kyoto University Research Reactor Institute, Kumatori, Osaka 590-0494, Japan.

using three ^{68}Zn targets. Since the production cross section of ^{68}Cu^{m} is 5 mb [27], the activity of the ^{68}Cu^{m} source was about 30 kBq at the beginning of the measurement.

Lifetimes of excited states in ^{68}Cu were measured using two BaF_2 detectors of 25 mm in diameter and 10 mm in thickness. These detectors were placed face to face at a distance of 20 mm and the ^{68}Cu^{m} source was placed at the center between them. A β-ray absorber made of a 3.5-mm-thick aluminum plate was attached to both of the detectors. The lifetimes were also measured by another detector configuration to reduce backscattering γ rays between the BaF_2 detectors. In this configuration, the BaF_2 detectors were placed at 90° and a 3-mm-thick lead absorber was placed between them. In Sec. III, the former detector configuration will be referred to as the 180° setup, while the latter will be referred to as the 90° setup. The purity of the ^{68}Cu^{m} source was monitored through the lifetime measurement by measuring γ rays with a Ge detector.

The BaF_2 scintillator was mounted on a Hamamatsu-H3378 photomultiplier tube and the time pickoff signals were generated by an ORTEC-583 constant fraction discriminator. An ORTEC-567 time-to-amplitude converter (TAC) was employed and was calibrated using an ORTEC-462 time calibrator. The γ-γ-t coincidence data were recorded event by event. An energy resolution was 9% for the 570-keV γ ray of ^{207}Bi. A typical time resolution of this system was 130 ps at full width at half maximum for the 1173-1332 keV γ-ray cascade of ^{60}Co.

A γ-ray singles measurement was performed in order to obtain the γ-ray energies and intensities in ^{68}Cu using an n type Ge detector of 33% relative efficiency. The distance between the source and the surface of the detector was 102 mm. No β-absorber was placed on this detector. The detection efficiency of the Ge detector was calibrated using a standard source of ^{152}Eu, ^{133}Ba, and ^{207}Bi, and was corrected for the self-absorption in the ^{68}Zn target. This absorption was estimated on the basis of the attenuation of the γ-ray intensities measured by putting the standard sources on the ^{68}Zn target.

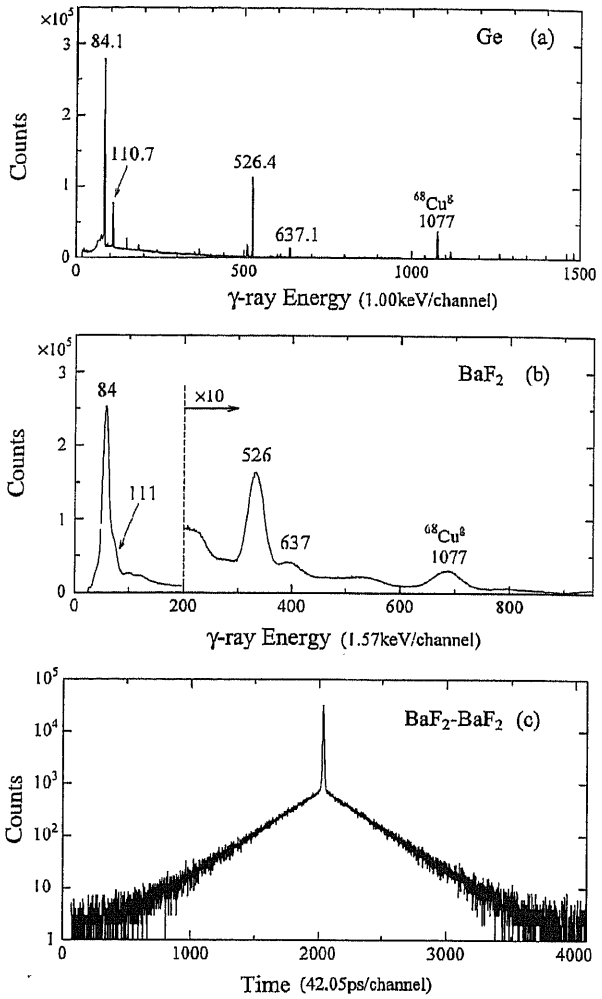

FIG. 1. (a) A γ-ray singles spectrum measured with a Ge detector. The γ-ray energies are depicted for the transitions descending from ^{68}Cu^{m}. The 1077-keV γ ray follows the β decay of the ground state in ^{68}Cu. (b) A γ-ray singles spectrum measured with a BaF_2 detector. (c) A time spectrum measured by the BaF_2-BaF_2-t coincidence with no gates on γ rays.

III. RESULTS

Figures 1(a) and 1(b) show γ-ray singles spectra measured with the Ge detector and with the BaF_2 detector, respectively, in the lifetime measurement. Most of the γ rays observed in the spectra are emitted by ^{68}Cu^{m}. Since the ground state of ^{68}Cu decays to ^{68}Zn with $T_{1/2}$=31 s, the γ rays in ^{68}Zn also appear in these spectra. Although γ rays following the β decay of ^{67}Cu ($T_{1/2}$=62 h), ^{65}Ni ($T_{1/2}$ =2.5 h), and ^{69}Zn ($T_{1/2}$=14 h) are also observed, these contributions are small. Figure 1(c) shows a time spectrum measured with the BaF_2 detectors. It is remarkable that more than half of the coincidence events are due to the decay with a long lifetime for the 84-keV level.

The decay scheme of ^{68}Cu^{m} is shown in Fig. 2. Coincidence relationships measured in this work are consistent with the previous scheme [28]. Spin-assignment of the 611-keV level will be discussed in Sec. IV. Figure 3(a) shows a γ-ray spectrum coincident with the 526-keV γ-ray energy (including the Compton continuum under the peak) and with the delayed part, between 4 ns and 87 ns from the prompt peak, of the TAC spectrum. This spectrum was derived from the data of the 180° setup. Figure 3(b) is a γ-ray spectrum coincident with the 526 keV energy and with the prompt part between −0.4 ns and +0.4 ns, derived from the data of the 90° setup. In Fig. 3(a), no other components except for the 84 keV peak are observed. This fact warrants the following lifetime analysis for the 84-keV level.

Decay curves for the 84-keV level were obtained by setting gates on a combination of γ-ray energies measured with the BaF_2 detectors. Figure 4(a) shows those curves derived from the data of the 180° setup by setting the gates of 526–84 keV and 637–84 keV. The experimental data were fitted with an exponential decay curve, $a\exp(-\lambda t)$, by a least squares method and the fitted lines are drawn, as shown in Fig. 4(a), in the range where the experimental data were used

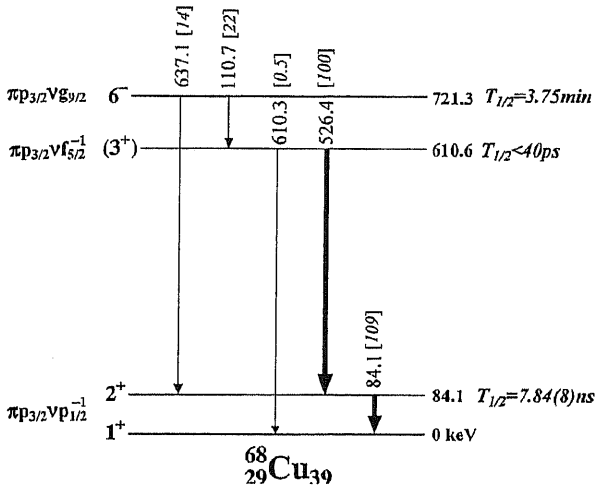

FIG. 2. A decay scheme of $^{68}Cu^{m}$. The γ-ray and level energies are in units of kilo-electron-volt. Relative intensities are shown in brackets. The lifetime of the 6^- isomer is taken from Ref. [28].

as the input values. We deduced the lifetime of the 84-keV level from the slopes of these fitted lines as well as from those of the decay curves gated on 111–84 keV. All the values of the slopes for the six decay curves are the same within measured uncertainties. Furthermore, the decay curves measured with the 90° setup give the same result. Consequently, we determined that the lifetime of this level is $T_{1/2}$ =7.84(8) ns. This error was estimated from the spread of all the values obtained in the experiment and from the variation of the values resulting from changing the fitting range. We also ascertained that the contaminant with a long lifetime component is negligible by fitting the experimental data with a curve consisting of an exponential decay and a constant background, $a\exp(-\lambda t)+b$.

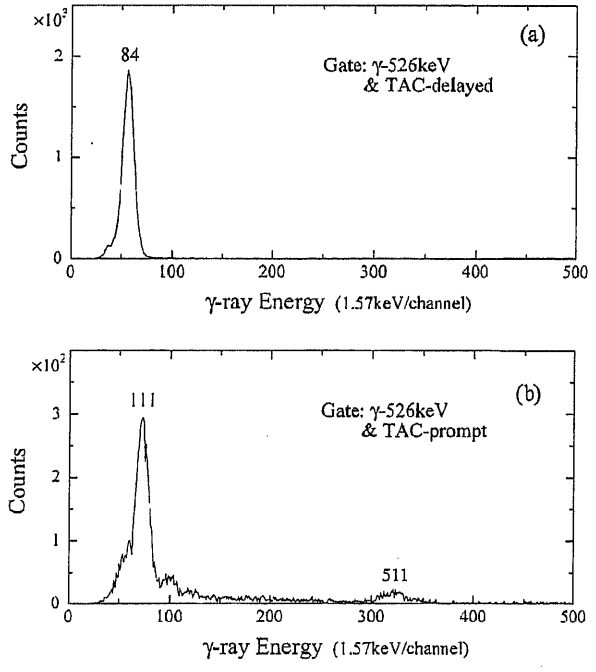

FIG. 3. (a) A γ-ray spectrum in coincidence with the 526-keV γ-ray energy and with the delayed part, between 4 ns and 87 ns from the prompt peak, of the TAC spectrum. (b) A γ-ray spectrum in coincidence with the 526-keV γ-ray energy and with the prompt part between −0.4 ns and +0.4 ns.

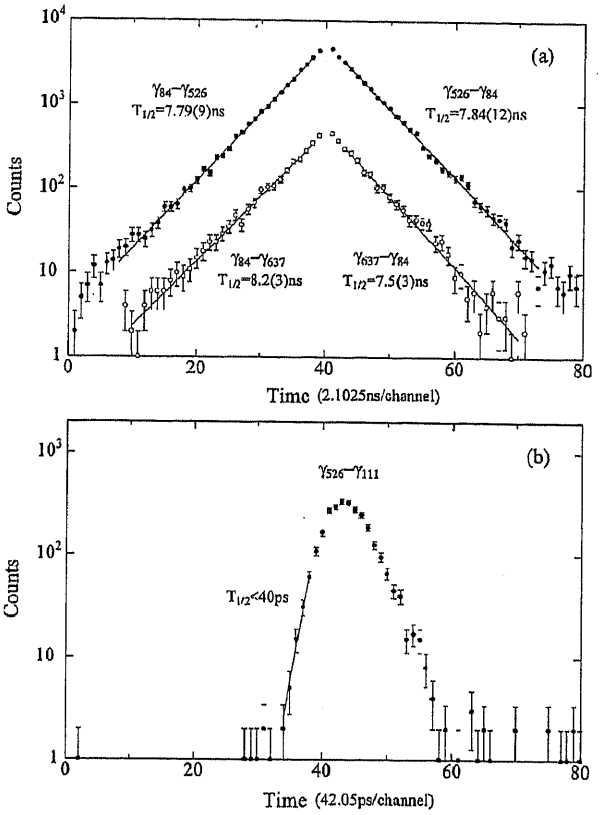

FIG. 4. (a) Decay curves due to the lifetime of the 84-keV level obtained by setting the gates on the γ-ray combinations of 526–84 keV and 637–84 keV. The lines fitted to an exponential decay are drawn in the fitting ranges. (b) A time spectrum for the 611-keV level obtained by the gate on the 526-keV γ-ray energy (start signal) and the 111-keV γ-ray energy (stop signal). The slope of the line drawn in this figure gives an upper limit for the lifetime of the 611-keV level.

Figure 4(b) shows a time spectrum obtained by setting the gate on the combination of the 526 keV energy (start signal) and the 111 keV energy (stop signal). This spectrum was derived from the data of the 90° setup. Although this time spectrum includes a component of the Compton continuum under the 111-keV peak as shown in Fig. 3(b), this contribution is only about 10%. Thus, the slope of the line drawn in this figure allows us to deduce an upper limit of 40 ps for the halflife of the 611-keV level.

γ-ray energies and intensities in ^{68}Cu are summarized in Table I. We derived the γ-ray intensities by taking into account the cascade summing effect, although the correction resulting from this effect was about 1% except for the weak 610-keV transition. The intensity of the 610-keV γ ray has a

TABLE I. γ-ray energies and intensities in ^{68}Cu.

E_γ (keV)	I_γ			α_T		
Present work	Present work	Swindle[a]	Tikku[b]	Present work	Swindle[a]	Tikku[b]
84.12(6)	109(4)	96.4(58)	95(5)	0.05(4)	0.156(25)	0.21(7)
110.74(6)	22.2(7)	22.3(13)	24.3(16)	3.52(12)		3.19(22)
526.44(6)	100	100	100			
610.3(3)	0.5(2)	1.4(4)	1.7(5)			
637.14(6)	14.3(4)	11.2(15)	14.7(15)			

[a]Reference [21].
[b]Reference [22].

large error, because it was corrected by considering the sum peak of the 526-keV and the 84-keV γ rays as well as the overlapped 609-keV γ ray following the decay of ^{214}Bi in the room background. The internal conversion coefficients (ICCs) calculated from the γ-ray intensity balance are also given in Table I. Intensities and ICCs in the previous work [21,22] are shown in this table for comparison.

IV. DISCUSSION

We first clarify the difference between the present results and those of previous reports [21,22]. The 611-keV level was previously proposed as 3^- on the basis of the ICC and the lifetime of the 111-keV transition [21,22]. However, the ICC of this transition α_T=3.52(12) only supports this transition as $M3$ or $E3$; a theoretical α_T is 3.71 and 3.75 for an $M3$ and an $E3$ transition, respectively [29]. The transition rate of the 111-keV γ ray corresponds to 1.0 W.u. and 0.02 W.u. for $M3$ and $E3$, respectively. There is no reason this transition rate favors an $M3$ multipolarity. We would rather propose that the spin parity of this level is 3^+ on the basis of the following shell model consideration. Low-lying negative-parity states in ^{68}Cu should have the $\pi p_{3/2}\nu g_{9/2}$ configuration. All the quartet members of this configuration were clearly observed by the $(t,{}^3\mathrm{He})$ transfer reaction [23]; the 6^- isomer is a member of this quartet and the other members lie above this isomer. Moreover, our recent experiment using heavy-ion deep-inelastic collisions suggests that one of the quartet members at 777 keV has the spin parity of 3^- [25]. On the other hand, the 3^+ state with the $\pi p_{3/2}\nu f_{5/2}^{-1}$ configuration very plausibly exists at 611 keV, because the $\nu f_{5/2}^{-1}$ state lies at 694 keV in the neighboring nucleus ^{67}Ni [3].

The intensity of the 84-keV γ ray measured by the present work is also different from the previous ones [19–22]. This intensity affects the estimation of the $B(M1)$ value of the 84-keV transition, because the $E2/M1$ mixing ratio of this transition is deduced from the ICC derived from the γ-ray intensity balance. Since all the previous data were measured in the early 1970s, one of the most likely reasons for this discrepancy is that the efficiency calibration of a Ge(Li) detector had a large error in the 80 keV energy region. To obtain a detection efficiency at about 80 keV, one usually uses the standard intensity of the 79.6- and 81.0-keV γ line of the ^{133}Ba source. This intensity in the references compiled in 1970s [30,31] was smaller than the present one [32] by about 10%. Therefore, the 1970s data of the 84-keV intensity would become smaller than that in the present result.

Now we discuss the $B(M1;2^+\rightarrow 1^+)$ value of the 84-keV transition. From the present result of the ICC of the 84-keV transition, α_T=0.05(4), we regard this transition as a pure $M1$ multipolarity; a theoretical α_T is 0.086 and 1.18 for a pure $M1$ and $E2$ transition, respectively [29]. Then, the $B(M1)$ value is obtained as $0.00777(8)\mu_N^2$, or 1/230 W.u., from the measured lifetime of the 84-keV level and the theoretical α_T for the pure $M1$ transition.

The $B(M1)$ value can be estimated by a shell model calculation which takes the core to be ^{68}Ni and uses experimental g factors of neighboring nuclei. The $B(M1)$ value with one proton (j_π) and one neutron (j_ν) outside the core is calculated as

$$B(M1;I_i\rightarrow I_f)=\frac{3}{4\pi}(2I_f+1)j_\pi(j_\pi+1)(2j_\pi+1)\times W^2(j_\nu j_\pi I_f 1;I_i j_\pi)\times(g_\pi-g_\nu)^2, \quad (1)$$

where g_π and g_ν are g factors of the j_π proton and the j_ν neutron, respectively [33]. The $B(M1)$ value of the 84-keV transition between the $\pi p_{3/2}\nu p_{1/2}^{-1}$ doublets is

$$B(M1;2^+\rightarrow 1^+)=\frac{3}{4\pi}\times\frac{3}{8}\times(g_\pi-g_\nu)^2=0.0427\mu_N^2, \quad (2)$$

where g_π=1.893μ_N and g_ν=1.202μ_N are taken from the experimental values of the $3/2^-$ ground state in $^{69}_{29}\mathrm{Cu}_{40}$ and the $1/2^-$ ground state in $^{67}_{28}\mathrm{Ni}_{39}$, respectively [13]. This calculation reproduces a small $B(M1)$ value, which originates from the cancellation of $g_\pi-g_\nu$. The g factor of the 1^+ ground state in ^{68}Cu was also measured recently by a laser-ion-source technique to be +2.48(2)(7)μ_N [24]. This g factor is calculated as

$$g(1^+)=\frac{1}{4}(5g_\pi-g_\nu)=+2.07\mu_N. \quad (3)$$

Thus, the calculation in the $\pi p_{3/2}\nu p_{1/2}^{-1}$ model space provides a good description of these $M1$ matrix elements in ^{68}Cu, using no free parameters. These results are shown in Table II as Cal-A. However, it is difficult to adjust the calculation more accurately for both the $B(M1)$ value and the g factor by only changing the g_π and g_ν effectively.

TABLE II. Shell model calculations of the $M1$ matrix elements in ^{67}Ni, ^{69}Cu, and ^{68}Cu. All the values in the table are in units of μ_N. Cal-A, $\pi p_{3/2}\nu p_{1/2}^{-1}$ model space using the experimental $g(1/2^-)$ value of ^{67}Ni and $g(3/2^-)$ value of ^{69}Cu. Cal-$B1$, $(p_{3/2}f_{5/2}p_{1/2})^n$ model space. Cal-$B2$, $f_{7/2}^{-r}(p_{3/2}f_{5/2}p_{1/2})^{n+r}(r=0, 1)$ model space. Two-body interactions used in Cal-$B1$ and Cal-$B2$ are described in the text.

Nucleus		Cal-A	Cal-$B1$	Cal-$B2$	Expt.
$^{67}_{28}Ni_{39}$	$g(1/2^-)$		1.28	0.93	1.20(1)[a]
$^{69}_{29}Cu_{40}$	$g(3/2^-)$		2.53	2.08	1.89(1)[a]
	$g(1^+)$	2.07	2.76	2.60	2.48(2)(7)[b]
$^{68}_{29}Cu_{39}$	$g(2^+)$	1.72	1.89	1.37	
	$\lvert\langle 2^+\lVert M1\rVert 1^+\rangle\rvert$	0.46	1.04	0.59	0.197(1)

[a]Reference [13].
[b]Reference [24].

This difficulty indicates a limit of this calculation using a minimum model space.

We have further studied the nuclear structure of ^{68}Cu by a shell model calculation in a fp model space. To investigate the effect of a $f_{7/2}$ particle excitation, a shell model calculation of the $(p_{3/2}f_{5/2}p_{1/2})^n$ model space was compared with that of the $f_{7/2}^{-r}(p_{3/2}f_{5/2}p_{1/2})^{n+r}(r=0, 1)$ model space. In the former calculation Cal-$B1$, the MSDI two-body interactions by Koops-Glaudemans were used [34]. In the latter calculation Cal-$B2$, two-body interactions derived from the folded diagram theory were used and single-particle energies were adjusted to reproduce low-lying levels in ^{67}Ni and ^{68,69}Cu. The results are summarized in Table II. In Cal-$B1$, the g factors of the $1/2^-$ state in ^{67}Ni and of the $3/2^-$ state in ^{69}Cu correspond to the Schmidt values of the $\nu p_{1/2}$ and the $\pi p_{3/2}$ single-particle states, respectively. In Cal-$B2$, the $g(3/2^-)$ value of ^{69}Cu is close to the experiment, while the $g(1/2^-)$ value of ^{67}Ni is slightly smaller than the experimental value.

These calculations give a measure of the purity of the $\pi p_{3/2}\nu p_{1/2}^{-1}$ doublet states in ^{68}Cu; the amplitude of the $\pi p_{3/2}\nu p_{1/2}^{-1}$ component in the 1^+ ground state is 0.91 and 0.78 in Cal-$B1$ and Cal-$B2$, respectively. The $g(1^+)$ value of ^{68}Cu in Cal-$B2$ is as large as that in Cal-$B1$. This is in contrast to the Cal-A result giving a smaller value than the experiment. On the other hand, the reduced matrix element of $\langle 2^+\lVert M1\rVert 1^+\rangle$ in Cal-$B2$ is much smaller than that in Cal-$B1$. These calculations show that this matrix element comprises the components originating from protons and from neutrons having a comparable magnitude but an opposite sign and that the difference between these components in Cal-$B2$ is smaller than that in Cal-$B1$. Therefore, this $\langle 2^+\lVert M1\rVert 1^+\rangle$ matrix element has a small value and is sensitive to a $f_{7/2}$ particle excitation. Although the experimental $\langle 2^+\lVert M1\rVert 1^+\rangle$ value is still smaller than the Cal-$B2$ result, the calculation may be improved by extending the model space to include the excitation to a $g_{9/2}$ orbital.

V. CONCLUSION

We have measured the lifetime of the first excited state in ^{68}Cu through the γ decay of ^{68}Cu^m produced by the ^{68}Zn(n,p) reaction using 14-MeV neutrons. We obtained a small $B(M1)$ value between the $\pi p_{3/2}\nu p_{1/2}^{-1}$ doublet states in ^{68}Cu. A parameter-free shell model calculation taking the core as ^{68}Ni gives a good prediction of this $B(M1)$ value by using experimental g factors of the $1/2^-$ state in ^{67}Ni and the $3/2^-$ state in ^{69}Cu. Both the $B(M1;2^+\rightarrow 1^+)$ and the $g(1^+)$ values in ^{68}Cu can be explained by a shell model calculation in the fp model space including a $f_{7/2}$ particle excitation.

ACKNOWLEDGMENTS

We would like to acknowledge Dr. T. Nishitani, the group leader of FNS, and the staff of FNS for supporting this experiment. We also thank Dr. A. Taniguchi for important suggestions regarding BaF_2 detectors and also thank Dr. Y. Kasugai for his advice on experiments using fast neutrons. We are grateful to Prof. K. Kawade for his fruitful discussions as well as for kindly allowing us to use the pneumatic tube system. One of us (L.H.) was supported by the MEXT scientist exchange program 2001.

[1] M. Bernas, Ph. Dessagne, M. Langevin, J. Payet, F. Pougheon, and P. Roussel, Phys. Lett. **113B**, 279 (1982).
[2] M. Girod, Ph. Dessagne, M. Bernas, M. Langevin, F. Pougheon, and P. Roussel, Phys. Rev. C **37**, 2600 (1988).
[3] T. Pawłat, R. Broda, W. Królas, A. Maj, M. Zięblíński, H. Grawe, R. Schubart, K. H. Maier, J. Heese, H. Kluge, and M. Schramm, Nucl. Phys. **A574**, 623 (1994).
[4] R. Broda *et al.*, Phys. Rev. Lett. **74**, 868 (1995).
[5] R. Grzywacz *et al.*, Phys. Rev. Lett. **81**, 766 (1998).
[6] S. Franchoo *et al.*, Phys. Rev. Lett. **81**, 3100 (1998).
[7] T. Ishii, M. Asai, I. Hossain, P. Kleinheinz, M. Ogawa, A. Makishima, S. Ichikawa, M. Itoh, M. Ishii, and J. Blomqvist, Phys. Rev. Lett. **81**, 4100 (1998).
[8] J. I. Prisciandaro, P. F. Mantica, A. M. Oros-Peusquens, D. W. Anthony, M. Huhta, P. A. Lofy, and R. M. Ronningen, Phys. Rev. C **60**, 054307 (1999).
[9] W. F. Mueller *et al.*, Phys. Rev. Lett. **83**, 3613 (1999).
[10] T. Ishii, M. Asai, A. Makishima, I. Hossain, M. Ogawa, J. Hasegawa, M. Matsuda, and S. Ichikawa, Phys. Rev. Lett. **84**, 39 (2000).
[11] W. F. Mueller *et al.*, Phys. Rev. C **61**, 054308 (2000).
[12] M. Asai, T. Ishii, A. Makishima, I. Hossain, M. Ogawa, and S. Ichikawa, Phys. Rev. C **62**, 054313 (2000).
[13] J. Rikovska *et al.*, Phys. Rev. Lett. **85**, 1392 (2000).
[14] A. M. Oros-Peusquens and P. F. Mantica, Nucl. Phys. **A669**, 81 (2000).
[15] O. Sorlin *et al.*, Phys. Rev. Lett. **88**, 092501 (2002).
[16] G. Georgiev *et al.*, J. Phys. G **28**, 2993 (2002).
[17] H. Grawe *et al.*, Nucl. Phys. **A704**, 211c (2002).
[18] O. Monnoye, S. Pittel, J. Engel, J. R. Bennett, and P. Van

Isacker, Phys. Rev. C **65**, 044322 (2002).
[19] T. E. Ward, H. Ihochi, and J. L. Meason, Phys. Rev. **188**, 1802 (1969).
[20] H. Singh, V. K. Tikku, B. Sethi, and S. K. Mukherjee, Nucl. Phys. **A174**, 426 (1971).
[21] D. L. Swindle, N. A. Morcos, T. E. Ward, and J. L. Meason, Nucl. Phys. **A185**, 561 (1972).
[22] V. K. Tikku and S. K. Mukherjee, J. Phys. G **1**, 446 (1975).
[23] J. D. Sherman, E. R. Flynn, Ole Hansen, Nelson Stein, and J. W. Sunier, Phys. Lett. **67B**, 275 (1977).
[24] L. Weissman *et al.*, Phys. Rev. C **65**, 024315 (2002).
[25] T. Ishii, M. Asai, P. Kleinheinz, M. Matsuda, A. Makishima, T. Kohno, and M. Ogawa, JAERI-Review Report No. 2002-029, 2002, p. 25.
[26] T. Ishii, M. Itoh, M. Ishii, A. Makishima, M. Ogawa, I. Hossain, T. Hayakawa, and T. Kohno, Nucl. Instrum. Methods Phys. Res. A **395**, 210 (1997).
[27] K. Kawade, H. Yamamoto, T. Yamada, T. Katoh, T. Iida, and A. Takahashi, JAERI-M Report No. 90-171, 1990.
[28] R. B. Firestone and V. S. Shirley, *Table of Isotopes*, 8th ed. (Wiley, New York, 1996).
[29] I. M. Band, M. B. Trzhaskovskaya, and M. A. Listengarten, At. Data Nucl. Data Tables **18**, 433 (1976).
[30] E. A. Henry, Nucl. Data Sheets **11**, 495 (1974).
[31] C. M. Lederer and V. S. Shirley, *Table of Isotopes*, 7th ed. (Wiley, New York, 1978), Appendixes-3.
[32] T. Horiguchi, T. Tachibana, H. Koura, and J. Katakura, *Chart of the Nuclides 2000* (Nuclear Data Center, JAERI, 2000).
[33] R. D. Lawson, *Theory of the Nuclear Shell Model* (Clarendon, Oxford, 1980), Chap. 5.
[34] J. Koops and P. M. W. Glaudemans, Z. Phys. A **280**, 181 (1977).

PHYSICAL REVIEW C 70, 054322 (2004)

Patterns of the ground states in the presence of random interactions: Nucleon systems

Y. M. Zhao,[1,2,3,*] A. Arima,[4] N. Shimizu,[5,†] K. Ogawa,[6,‡] N. Yoshinaga,[7,§] and O. Scholten[8,‖]
[1]*Department of Physics, Shanghai Jiao Tong University, Shanghai 200030, China*
[2]*Cyclotron Center, Institute of Physical Chemical Research (RIKEN), Hirosawa 2-1, Wako-shi, Saitama 351-0198, Japan*
[3]*Department of Physics, Southeast University, Nanjing 210018, China*
[4]*Science Museum, Japan Science Foundation, 2-1 Kitanomaru-koen, Chiyodaku, Tokyo 102-0091, Japan*
[5]*Department of Physics, University of Tokyo, Bunkyo-ku, Tokyo 113-0033, Japan*
[6]*Department of Physics, Chiba University, Yayoi-cho 1-33, Inage, Chiba 263-8522, Japan*
[7]*Department of Physics, Saitama University, Saitama 338, Japan*
[8]*Kernfysisch Versneller Instituut, University of Groningen, 9747 AA Groningen, The Netherlands*
(Received 16 April 2004; published 29 November 2004)

We present our results on properties of ground states for nucleonic systems in the presence of random two-body interactions. In particular, we calculate probability distributions for parity, seniority, spectroscopic (i.e., in the laboratory frame) quadrupole moments, and discuss α clustering in the ground states. We find that the probability distribution for the parity of the ground states obtained by a two-body random ensemble simulates that of realistic nuclei with $A \geq 70$: positive parity is dominant in the ground states of even-even nuclei, while for odd-odd nuclei and odd-mass nuclei we obtain with almost equal probability ground states with positive and negative parity. In addition, assuming pure random interactions, we find that, for the ground states, low seniority is not favored, no dominance of positive values of spectroscopic quadrupole deformation is observed, and there is no sign of α-clustering correlation, all in sharp contrast to realistic nuclei. Considering a mixture of a random and a realistic interaction, we observe a second-order phase transition for the α-clustering correlation probability.

DOI: 10.1103/PhysRevC.70.054322 PACS number(s): 21.60.Ev, 21.60.Fw, 05.30.Jp, 24.60.Lz

I. INTRODUCTION

It was discovered in Ref. [1] that the dominance of spin-zero ground states (0 g.s.) can be obtained by diagonalizing a scalar two-body Hamiltonian with random valued matrix elements, a so-called two-body random ensemble (TBRE) Hamiltonian. The 0 g.s. dominance was soon confirmed in Ref. [2] for *sd*-boson systems. This feature was found to be robust and insensitive to the detailed statistical properties of the random Hamiltonian, suggesting that the 0 g.s. dominance holds for a very large ensemble of two-body interactions other than a simple monopole paring interaction. An understanding of this discovery is very important, because this observation seems to be contrary to what is traditionally assumed in nuclear physics, where the 0 g.s. dominance in even-even nuclei is usually explained as a reflection of attractive pairing interaction between like nucleons.

There have been many efforts to understand this observation, but a fundamental understanding is still out of reach [3]. There are also many works [4] studying other robust phenomena of many-body systems in the presence of the TBRE, for example the studies of odd-even staggering of binding energies, generic collectivity, the behavior of energy centroids of fixed spin states, correlations, etc.

The purpose of the present paper is to focus our attention on some physical quantities in the ground states which have not been studied yet, specifically parity, seniority, spectroscopic quadrupole moments (i.e., measured in the laboratory frame), and α-clustering probability. For realistic nuclei, these quantities show a very regular pattern. In this paper, we shall discuss whether these regular patterns are robust in the presence of random interactions.

As is well known, all even-even nuclei have positive-parity ground states (i.e., 100%), whereas the ground states of nuclei with odd mass numbers have only a slightly higher probability for positive parity than for negative parity. Odd-odd nuclei have almost equal probabilities for positive- and negative-parity ground states ($\sim$50%). The statistics for the ground-state parity of nuclei with mass number $A \geq 70$ are summarized in Table I. As the first subject, we will study the ground-state parity distribution using random interactions.

TABLE I. The positive parity distribution of the ground states of atomic nuclei. We included all ground-state parities of nuclei with mass number $A \geq 70$. The data are taken from Ref. [5]. We have not taken into account those nuclei for which the ground-state parity was not measured.

Counts	Even-even	Odd-A	Odd-odd
verified (+)	487	281	118
verified (−)	0	215	104
tentative (+)	0	159	70
tentative (−)	0	126	60

*Electronic address: ymzhao@riken.jp
†Electronic address: shimizu@nt.phys.s.u-toyo.ac.jp
‡Electronic address: ogawa@physics.s.chiba-u.ac.jp
§Electronic address: yosinaga@phy.saitama-u.ac.jp
‖Electronic address: scholten@kvi.nl

The next subject that we shall discuss in this paper is the distribution of seniority in the ground states. Seniority [6] has been proven to be a very relevant concept in nuclear physics, in particular for spherical or transitional nuclei. Seniority (v) is uniquely defined for a single-j shell; it was generalized to the case of many-j shells by Talmi in Ref. [7]. In Refs. [1,8] it was reported that the pairing phenomenon seems to be favored simply as a consequence of the two-body nature of the interaction. The "pairing" of Refs. [1,8] was characterized by a large matrix element of the S pair annihilation operator between the ground states of an n fermion system and an $n-2$, $n-4$,... system, where the S pair structure is determined by using the procedure of Talmi's generalized seniority scheme. This indicated that the S-pair correlation is dominant for the spin-0 g.s. of these systems. However, an examination of this "pairing" correlation of fermions in a single-j shell in Ref. [9] showed that an enhanced probability for low seniority in the spin-0 g.s. is not observed in most of the calculations using a TBRE Hamiltonian. For many-j shells, there have been only a few discussions to clarify this point so far.

Another subject that we shall discuss is the α-clustering correlation in the presence of random interactions. The importance of the α-clustering correlation in light and medium nuclei has been emphasized by many authors [10]. The α-clustering correlation also plays an important role in astrophysical processes, such as the Salpeter process in the formation of ^{12}C. Many calculations of low-lying states, using the antisymmetrized molecular-dynamics model, have been done in recent years [11] to study the α-clustering and other clustering correlations for both stable and unstable light nuclei. α-cluster condensation was suggested by Horiuchi, Schuck, and collaborators in Ref. [12]. As a function of the admixture of a realistic to the TBRE interaction, a phase transition is observed for the α-clustering probability in the ground state.

In this paper, we also discuss the spectroscopic quadrupole moments (i.e., measured in the laboratory frame) of the ground states. A positive value of spectroscopic quadrupole deformation is dominant in the low-lying states of atomic nuclei. Recently, it has been argued in Ref. [13] that this is due to the interference of spin-orbit and l^2 terms of the Nilsson potential.

Our calculations are based on the use of TBRE interactions. The single-particle energies are set to be zero. The Hamiltonian that we use conserves the total angular momentum and isospin,

$$H=\sum_{j_1j_2j_3j_4}^{JT}\sqrt{2J+1}\sqrt{2T+1}G^{JT}_{j_1j_2j_3j_4}\frac{1}{\sqrt{1+\delta_{j_1j_2}}\sqrt{1+\delta_{j_3j_4}}}\times[(a^{\dagger}_{j_1t}\times a^{\dagger}_{j_2t})^{(JT)}\times(\tilde{a}_{j_3t}\times\tilde{a}_{j_4t})^{(JT)}]^{(00)}, \quad (1)$$

where the $G^{JT}_{j_1j_2j_3j_4}$ are defined as $\langle j_1j_2JT|V|j_3j_4JT\rangle$ and follow the following distribution:

$$\rho(G^{JT}_{j_1j_2j_3j_4})=\frac{1}{\sqrt{2\pi}x}\exp\left(-\frac{(G^{JT}_{j_1j_2j_3j_4})^2}{2x}\right) \quad (2)$$

with

$$x=\begin{cases}1 & \text{if } |(j_1j_2)JT\rangle=|(j_3j_4)JT\rangle\\ \frac{1}{2} & \text{otherwise.}\end{cases} \quad (3)$$

The Hamiltonian so defined is called a TBRE Hamiltonian. Here j_1, j_2, j_3, and j_4 denote the respective single-particle orbits, and $J(T)$ denotes the total angular momentum (isospin) of two nucleons. For each system, 1000 runs of calculations are performed in order to accumulate stable statistics.

This paper is organized as follows. In Sec. II, we present our results for parity distributions for a variety of systems. In Sec. III, we discuss the distribution of seniority in the ground states using random interactions. In Sec. IV, we show our results for spectroscopic quadrupole moments of the ground states which suggest prolate or oblate shapes. In Sec. V, we discuss the α-clustering correlation in the ground states. A summary will be given in Sec. VI.

II. PARITY

We select four model spaces for studying the parity distribution in the ground states obtained by random interactions.

(A) Both protons and neutrons are in the $f_{5/2}p_{1/2}g_{9/2}$ shell, which corresponds to nuclei with both proton number Z and neutron number $N\sim 40$.

(B) Protons in the $f_{5/2}p_{1/2}g_{9/2}$ shell and neutrons in the $g_{7/2}d_{5/2}$ shell, which corresponds to nuclei with $Z\sim 40$ and $N\sim 50$.

(C) Both protons and neutrons are in the $h_{11/2}s_{1/2}d_{3/2}$ shell, which corresponds to nuclei with Z and $N\sim 82$.

(D) Protons in the $g_{7/2}d_{5/2}$ shell and neutrons in the $h_{11/2}s_{1/2}d_{3/2}$ shell, which corresponds to nuclei with $Z\sim 50$ and $N\sim 82$.

These four model spaces do not correspond to a complete major shell but have been truncated in order to make the calculations feasible. These truncations are based on the subshell structures of the involved single-particle levels. We study the dependence on valence-proton number N_p and valence-neutron number N_n in these four model spaces. It is noted that the numbers of states [denoted as $D(I)$] for positive and negative parity are very close to each other for all these examples. The $D(I)$'s for a few examples are shown in Fig. 1. One thus expects that the probability of the ground states with positive parity is around 50%, if one assumes that each state of the full shell model space is equally probable in the ground state.

The calculated statistics for the parity of the ground states, using a TBRE Hamiltonian, is given in Table II. This clearly shows that positive parity is favored, and dominant for most examples, for the ground states of even-even nuclei in the presence of random interactions.

The statistics for nuclei with odd mass numbers and nuclei with odd values of both N_p and N_n (the number of protons and the number of neutrons, respectively) is also given in Table II. These statistics show that the probabilities to have positive or negative parity in the ground states are almost equal to each other with some exceptions. In general, there is no favoring for either positive parity or negative

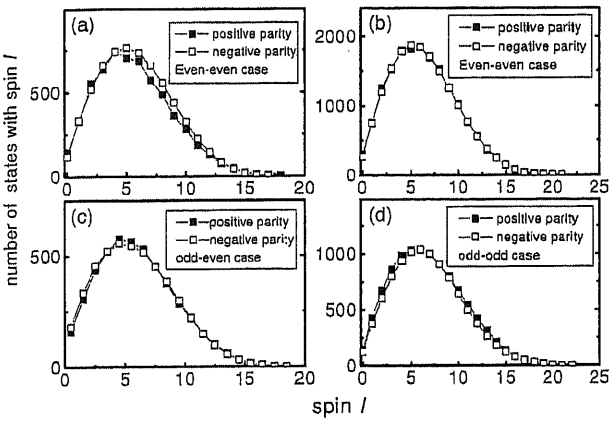

FIG. 1. Number of states with total angular momentum I [denoted as $D(I)$] vs I. One sees that the $D(I)$ of positive parity levels and that of negative parity levels are very close to each other. (a) Two protons in the $1g_{9/2}2p_{1/2}1f_{5/2}$ shell and four neutrons in the $2d_{5/2}1g_{7/2}$ shell; (b) two protons and two neutrons in the $1g_{9/2}2p_{1/2}1f_{5/2}$ shell; (c) two protons and three neutrons in the $1g_{9/2}2p_{1/2}1f_{5/2}$ shell; (d) three protons in the $1h_{11/2}3s_{1/2}2d_{5/2}$ shell and three neutrons in the $2d_{5/2}1g_{7/2}$ shell.

parity in the ground states of odd mass nuclei and doubly odd nuclei in the presence of random interactions. It is noted that these calculations are done for the beginning of the shell. For the end of the shell, the results show a similar trend.

TABLE II. The positive parity probability for the ground states (in %). Numbers of neutrons and protons (N_p,N_n) are given in parentheses for each configuration.

Basis A							
(0,4)	(0,6)	(2,2)	(2,4)	(2,6)			
86.8%	86.2%	93.1%	81.8%	88.8%			
(2,3)	(1,4)	(1,3)	(0,5)	(1,5)	(6,1)	(2,1)	
42.8%	38.6%	77.1%	45.0%	69.8%	38.4%	31.2%	
Basis B							
(2,2)	(2,4)	(4,2)					
72.7%	80.5%	81.0%					
(3,4)	(3,3)	(2,3)	(5,1)	(3,2)	(4,1)	(1,4)	(5,0)
42.5%	74.9%	72.4%	42.9%	39.1%	75.1%	26.4%	44.1%
Basis C							
(2,2)	(2,4)	(4,0)	(6,0)				
92.2%	81.1%	80.9%	82.4%				
(1,3)	(1,5)	(2,3)	(5,0)	(4,1)			
73.0%	64.4%	52.0%	42.6%	56.5%			
Basis D							
(2,2)	(4,2)	(2,4)	(0,6)				
67.2%	76.1%	74.6%	83.0%				
(3,3)	(3,2)	(2,3)	(0,5)				
54.5%	54.2%	54.0%	45.9%				

We also find that the above regularities for parity distributions also hold for very simple cases, namely single-closed two-j shells with one positive and one negative parity. We have checked this explicitly in the cases $(2j_1,2j_2)=(9,7)$, (11,9), (13,9), (11,3), (13,5), (19,15), (7,5), and (15,1). The statistics is very similar to the above results: The probability of ground states with positive parity is about 85% for an even number of nucleons, and about 50% for an odd number of nucleons.

It is interesting to note that for all even-even nuclei, the $P(0^+)$ is usually two orders of magnitude larger than $P(0^-)$. It would be very interesting to investigate the origin of this large difference, i.e., why the 0^- is not favored in the ground states. As is the case for an odd number of bosons with spin l [14], spin $I=0$ is *not* a sufficient condition to be favored in the ground states of a many-body system in the presence of the random interactions. It should be noted that for a realistic g.s., not only is $I=0$ required but also positive parity.

One simple and schematic system to study the parity distribution of the ground states in the presence of random interactions is the sp-boson system. First, we note that an sp-boson system with an odd number of particles (denoted as n) has the same number of states with positive and negative parity, and for an even value of n there are *slightly* more states with positive parity (the difference is only $n+1$). The calculated results of Ref. [15] showed that when the number n of sp bosons is even, the dominant I of the ground states is 0 or n (about 99%), with positive-parity dominance [the parity for sp bosons is given by $(-)^I$]. When n is odd, only about 50% of the ground states in the ensemble have spin 0, and about 50% have $I=1$ or $I=n$. This leads to about equal percentages for positive- and negative-parity ground states. This pattern is very similar to that observed for fermion systems.

III. SENIORITY

In this section, we discuss the distribution of the seniority, the number of particles not pairwise coupled to angular momentum 0, of the ground states of nuclei in the sd shell in the presence of random interactions. Because seniority is used in classifying the states in our basis, we define the expectation value for seniority in the ground states as follows [16]:

$$\langle v\rangle = \sum_i f_i^2 v_i, \tag{4}$$

where f_i is the amplitude of the ith component in the ground-state wave function, and v_i is the seniority number of the corresponding component.

For even-even nuclei, we consider the spin-0 g.s. because previous discussions [8,9] were focused on spin-0 ground states. For odd-mass nuclei, we consider the $I=\frac{1}{2}$, $\frac{3}{2}$, and $\frac{5}{2}$ ground states, because these spin I's are equal to the angular momenta of the single-particle levels in the sd shell and are favored as the ground states in the presence of random interactions. For odd-odd nuclei in this section we consider the ground states with $I=1$ (most favored) and $I=0$ states. The examples that we have calculated include $(N_p,N_n)=(0,4)$, (0,6), (2,2), (2,4), (2,6), (4,6), (0,5), (2,3), (2,5), (4,3), (4,5), (3,3), (1,5), and (3,5).

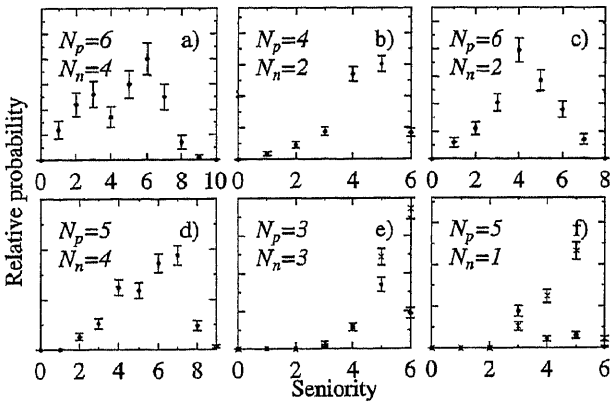

FIG. 2. Distribution of seniority in the ground states with spin zero for even-even nuclei [refer to panels (a), (b), and (c)], spin $I=j_1,j_2,j_3$ for the odd-A case [refer to panel (d)], or spin $I=1,0$ for odd-odd nuclei [refer to panels (e) and (f)]. The error bar is defined by the square root of the count (statistics) for each seniority bin (step width is 1). The dominance of seniority zero components of ground states is not observed.

Typical examples of the distribution of average seniority ($\langle v \rangle$) in the ground states are shown in Fig. 2 in arbitrary units (i.e., relative probability). The figure shows that for none of the cases is a small value for $\langle v \rangle$ preferred. These distributions of seniority in the ground states show that the large matrix elements of the S-pair operator between the spin-0 g.s. of an n-nucleon system and that of an $(n+2)$-nucleon system, as observed in Ref. [8], should not be understood as an indication of a large S pair condensate in the spin-0 g.s. of TBRE Hamiltonians. Further studies are necessary to understand the implications of Ref. [8].

IV. SPECTROSCOPIC QUADRUPOLE MOMENT

In this section, we study the quadrupole moments of the ground or low-lying states. If the ground-state spin I is smaller than 1 (i.e., 0 or $\frac{1}{2}$), the spectroscopic quadrupole moment necessarily vanishes (even though there could be a finite intrinsic moment) because the triangle relationship of angular momentum coupling cannot be obeyed by the two I's ($I \leqslant \frac{1}{2}$) and the angular momentum for the quadrupole operator (=2). For these cases, one can use an alternative, namely the quadrupole moment of the next lowest state with $I > \frac{1}{2}$. For all cases that we have checked, it is found that the essential statistics for positive and negative quadrupole moments obtained by this alternative is very close to that obtained by neglecting cases with ground state $I < \frac{1}{2}$. In this paper, we show the statistics which does not include the runs of spin-0 and spin-$\frac{1}{2}$ ground states. The total number of calculated spectroscopic quadrupole moments is thus much less than 1000. We note that a negative spectroscopic quadrupole moment implies a positive quadrupole moment in the intrinsic frame and thereby a prolate deformation.

The spectroscopic quadrupole moment is defined by

$$Q = \langle \beta I | r^2 Y_{2M} | \beta I \rangle \tag{5}$$

for both proton and neutron degrees of freedom. In Eq. (5), $|\beta I\rangle$ is the wave function of the ground state. In this paper, Q will be used to refer to the spectroscopic quadrupole moment following from Eq. (5).

We have calculated Q for a number of cases in the sd shell and for several fillings of the four single-particle bases mentioned in Sec. II. The results are given in Table III. One sees that negative values for Q (corresponding to prolate deformations) are dominant with two exceptions, $(N_p,N_n)=(4,3),(6,5)$ in the sd shell. In general we observe that for the sd shell, the statistics for positive and negative values for Q is comparable if N_p and/or N_n are close to their midshell values.

From Table III, we conclude that at the beginning of the shell, negative values for Q are dominant, while at the end of the shell, positive value dominate. This is similar to the result for a harmonic-oscillator potential, for which prolate deformation occurs at the beginning and oblate deformation at the end of the shell [17].

V. α CLUSTERING

It was shown in Ref. [18] that the essential parts of the $I=0,T=0$ ground state for ^{20}Ne with two protons and two neutrons in the sd shell are dominated by components with the highest orbital symmetry [4]; 91.8% of the ground state is given by components with orbital symmetry [4] which corresponds to a pure α-clustering configuration. One may use the expectation value of the Majorana interaction, P_M, as the fingerprint for the α-cluster wave function. Another similar example is the $I=0,T=0$ ground state for ^{8}Be with two protons and two neutrons in the p shell. If one uses the Cohen-Kurath interaction, one sees that the expectation value of P_M is -5.76, close to -6, which is the eigenvalue of Majorana force. The overlap between the g.s. wave function obtained by diagonalizing the Cohen-Kurath interaction for ^{8}Be and that for exact SU(4) symmetry (namely, full symmetry [4] for the ground state) is 0.97.[1] This dominance of the full symmetry [4] with respect to the permutation of orbital degrees of freedom in the $I=0$ and $T=0$ ground states of these nuclei is an indication of α-clustering correlation from the perspective of the shell model. In this paper, we concentrate on these two examples using random interactions.

To set the scale, we can calculate the matrix element of P_M in the $I=T=0$ (spin-isospin singlet) ground state by assuming that all the possible $I=T=0$ states with different symmetries with respect to the exchange of the orbital degrees of freedom appear at an equal probability. We call the P_M so obtained the geometric P_M. To do so, one needs the number of $(I=0,T=0)$ states for each orbital symmetry.

The procedure to construct the states with particular spin-isospin symmetry is given in Ref. [19], while that for constructing wave functions with certain orbital symmetry is given in Ref. [20] for the Elliott model [21], with tables for the sd, pf, and sdg shells. Finally, the spin-isospin functions should be coupled to the orbital functions with their conju-

[1] In this paper we set the single particle energies to zero. If we take the single particle energies of Cohen-Kurath interaction, this overlap becomes 0.99.

TABLE III. The number of cases with positive (negative) spectroscopic quadrupole moments are given in bold (*italic*) font, respectively. We omitted the cases for which the spin of the ground state is less than 1; see the text for further details.

Both protons and neutrons in the *sd* shell									
(N_p,N_n)		(2, 1)			(2, 3)			(2, 5)	
	280		*418*	**338**		*430*	**306**		*402*
(N_p,N_n)		(2, 1)			(4, 3)			(4, 5)	
	287		*425*	**434**		*374*	**320**		*370*
(N_p,N_n)		(6, 1)			(6, 3)			(6, 5)	
	201		*530*	**400**		*444*	**420**		*348*
Basis (A): protons and neutrons in $f_{5/2}p_{1/2}g_{9/2}$									
(N_p,N_n)		(1, 2)			(1, 3)			(1, 4)	
	267		*469*	**283**		*481*	**246**		*535*
(N_p,N_n)		(1, 6)			(2, 3)			(0, 5)	
	207		*566*	**284**		*564*	**447**		*459*
Basis (B): protons $(f_{5/2}p_{1/2}g_{9/2})$, neutrons $(g_{7/2}d_{5/2})$									
(N_p,N_n)		(1, 4)			(4, 1)			(2, 4)	
	374		*507*	**278**		*632*	**253**		*428*
(N_p,N_n)		(3, 4)			(4, 3)			(6, 1)	
	278		*620*	**330**		*560*	**233**		*660*
Basis (C): protons and neutrons in $s_{1/2}d_{3/2}h_{11/2}$									
(N_p,N_n)		(2, 3)			(2, 5)			(4, 3)	
	231		*657*	**238**		*472*	**392**		*498*
(N_p,N_n)		(5, 1)			(5, 0)			(3, 3)	
	213		*628*	**212**		*659*	**349**		*449*
Basis (D): protons $g_{7/2}d_{5/2}$, neutrons $s_{1/2}d_{3/2}h_{11/2}$									
(N_p,N_n)		(14, 13)			(15, 12)				
	781		*183*	**610**		*333*			

gate symmetry to obtain the fully antisymmetric wave functions with respect to an exchange of two particles. The angular momentum for each state is given by coupling S and L.

Table IV presents the number of $I=0$ states for two protons and two neutrons in the p shell and the sd shell with all possible orbital symmetries. From Table II, one obtains the geometric P_M for the $I=T=0$ states: P_M is $-\frac{6}{5}$ for the p shell and $-\frac{22}{21}$ for the sd shell.

Using a TBRE Hamiltonian, we obtain the following probabilities for spin-I ground states: For 1000 runs, one obtains 485 and 365 runs with $(I,T)=(0,0)$ ground states for ^{8}Be and ^{20}Ne, respectively. This is consistent with the result [1,8] of the $I=T=0$ g.s. dominance in the presence of random interactions. The average value of P_M for the $(I,T)=(0,0)$ g.s. that we obtain is -1.26 (the geometric value is $-\frac{6}{5}=-1.20$) and -1.66 (the geometric value is $-\frac{22}{21}=-1.05$) for the p shell and the sd shell, respectively. The average value of P_M for a TBRE Hamiltonian and the corresponding geometric value are very close to each other for the p shell, indicating that α-clustering correlation is not favored by random interactions. For the case of the sd shell, the average value of P_M for a TBRE Hamiltonian deviates sizably from its geometric value.

To check whether this deviation becomes larger for larger shells, we calculate the case of two protons and two neutrons in the sdg shell, for which we obtained 385 cases with $(I,T)=(0,0)$ ground states among 1000 sets of TBRE Hamiltonians. The average P_M value for these states is -0.629, while that obtained by assuming a random orbital symmetry is $-\frac{2}{5}$, which is close to the above value.

It is also interesting to study the distribution of overlaps between the $I=T=0$ ground state obtained from the realistic interactions and those obtained by pure random interactions or by a combination of realistic and random interactions. As an example, we discuss here the case of two protons and two neutrons in the p shell where the realistic interaction is chosen as the Cohen-Kurath interaction. We thus define a Hamiltonian

$$H=(1-\lambda)H_{\mathrm{TBRE}}+\lambda H_{\mathrm{real}}. \tag{6}$$

Here $\lambda=0$ corresponds to the pure TBRE Hamiltonian and $\lambda=1$ corresponds to the realistic Cohen-Kurath interaction.

TABLE IV. The number of $I=0$ states for two valence protons and two valence neutrons in the p shell and the sd shell with definite symmetry with respect to exchange orbital degree of freedom of two particles and the corresponding conjugate symmetry with respect to exchange spin-isospin ($S-T$) degrees of freedom. L is the total orbital angular momentum and S is the total spin. The last column gives number of the $I=0$ states with $T=0$.

L	S	$I=0$	$I=T=0$
	The p shell		
[4] 0,2,4	0	0	0
[31] 1,2,3	$0,1^2$	0^2	0
[22] 0,2	$0^2,1,2$	0^3	0^2
[211] 1	$0,1^3,2$	0^3	0
	The sd shell		
[4] $0^4,2^5,3,4^4,5,6^2,8$	0	0^4	0^4
[31] $0^2,1^4,2^7,3^6,4^5,5^3,6^2,7$	$0,1^2$	0^{10}	0^4
[22] $0^3,1,2^5,3^2,4^3,5,6$	$0^2,1,2$	0^{12}	0^8
[211] $1^5,2^3,3^5,4^2,5^2$	$0,1^3,2$	0^{18}	0^5
[1111] 1,2,3	0,1,2	0^2	

We will vary λ in the range from 0 to 1, corresponding to the situation of nuclear forces with different mixtures of random noise.

The results for $\lambda=0$, 0.3, 0.5, 0.7, and 0.9 are shown in Figs. 3(a)–3(e). The error bars indicate the statistical errors in determining the numbers, defined by the square root of the number of counts for each bin. For case (a) with $\lambda=0$ one sees that the overlaps distribute "randomly" from 0 to 1. This suggests that pure random interactions produce "random" overlaps of the $I=T=0$ ground states with the realistic ground state. However, for $\lambda>0.5$, the $I=T=0$ ground states are close to that of the realistic interactions for most of the cases. This is especially clear from Fig. 4, where the overlap, averaged over the different Hamiltonians in the ensemble Eq. (6), is plotted versus λ. The statistical inaccuracies are indicated by the error bars in this figure. For values of λ exceeding 0.6, the overlap is very close to unity, while for larger admixtures of the random component in the interaction, the overlap decreases approximately linearly with λ. This trend has all the signatures of a second-order phase transition. Only for limited magnitude of the random interaction does the g.s. have a realistic structure, which breaks down when a critical value is exceeded.

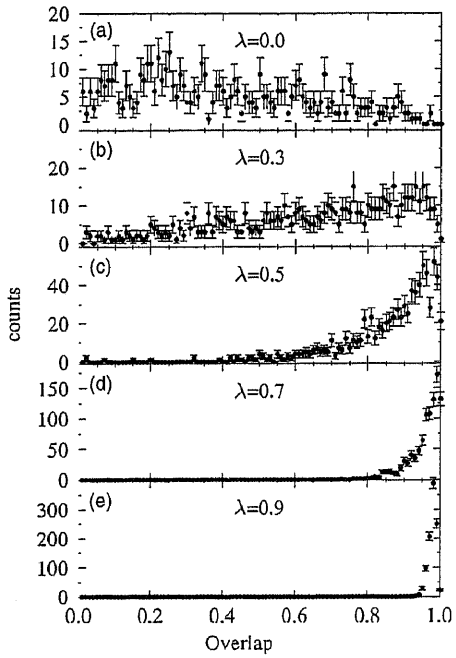

FIG. 3. The overlaps between the $I=T=0$ ground states for two protons and two neutrons in the p shell obtained by Cohen-Kurath interactions and those obtained by the Hamiltonian Eq. (6). (a)–(e) correspond to $\lambda=0$, 0.3, 0.5, 0.7, and 0.9, respectively.

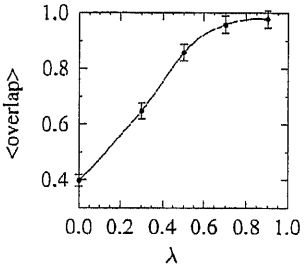

FIG. 4. Average overlap of the g.s. of the Hamiltonian of Eq. (6) with that of the realistic Hamiltonian as a function of the mixing parameter λ. The line is plotted to guide the eyes.

VI. DISCUSSION AND SUMMARY

The present paper was stimulated by the discovery of the spin-zero ground-state dominance (0 g.s.) of even fermion systems [1] and boson systems [2] in the presence of the random two-body ensemble (TBRE). This discovery sparked off a sudden interest in many-body systems under the TBRE. It also led to extensive studies of other physical quantities [4], such as energy centroid of fixed spin states, collectivity, etc. The purpose of this paper was to study the robustness of some features which are well known in nuclear physics but have not been studied under the TBRE.

First, we calculated in Sec. II the parity distribution of the g.s. for a TBRE Hamiltonian. It was found that positive parity is dominant for the g.s. of systems with even numbers of valence protons and neutrons. For odd-A and doubly odd systems, the TBRE Hamiltonian leads to ground states with comparable probability for both positive and negative parity. This is similar to the global statistics for realistic nuclei with $A \geq 70$ (refer to Table I). Unlike the spin-0 g.s. dominance in the presence of random interactions, the dominance of positive parity in the ground states of even-even nuclei has not been pointed out explicitly so far. Since parity is a much simpler quantity than angular momentum, an understanding of the parity dominance of even-even systems may be helpful in understanding the spin-0 g.s. dominance of even-even nuclei in the presence of random interactions.

Second, our investigation showed that the seniority distribution for the g.s. of *sd*-shell nuclei is not dominated by low seniority components, contrary to the situation for realistic nuclei. Our investigation also suggests that the correlation between the wave function of the spin-0 g.s. for A nucleons and that for $A+2$ nucleons discussed in Ref. [8] should not be understood as an indication of the dominance of the seniority zero component.

Third, the dominance of negative spectroscopic quadrupole moments at the beginning of the shell and positive quadrupole moments at the end of the shell is also observed in the g.s. obtained by using the TBRE interactions. This situation is similar to the prediction obtained from a simple harmonic-oscillator potential. This means that the TBRE Hamiltonians do not lead to an overall dominance of the prolate deformation. However, also in realistic nuclei a dominance of prolate deformation is observed when both valence protons and neutrons are in the first half of a major shell.

Last, we studied the α-clustering correlation by calculating the expectation value of the Majorana operator in the $I=0$, $T=0$ g.s. of TBRE interactions. We also calculated the overlaps between the $I=0$, $T=0$ ground states of the TBRE Hamiltonian and the ground state obtained from realistic interactions. Our calculations on ^{8}Be and ^{20}Ne showed that the α-clustering structure is not favored by a pure TBRE Hamiltonian. It is interesting to note that, as a function of the admixture of a realistic Hamiltonian to a TBRE Hamiltonian, a second-order phase transition is observed. For Hamiltonians that contain less than ~ 0.4 admixture of random interactions, the structure of the g.s. is close to the realistic case, but for higher admixtures the overlap with a realistic wave function becomes progressively worse.

In conclusion, we have observed in this paper the dominance of positive parity in the ground states of even-even nuclei in the presence of pure random two-body interactions. Because parity is intrinsically a simpler quantum number than angular momentum, it will be interesting to understand the mechanism for this. In addition, it has been shown that, even though the quantum numbers for the g.s. are realistic, the dynamical properties of the ground states under the TBRE Hamiltonian, such as seniority, which is a signature of pairing correlation, the α-clustering probabilities, and the sign of quadrupole moments, are in sharp disagreement with those of realistic nuclei.

ACKNOWLEDGMENTS

Part of this work was performed as part of the research program of the Stichting voor Fundamenteel Onderzoek der Materie (FOM) with financial support from the Nederlandse Organisatie voor Wetenschappelijk Onderzoek (NWO). This work was also supported in part by a Grant-in-Aid for Specially Promoted Research (Grant No. 13002001) from the Ministry of Education, Science and Culture in Japan. One of the authors (Y.M.Z.) acknowledges a grant from the NWO.

[1] C. W. Johnson, G. F. Bertsch, and D. J. Dean, Phys. Rev. Lett. **80**, 2749 (1998).

[2] R. Bijker and A. Frank, Phys. Rev. Lett. **84**, 420 (2000); Phys. Rev. C **62**, 014303 (2000).

[3] R. Bijker, A. Frank, and S. Pittel, Phys. Rev. C **60**, 021302 (1999); D. Kusnezov, N. V. Zamfir, and R. F. Casten, Phys. Rev. Lett. **85**, 1396 (2000); D. Mulhall, A. Volya, and V. Zelevinsky, *ibid.* **85**, 4016 (2000); Y. M. Zhao and A. Arima, Phys. Rev. C **64**, R041301 (2001); R. Bijker and A. Frank, *ibid.* **65**, 044316 (2002); P. H-T. Chau, A. Frank, N. A. Smirnova, and P. V. Isacker, *ibid.* **66**, R061302 (2002); V. Velazquez and A. P. Zuker, Phys. Rev. Lett. **88**, 072502 (2002); Y. M. Zhao, A. Arima, and N. Yoshinaga, Phys. Rev. C **66**, 034302 (2002); **66**, 064323 (2002); T. Papenbrock and H. A. Weidenmueller, Phys. Rev. Lett. **93**, 132503 (2004); for a recent review, Y. M. Zhao, A. Arima, and N. Yoshinaga, Phys. Rep. **400**, 1 (2004).

[4] D. Mulhall, A. Volya, and V. Zelevinsky, Phys. Rev. Lett. **85**, 4016 (2000); Lev Kaplan, Thomas Papenbrock, and Calvin W. Johnson, Phys. Rev. C **63**, 014307 (2001); M. Horoi, B. A. Brown, and V. Zelevinsky, Phys. Rev. Lett. **87**, 062501 (2001); M. Horoi, A. Volya, and V. Zelevinsky, Phys. Rev. C **66**, 024319 (2002); Y. M. Zhao, S. Pittel, R. Bijker, A. Frank, and A. Arima, *ibid.* **66**, R041301 (2002); Y. M. Zhao, A. Arima, and N. Yoshinaga, *ibid.* **66**, 064323 (2002); Y. M. Zhao, A. Arima, J. N. Ginocchio, and N. Yoshinaga, *ibid.* **68**, 044320 (2003); V. Velazquez, J. G. Hirsch, A. Frank, and A. P. Zuker, *ibid.* **67**, 034311 (2003).

[5] *Table of Isotopes*, edited by R. B. Firestone, V. S. Shirley, C. M. Baglin, S. Y. F. Chu, and J. Zipkin (John Wiley and Sons, Inc., New York, 1996).

[6] G. Racah, Phys. Rev. **63**, 367 (1943); B. H. Flowers, Proc. R. Soc. London, Ser. A **212**, 248 (1952).

[7] I. Talmi, Nucl. Phys. **A172**, 1 (1971).

[8] C. W. Johnson, G. F. Bertsch, D. J. Dean, and I. Talmi, Phys. Rev. C **61**, 014311 (1999).

[9] Y. M. Zhao, A. Arima, and N. Yoshinaga, Phys. Rev. C **66**, 064322 (2002).

[10] A. Arima, H. Horiuchi, K. Kubodera, and N. Takigawa, *Advances in Nuclear Physics* (Plenum Press, New York, 1972), Vol. 5, p. 345.

[11] Y. Kanada-En'yo and H. Horiuchi, Prog. Theor. Phys. Suppl. **142**, 205 (2001).

[12] P. Schuck, H. Horiuchi, G. Ropke, and A. Tohsaki, nucl-th/0302076.

[13] N. Tajima and N. Suzuki, Phys. Rev. C **64**, 037301 (2001).

[14] Y. M. Zhao, A. Arima, and N. Yoshinaga, Phys. Rev. C **68**, 014322 (2003).

[15] R. Bijker and A. Frank, Phys. Rev. C **64**, 061303 (2001).

[16] N. Auerbach, Phys. Rev. **163**, 1203 (1967); there are other definitions possible for the seniority number for many-j shells, but the essential physics remains the same.

[17] A. Bohr and B. R. Mottelson, *Nuclear Structure* (Benjamin, New York, 1975), Vol. II, pp. 45 and 136.

[18] T. Inoue, T. Sebe, H. Higawara, and A. Arima, Nucl. Phys. **59**, 1 (1964).

[19] M. Hamermesh, *Group Theory and Its Application to Physical Problems* (Addison-Wesley Publishing Company, Reading, MA., 1964), p. 435.
[20] M. Harvey, *Advances in Nuclear Physics* (Plenum Press, New York, 1968), Vol. 1, p. 67.
[21] J. P. Elliott, Proc. R. Soc. London, Ser. A **245**, 128 (1958); **245**, 562 (1958).

PHYSICAL REVIEW C 71, 017304 (2005)

Energy centroids of spin I states by random two-body interactions

Y. M. Zhao,*,†,‡ A. Arima,§ and K. Ogawa‖

*Department of Physics, Shanghai Jiao Tong University, 200240, China

†Cyclotron Center, Institute of Physical Chemical Research (RIKEN), Hirosawa 2-1, Wako-shi, Saitama 351-0198, Japan

‡Center of Theoretical Nuclear Physics, National Laboratory of Heavy Ion Accelerator, Lanzhou 730000, China

§The Science Museum, Japan Science Foundation, 2-1 Kitanomaru-koen, Chiyodaku, Tokyo 102-0091, Japan

‖Department of Physics, Chiba University, Yayoi-cho 1-33, Inage, Chiba 263-8522, Japan

(Received 6 October 2004; published 31 January 2005)

In this paper we study the behavior of energy centroids (denoted as $\overline{E_I}$) of spin I states in the presence of random two-body interactions, for systems ranging from very simple systems (e.g., single-j shell for very small j) to very complicated systems (e.g., many-j shells with different parities and with isospin degree of freedom). Regularities of $\overline{E_I}$'s discussed in terms of the so-called geometric chaoticity (or quasi-randomness of two-body coefficients of fractional parentage) in earlier works are found to hold even for very simple systems in which one cannot assume geometric chaoticity. It is shown that the inclusion of isospin and parity does not "break" the regularities of $\overline{E_I}$'s.

DOI: 10.1103/PhysRevC.71.017304 PACS number(s): 21.10.Re, 21.60.Ev, 23.20.Js

Low-lying spectra of many-body systems with an even number of particles were examined by Johnson, Bertsch, and Dean in Ref. [1] by using random two-body interactions (TBRE). Their results showed a preponderance of spin$^{\text{parity}} = 0^+$ ground states. Many efforts have been made to understand this very interesting observation and to study other regularities of many-body systems in the presence of random interactions. For instance, studies of odd-even staggering of binding energies, generic collectivity, behavior of energy centroids for spin I states, and correlations have attracted much attention in recent years. See Ref. [2] for a recent review.

Among many works along the context of regularities under the TBRE Hamiltonian, regularities of energy centroids (denoted as $\overline{E_I}$'s) of spin I states are very interesting. We denote by $\mathcal{P}(I)$ the probability that $\overline{E_I}$ is the lowest energy among all $\overline{E_{I'}}$'s. It was shown in Refs. [3,4] that $\mathcal{P}(I)$ is large only when $I \simeq I_{\min}$ or $I \simeq I_{\max}$. One thus divides the TBRE into two subsets; one subset has $\overline{E_{I\simeq I_{\min}}}$ as the lowest energy, and the other has $\overline{E_{I\simeq I_{\max}}}$ as the lowest energy. We define $\langle\overline{E_I}\rangle_{\min}$ ($\langle\overline{E_I}\rangle_{\max}$) as the value obtained by averaging $\overline{E_I}$ over the subset where $\overline{E_{I\simeq I_{\min}}}$ ($\overline{E_{I\simeq I_{\max}}}$) is the lowest energy. It was shown in Ref. [4] that $\langle\overline{E_I}\rangle_{\min} \simeq C\,I(I+1)$ and $\langle\overline{E_I}\rangle_{\max} \simeq C\,[I_{\max}(I_{\max}+1) - I(I+1)]$, where C is a constant depending on the occupied single-particle orbits and the choice of the ensemble. These features were discussed by using the quasi-randomness of two-body coefficients of fractional parentage (cfps) in Ref. [4], and by using other statistical views in Refs. [5,6].

The purpose of this Brief Report is to revisit regularities of $\overline{E_I}$. We shall show that the aforementioned regularities of $\mathcal{P}(I)$'s and $\langle\overline{E_I}\rangle_{\min}$'s hold even for very simple systems in which one cannot assume that two-body cfps are random. Previous studies of $\overline{E_I}$ under random two-body interactions have been restricted to identical fermions in one-j shell or two-j shells. Here we shall extend the study of $\overline{E_I}$ under random interactions to systems of many-j shells with the inclusion of parity and/or isospin.

In this paper we use the general shell model Hamiltonians defined in Ref. [2] and take the TBRE of Ref. [1] for two-body matrix elements. $\overline{E_I}$ and $\mathcal{P}(I)$ for "$\pm$" parity states are denoted by $\overline{E_{I^\pm}}$ and $\mathcal{P}(I^\pm)$, respectively. The number of particles is denoted by n. Proton (neutron) degree of freedom is denoted by "p" ("n"). Our statistics are based on 1000 sets of the TBRE Hamiltonian.

We begin with simple systems, that is, fermions in a small single-j shell ($j \leqslant 7/2$) and bosons with a small spin l. First we study fermions in a $j = 5/2$ or $7/2$ shell. $\overline{E_I}$ for three fermions were given in Eqs. (2.1) and (D1) of Ref. [7]. $\overline{E_I}$ for four fermions in a $j = 7/2$ shell can be obtained based on Eq. (5) of Ref. [8]. $\mathcal{P}(I)$'s obtained by using the TBRE Hamiltonian and those by applying the empirical rule of Ref. [7] are plotted and compared in Figs. 1(a)–1(c), where reasonable agreement is achieved. One sees that $\mathcal{P}(I)$'s are large for $I \simeq I_{\min}$ or $I \simeq I_{\max}$, except that this pattern is not very striking for Fig. 1(a) where there are only three $\overline{E_I}$'s given by three two-body matrix elements. For $j = 7/2$, $\mathcal{P}(I)$'s are small for "medium" I.

Let us look at $\langle\overline{E_I}\rangle_{\min}$'s, which are obtained by averaging $\overline{E_I}$ over the subset with $\overline{E_{I\simeq I_{\min}}}$ being the lowest energy. We plot $\langle\overline{E_I}\rangle_{\min}$'s for $n = 3$ with $j = 5/2$, $n = 3$ with $j = 7/2$, and $n = 4$ with $j = 7/2$ in Figs. 1(a′)–1(c′), respectively. We see that $\langle\overline{E_I}\rangle_{\min}$'s are approximately proportional to $I(I+1)$.

Now we study bosons with small spin l. The case with $l = 1$ (p bosons) can be easily understood: There is only one state for each I; $\mathcal{P}(I) = 50\%$ for $I = I_{\min}$ or $I = I_{\max}$, and $\mathcal{P}(I) = 0$ for other I values; $\overline{E_I}$ follows the $\overline{E_I} = C\,I(I+1)$ relation precisely.

As for $l = 2$ (d) bosons, we predict $\mathcal{P}(I)$ values for $n = 3$, 4, 5, and 6 by applying the empirical rule of Ref. [7] and compare them with those obtained using the TBRE Hamiltonian in Figs. 2(a)–2(d). Figures 2(a′)–2(d′) plot $\langle\overline{E_I}\rangle_{\min}$ versus $I(I+1)$. A linear correlation between these two quantities is easily noticed. Because all eigenvalues of d-boson systems are known, one can study

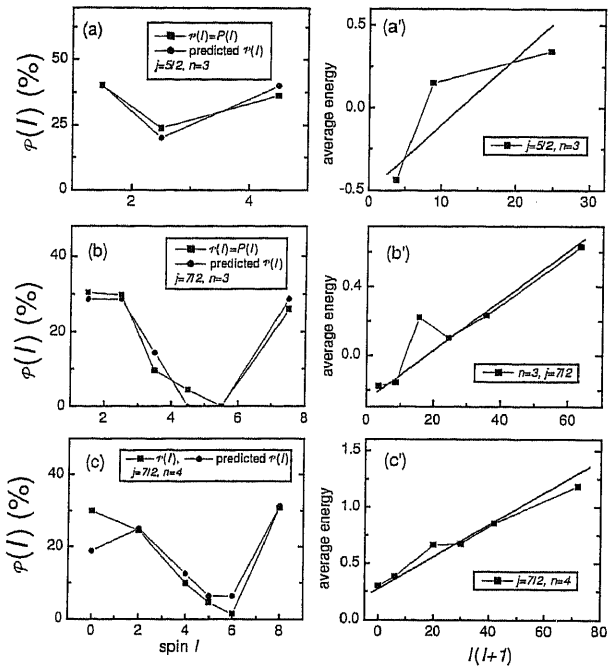

FIG. 1. $\mathcal{P}(I)$'s and $\langle \bar{E}_I \rangle_{\min}$'s for three fermions in a $j = 5/2$ or $7/2$ shell, and for four fermions in a $j = 7/2$ shell. $\langle \overline{E_I} \rangle_{\min}$'s are obtained by averaging over the subset of $\overline{E_{I \simeq I_{\min}}}$. One sees that $\mathcal{P}(I)$'s are large for $I \simeq I_{\min}$ and $I \simeq I_{\max}$, except in the case with $n = 3$ and $j = 5/2$ for which three states are given by three random two-body interactions. A good agreement between $\mathcal{P}(I)$ obtained using the TBRE Hamiltonian and that using the empirical rule of Ref. [7] is easily seen. The dotted lines in (a')–(c') are plotted to guide the eyes.

$\mathcal{P}(I)$ and the correlation between $\langle \overline{E_I} \rangle_{\min}$ and $I(I+1)$ at a more sophisticated level. From Eqs. (2.7) and (2.8) of Ref. [7], we have

$$\overline{E_I} = E'(n) + \frac{1}{70}(10c_2 - 7c_0 - 3c_4) \times \overline{v(v+3)} + \frac{1}{14}(c_4 - c_2)I(I+1). \quad (1)$$

Equation (1) shows that there are three terms in the $\overline{E_I}$'s: The first is just a constant and the second is related to $\overline{v(v+3)}$, the difference of which between neighboring I is large for low I and is negligible for $I \gg I_{\min}$; the third one is $I(I+1)$, which is small for low I and becomes dominant for large I. Thus $\mathcal{P}(I)$ is sensitive to the value of $\overline{v(v+3)}$ only for low I. Let us evaluate C in the formula $\langle \overline{E_I} \rangle_{\max} \simeq C\,[I_{\max}(I_{\max}+1) - I(I+1)]$ for d-boson systems. A simple assumption here is $(c_4 - c_2) \leqslant 0$. The C value can be evaluated by averaging $\frac{1}{14}(c_4 - c_2)$ under such a requirement:

$$C = \frac{1}{14} \times 2 \times \frac{1}{\sqrt{2\pi}} \frac{1}{\sqrt{2}} \int_0^{-\infty} x e^{-\frac{x^2}{4}} dx = -\frac{1}{7\sqrt{\pi}} \simeq -0.0806. \quad (2)$$

The value of C obtained by using the TBRE Hamiltonian is ~ -0.73 if $\overline{E_{I \simeq I_{\max}}}$ is the lowest energy and ~ 0.070 if $\overline{E_{I \simeq I_{\min}}}$ is the lowest energy. The difference between our predicted $|C|$ of

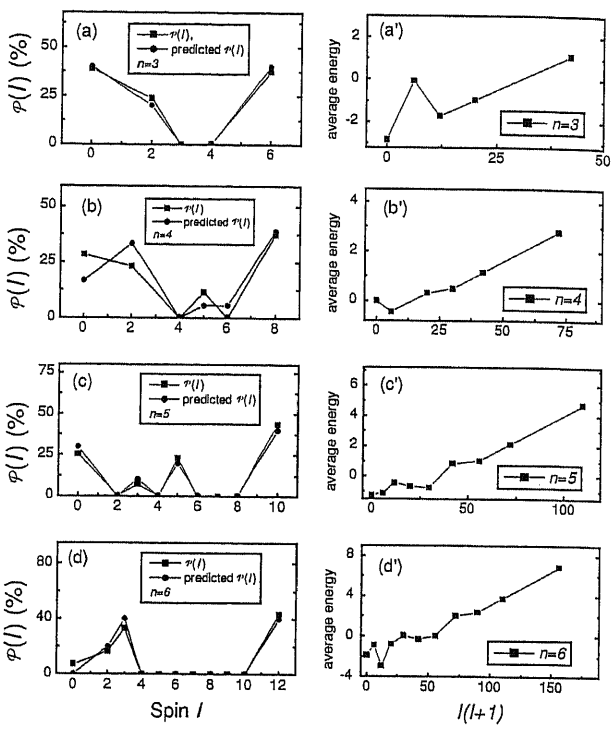

FIG. 2. $\mathcal{P}(I)$'s and $\langle \bar{E}_I \rangle_{\min}$'s for d bosons with $n = 3, 4, 5$, and 6. $\mathcal{P}(I)$'s are large when $I \simeq I_{\min}$ or $I \simeq I_{\max}$. $\mathcal{P}(I)$'s predicted by using the empirical rule are reasonably consistent with those obtained using the TBRE Hamiltonian. $\langle \bar{E}_I \rangle_{\min}$'s of these systems are proportional to $I(I+1)$ with fluctuations.

Eq. (2) and those obtained by the TBRE Hamiltonian comes from the complexity of $\overline{v(v+3)}$, which can be formulated analytically for any I.[1]

Now we come to systems of many-j shells with the inclusion of parity. Let us exemplify by a system with four identical nucleons in two-j shells: $j_1^{\pi} = 5/2^+$ and $j_2^{\pi} = 3/2^-$. Figure 3 plots our calculated $\mathcal{P}(I^{\pm})$ in terms of $I^{\pm}$ and $\langle \bar{E}_{I^{\pm}} \rangle_{\min}$ in terms of $I^{\pm}(I^{\pm}+1)$. One sees that both $\mathcal{P}(I^{\pm})$ and $\langle \bar{E}_{I^{\pm}} \rangle_{\min}$ behave similarly as $\mathcal{P}(I)$ and $\langle \overline{E_I} \rangle_{\min}$ in Ref. [7]. The $\mathcal{P}(I^{\pm})$'s predicted using the empirical rule of Ref. [7] are reasonably consistent with those obtained numerically using the TBRE Hamiltonian. According to our statistics, $\sum_{I^+} \mathcal{P}(I^+) = 41.3\%$, whereas $\sum_{I^-} \mathcal{P}(I^-) = 58.7\%$; $C^+ = 0.0372 \pm 0.0017$ and $C^- = 0.0359 \pm 0.0029$. These $C^{\pm}$ values are close to those obtained for $d_{3/2}d_{5/2}$ shells. For four identical nucleons in $d_{3/2}d_{5/2}$ shells, $C = 0.0401 \pm 0.0017$. This suggests that the relation $\langle \bar{E}_{I^{\pm}} \rangle_{\min} \simeq C^{\pm} I^{\pm}(I^{\pm}+1)$ and the value of C are not sensitive to parity of single-particle levels in the model space.

[1]We can see this point from the following numerical experiment. Let us take the subset where $\overline{E_{|\simeq I_{m\,\max}}}$ is the lowest energy, and confine our data of $\overline{E_I}$ to large I cases where the contribution from $\overline{v(v+3)}$ is small. The value of C such obtained is well consistent with that predicted by using Eq. (2). For example, if we adopt only $I \geqslant 55$ for $n = 33$, $C = -0.08146 \pm 0.00191$ for $\langle \overline{E_I} \rangle_{m\,\max}$.

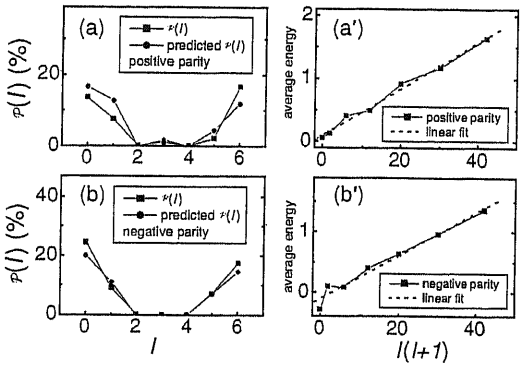

FIG. 3. $\mathcal{P}(I^{\pm})$'s and $\langle \bar{E}_{I^{\pm}} \rangle_{\min}$'s for four fermions in a two-j shell: $\frac{5}{2}^{+}$, $\frac{3}{2}^{-}$. $\mathcal{P}(I^{\pm})$'s for both negative parity and positive parity are large for $I \simeq I_{\min}$ or $I_{\max}$. The linear correlation between $\langle \bar{E}_{I^{\pm}} \rangle_{\min}$ and $I(I+1)$ holds for both positive and negative parity states of this simple system, with $C^{\pm}$ very close to each other.

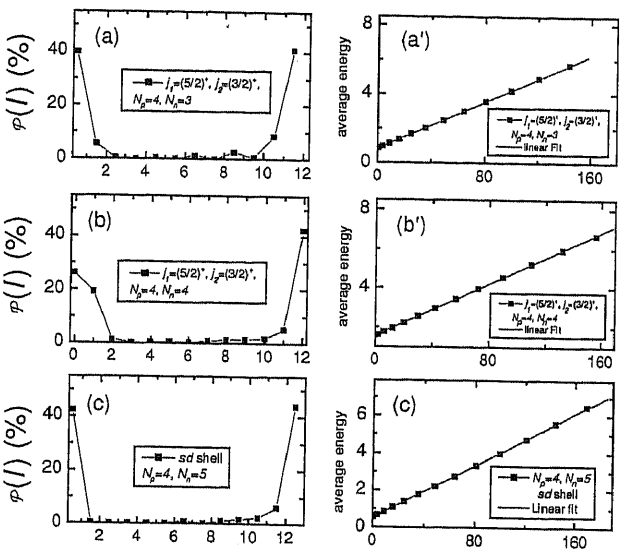

FIG. 4. $\mathcal{P}(I)$ and $\langle \bar{E}_I \rangle_{\min}$ for a few systems with both valence neutrons and protons.

We next study many systems with the inclusion of isospin degree of freedom. Figure 4 presents a few typical examples of $\mathcal{P}(I)$ and $\langle \overline{E_I} \rangle_{\min}$. We see that $\mathcal{P}(I)$ is large only when $I \simeq I_{\min}$ or $I \simeq I_{\max}$, and that $\langle \overline{E_I} \rangle_{\min} \simeq CI(I+1)$. According to our calculations, $C = 0.0354 \pm 0.0003$, 0.0341 ± 0.0001, 0.0350 ± 0.0001, and 0.0341 ± 0.0002 for $(n_{\rm p}, n_{\rm n})$=(4,4), (4,5), (4,6), and (6,6), respectively, in $s_{1/2}d_{3/2}d_{5/2}$ shells. $C = 0.0331 \pm 0.0002$, 0.0331 ± 0.0001, and 0.0338 ± 0.0001 for $(n_{\rm p}, n_{\rm n}) = (2, 4)$, (4,3), and (4,4), respectively, in fictitious two-j shells $d_{3/2}d_{5/2}$. C values are very close to those given by the empirical formula $C \simeq 1/(4\sum_i j_i^2)$ suggested on the basis of numerical experiments in Ref. [4].

We have also studied systems that include both parity and isospin. Our results present similar regularities and suggest that $C^{\pm}$ values are sensitive to j shells but not sensitive to particle numbers, nor to the isospin degree offreedom.

Now we discuss the formula of $\overline{E_I}$ obtained in Refs. [5,6] by evaluating the C value in $\langle \overline{E_I} \rangle_{\min} \simeq CI(I+1)$. The coefficient of the third term in Eq. (9) of Ref. [6] is a Gaussian random number with width

$$\sigma = \sqrt{\sum_{m \text{ even } J} \left((2J+1) \frac{3(J(J+1) - 2j(j+1))}{2j^2(j+1)^2(2j+1)^2} \right)^2}$$
$$= \sqrt{\frac{3(1408j^6 + 864j^5 - 4296j^4 - 512j^3 + 5688j^2 + 558j - 945)}{560j^4(j+1)^4(2j+1)^3}}. \quad (3)$$

One sees that $\sigma \propto j^{-5/2}$ when $j \to \infty$. The coefficient C in $\langle \overline{E_I} \rangle_{\min} = CI(I+1)$ is given by $\sigma \times \sqrt{2/\pi}$. The C value based on Refs. [5,6] is therefore proportional to $1/\sqrt{j^5}$ at the large-j limit. This is different from the empirical formula $C \simeq 1/4j^2$. In Table I we list a few C values obtained by different methods. This table shows that there is a systematic discrepancy between the predicted $C = \sqrt{2/\pi}\sigma$ with σ given by Eq. (3) and that obtained by using the TBRE Hamiltonian. The reason for this discrepancy should be clarified in the future.

To summarize, in this paper we have studied energy centroids of spin I states in the presence of random two-body interactions. First, we have shown that the regularities—$\mathcal{P}(I)$'s are large only when $I \simeq I_{\min}$ or $I \simeq I_{\max}$, and $\langle \overline{E_I} \rangle_{\min} \simeq I(I+1)$—hold approximately even for very simple systems in which cfps cannot be assumed "random." These simple systems include fermions in a $j = 5/2$ or $j = 7/2$ shell, $l = 1$ (p) bosons, and $l = 2(d)$ bosons. We point out that, although these regularities of energy centroids of spin I states are noticed and argued in Refs. [4–6], a *sound* understanding of $\overline{E_I}$ is not yet available. The arguments of Refs. [4–6] might be part of the story, and the randomness of cfps is not the unique origin of these regularities.

Second, we have shown that the these regularities are also robust with the inclusion of parity and/or isospin: $\mathcal{P}(I^{\pm})$'s are large only when $I^{\pm} \simeq I_{\min}$ or $I^{\pm} \simeq I_{\max}$, and $\langle \overline{E_{I^{\pm}}} \rangle_{\min} \simeq C^{\pm} I^{\pm}(I^{\pm}+1)$. $C^{\pm}$ is not sensitive to parity or isospin but

TABLE I. The coefficients C for a single-j shell. The column "TBRE" is obtained by 1000 runs of the TBRE Hamiltonian. The column "Empirical" is obtained by the simple formula $1/4j^2$ suggested in Ref. [4]. The column "Z-K" is obtained by the formulas given in Refs. [5,6]. Because C is not sensitive to particle number n, all results are given by $n = 4$. It is noted that C values obtained by the formula of Refs. [5,6] are systematically smaller than (about 70–80% of) the "experimental" values for a single-j shell.

$2j$	TBRE	Empirical	Z-K
9	0.01374	0.01235	0.01026
11	0.00826	0.00826	0.006907
15	0.00474	0.004444	0.003604
21	0.00231	0.002268	0.001712
27	0.00131	0.001372	0.000963

is sensitive to the value of j. We note without detail that this pattern also holds for two-body random interactions that are uniformly distributed.

Finally, we would like to mention two works on the energy centroids and other trace quantities such as spectral variances. In Ref. [9] Velazquez and Zuker used energy centroids and spectral variances to obtain the lower bound of energy for spin I states in the presence of random two-body interactions. In Ref. [10] Papenbrock and Weidenmueller derived the distribution of and the correlation between spectral variances of different spin I states, and they discovered a correlation between spin I ground-state probability and its spectral variance multiplied by a scaling factor. These studies are very interesting, and further studies along this line are called for.

We would like to thank Drs. V. K. B. Kota and W. Bentz for discussions and communications.

[1] C. W. Johnson, G. F. Bertsch, and D. J. Dean, Phys. Rev. Lett. **80**, 2749 (1998).
[2] Y. M. Zhao, A. Arima, and N. Yoshinaga, Phys. Rep. **400**, 1 (2004).
[3] A. Arima, N. Yoshinaga, and Y. M. Zhao, Eur. Phys. J. A **13**, 105 (2002); N. Yoshinaga, A. Arima, and Y. M. Zhao, J. Phys. A **35**, 8575 (2002).
[4] Y. M. Zhao, A. Arima, and N. Yoshinaga, Phys. Rev. C **66**, 064323 (2002).
[5] D. Mulhall, A. Volya, and V. Zelevinsky, Phys. Rev. Lett. **85**, 4016 (2000).
[6] V. K. B. Kota and K. Kar, Phys. Rev. E **65**, 026130 (2002).
[7] Y. M. Zhao, A. Arima, and N. Yoshinaga, Phys. Rev. C **66**, 034302 (2002); **66**, 064322 (2002).
[8] Y. M. Zhao and A. Arima, Phys. Rev. C **64**, 041301 (2001).
[9] V. Velazquez and A. P. Zuker, Phys. Rev. Lett. **88**, 072502 (2002).
[10] T. Papenbrock and H. A. Weidenmueller, Phys. Rev. Lett. **93**, 132503 (2004).